3D Microfabrication of Waveguides using Two-Photon Polymerization

A Major Qualifying Project
submitted to the faculty of
Worcester Polytechnic Institute
in partial fulfillment of the requirements for the degree of
Bachelor of Science in Physics

By
Brady B. Jeong

Date:
April 28, 2022

Report Submitted to:
Professor Douglas T. Petkie
Worcester Polytechnic Institute

Acknowledgements

Table of Contents

List of Figures

Abbreviations and Notations

WPI: Worcester Polytechnic Institute

QCC: Quinsigamond Community College

IC: Integrated Circuit

PIC: Photonic Integrated Circuit

LEAP: Lab for Education & Application Prototypes

2PP: Two-Photon Polymerization

Abstract

This project set a foundation for future related projects at the new photonics laboratory at WPI. Integrated photonics is a rapidly growing industry with applications in communications, sensing, medicine, defense, computing, and beyond. To illustrate the capabilities of the new laboratory, we developed a straight waveguide and a waveguide with an S-bend. The design was simulated using the finite element method and fabricated using two-photon polymerization-based direct laser writing. For characterization, we measured the insertion loss of the waveguides and inspected the quality of the prints. As a recommendation for future potential projects, we proposed applications that could build upon this project and made several process recommendations based upon the challenges we encountered.

Chapter 1: Introduction

The invention of the transistor and the discovery of minority carrier launched the modern electronics era [1]. However, it wasn't until the coming scalability of semiconductor technology and the invention of the integrated circuit [2, 3] that the incredible advances of modern electronics could come into fruition. The very fact that it is difficult to imagine a world without electronics today is a testament to the unparalleled impact of modern electronics and semiconductor technology which continues to increase in functionality, performance and reliability while decreasing in size, power, and costs [4]. The exponential scaling of integrated has been exponential with the cost per transistor of 0.1 micro-cents and chips with billions of transistors. Integration results in eliminating the need to package and assemble several parts by providing the device and connections in a single batch.

Several developments have created the foundation for modern optoelectronics and the potential for extending the concept of integration to photonics. The semiconductor laser [5], semiconductor alloy laser [6], and "tunable" bandgap materials [6] have led the groundwork of photonic integrated circuits. First proposed in 1969 by Miller [7], photonic integrated circuits have not made as much progress as its electronic counterparts. In the coming years however, the photonics industry is expected to experience strong growth. For example, photonic sensors are expected to grow 9% annually through 2025 with demand in automotive application expected to grow at 21 percent a year [8]. Waveguides are one of the basic building blocks of a photonic integrated circuit, the photonic counterpart to an electrical connection.

Two-photon polymerization allows for maskless rapid prototyping of nano and microstructures. Polymers are advantageous over its counterparts because of their low cost, high

transmission, plasticity, and mechanical stability. Because direct laser writing using two-photon polymerization can significantly reduce the fabrication time of microstructures using polymers, it is useful in the fields of micro-optics, biomedicine, and microelectronics.

Within the past few years, a new photonics laboratory has been built at WPI. The facility, LEAP@WPI/QCC, is designed to be an intersection of industry, government, and academia that fosters collaborations without barriers to develop mass production technology. It was funded through the Massachusetts Manufacturing Innovation Initiative (M2I2) and contains state of the art equipment to develop photonic integrated devices and support the sector in central Massachusetts through connections to the Manufacturing USA Institute AIM Photonics located in Albany, NY on the campus of SUNY Polytechnic Institute.

The aim of this project was to showcase the capabilities of the new photonics laboratory at WPI and set a foundation for similar future projects at the laboratory. We conducted background research into existing design rules and modeled and simulated our own waveguides. Using the Nanoscribe Photonics Professional GT+, we fabricated these air-clad polymer waveguides and conducted basic tests to characterize them.

This project informed us on potential improvements to the process we took that could benefit a related future project. We analyzed our approach in developing the waveguides and provided recommendations for project approach and process based on the different challenges we faced. Additionally, we proposed future projects that could reasonably build upon this project without significant challenges.

Chapter 2: Literature Review and Background

Photonic technology is a promising industry with great future prospects. The photonics market is expected to surge in the coming years due to the expanding applications in a wide range of industries from life sciences and manufacturing to information technology and sensing [9]. The first section of this background chapter introduces photonics, with a focus on miniaturized photonic technology. Sections 2-6 delves into the core technology and components of photonics that are used during the project. These include lasers, fiber optics, waveguides, photonic integrated circuits, and direct laser writing. Section 7 introduces research tools the team used to complete this project. Lastly, the chapter concludes with a brief analysis of the stakeholders and beneficiaries of this project.

2.1 Photonics

The word photonics comes from the quantum of the electromagnetic field, photons. Photonics is the science of generating, detecting, and manipulating light through various methods [10]. The development of photonic integrated circuits and demand for miniaturization and high-speed photonic technology has increased interest in the subject matter in recent years. Photonics technology is used for a variety of applications across industries such as spectroscopy, lithography, surgery, welding, electronics, manufacturing, military technology, telecommunications, information processing, and sensing. Analogous to the microelectronics revolution, the photonics industry is set to take off into a new age of miniaturized devices. Lasers, integrated with optics and sensors at much smaller size, allow for much more sophisticated applications in photonic sensing and precision optics.

2.2 Lasers

A laser is a core component of a photonic device as light is to photonics as electricity is to electronics. Lasers use different methods for optical amplification and create a coherent beam of light where all the photons have uniform frequency and waveform. Modulation of the light from the laser carries the information for communication applications and the interaction of light with the environment enables sensing applications and is an obvious and critical component to photonics applications. The industries that combine lasers with other technologies are seeing the strongest growth [8].

2.2.1 Historical Background

A discussion on the origins of lasers can't be had without Albert Einstein. In 1917, Einstein laid the theoretical groundwork for the laser in his paper, "On the Quantum Theory of Radiation" by rederiving Max Planck's law of radiation using the concepts of Einstein coefficients for absorption, spontaneous, and stimulated emission [11]. In the coming decades, there were few advancements in this area. In 1928, Rudolf W. Ladenburg indirectly confirmed the evidence of stimulated emission and negative absorption [12]. In 1939, a Russian physicist named Valentin A. Fabrikant predicted that stimulated emission in a gas discharge could amplify light under certain conditions [13]. And sometime after WWII, Willis E. Lamb and R.C. Retherford observed stimulated emission in hydrogen spectra [14].

Using Joseph Weber's paper on using stimulated emission to create a maser, Charles Hard Towne worked to develop a maser [15]. In 1954, Charles Hard Townes and his students James P. Gordon and Herbert J. Zeiger produced the first microwave maser, amplifying microwave radiations rather than light, as a laser would [16]. A few years later, in April 1957, a

Japanese engineer named Jun-ichi Nishizawa applied for a patent for the concept of a "semiconductor optical maser" [17]. Interest in maser development boomed soon after, and some began to think about extending the concept to higher frequencies of the electromagnetic spectrum. Dismissing the idea at first, Townes began investigating the possibility of an optical oscillator that generates coherent by amplifying stimulated emission. After conversations with Gordan Gould about optical pumping, both men went off separately and succeeded in solving the problem. Townes teamed with Arthur Schawlow and published a detailed proposal on a "optical maser" in *Physical Review* in 1958 [18].

The difficulty in creating a laser were the following: what to use as an active medium and how to excite a population inversion. Townes and Schawlow's proposal had been based on the optical pumping of a vaporized alkali metal with a lamp emitting on the lines of the same element. At Bell labs, Ali Javan proposed using electric discharge to excite helium gas, which would emit light by transferring energy to the neon atoms [19]. Gould also had a variety of methods which had potential to solve the problem at hand. Despite these developments, progress was slow. Theodore Maiman had designed a compact microwave maser using ruby crystals and was investigating its potential use in lasers. His calculations showed that using intense white pulses, he could raise chromium atoms in the ruby to the excited laser level [20]. On May 16, 1960, Maiman tested his design, marking the first experiment of a working laser [21, 22].

The term *laser* was first coined by Gordon Gould at a conference in 1959 [23]. The "LASER" was an acronym for Light Amplification by Stimulated Emission of Radiation". After Maiman's discovery, engineers and physicists replicated and improved upon the ruby laser and developed a variety of laser types. The first notable companies in the laser market were Hughes Aircraft, American Optical, TRG, AT&T (Bell Labs), and Raytheon. Some of the early laser

applications included increasing the bandwidth of Bell System's backbone telephone network, military technology, and holography.

The following decades saw great improvement and the introduction of new laser types. In recent years, the solid-state laser revolution has taken place. The major driving force of this shift is due to the remarkable efficiency of the high-power diode lasers. The development of the quantum-cascade laser gave terahertz research another source for terahertz radiation, a band that has seen increasing interest in recent years. Lasers have become a fundamental part of our modern life. Whether we realize it or not, lasers have contributed to an immense amount of human knowledge and make the core of the Internet. Lasers have and will continue to evolve and impact the world as technology advances.

2.2.2 Types and Operating principles

There are many laser types available today with varying applications. In this review, we will discuss some of the major laser types and their operating principles. The key difference between the laser types is the gain medium, or source of optical amplification that is used, a requirement to create the desired coherent beam of light. All lasers use population inversion, but different mechanisms/mediums/pumping separate them apart. The gain medium of the lasers can be solids, liquids, or gases as a gain medium [8]. Photons of the same frequency and waveform form these coherent beams and is prevented from spreading and diffusing due to their uniformity.

Gas lasers use gas as the medium to generate light. Electric current is sent through a gas (CO_2, helium-neon, argon, krypton, and excimer lasers), which produces coherent light. Gas lasers usually emit less lossy and more uniform emission than its counterparts (solid and liquid lasers). CO_2 lasers are some of the most widely used devices tend to be less costly than other

types of lasers. They produce the highest power continuous wave gas lasers available, but their maintenance costs often outweigh the benefits in frequent use applications. Excimer lasers are a type of gas laser with an excimer lasing medium. Excimer lasers operate at UV wavelengths and are used in applications such as photolithography and LASIK surgery. These are very concentrated light in the UV region and can produce high power at lower wavelengths but are much more expensive than fiber. Solid state lasers use doped ions that provide energy states required to maintain population inversion. These have been overshadowed by fiber lasers due to its lower efficiency and higher maintenance costs. Fiber lasers use rare earth elements such as erbium or thulium to turn optical fiber into the active gain medium. Their simple and robust design has cost advantages that have fueled its steady growth. Semiconductor lasers, or diode lasers operate by electrically pumping the diodes and introducing optical gain. Their costs have been falling and their versatility has been increasing, which has led to some growth in their demand. Commercial applications include laser pointers, laser printers, CD/DVDs. Quantum cascade lasers produce beams in the mid to far infrared spectrum. These have potential in optical communications, medical diagnostics, and industrial process control and are often used in defense applications. These like some others, are still too costly for many cases.

2.2.3 Applications

Lasers have a wide range of applications. Some scientific research applications include spectroscopy, laser interferometry, and laser scattering. The military has developed uses of the laser for its weapons and defense systems. These include guided munitions, missile defense, and electro-optical countermeasures. Lasers have also made huge advancements in modern medicine and are used in eye surgery, cancer treatments, and lithotripsy. Lastly, lasers are used extensively in industry for processing materials including cutting, welding, marking, 3D printing, and laser

cleaning. Commercially, laser printers, barcode scanners, holograms, and laser printers are all examples of uses of lasers.

2.3 Fiber Optics

The fundamental principle underlying optical fibers, refraction, was first demonstrated in the early 1840s. Refraction is the change in direction of light due to entering a material with a different index of refraction. In 1965, Charles Kao and George Hockman described a method that could reduce the attenuation of optical fibers below 20 dB/km, making optical fiber a potentially viable communication medium [24]. By using the right materials with high purity levels, they theorized that it was possible to reduce the attenuation. This realization led to Kao's Nobel Prize in Physics in 2009 and over the next several decades, higher quality optical fiber with lower attenuation were developed. Today, optical fiber cables are used as the main medium for computer networking because of the low attenuation across long distances, higher bandwidth, and immunity to electromagnetic interfaces [25]. Fiber optic sensors are also another use of optical fibers. Optical fiber sensors can be used to measure strain, temperature, pressure, and other quantities by exploiting the properties of the fiber such that the phase, wavelength polarization, or intensity of the light in fiber is changed.

2.3.1 Principle of Operation

An optical fiber is a cylindrical dielectric waveguide, or a nonconducting waveguide that uses total internal reflection to transmit light through its axis. The fiber construction includes the core that is surrounded by a cladding layer, as shown in Fig. 1. Both materials are dielectric materials, but the refractive index of the core is higher than the refractive index of the cladding to

confine the light in the core. The refractive index of a material is a property that measures the speed of light in a certain material. The higher the refractive index, the slower the speed of light through the material [26], making the speed of light in a vacuum the ultimate speed limit of light. The change in refractive index between the core and cladding can be either abrupt or gradual, step-index fiber and graded-index fiber respectively. Light is propagated through the fiber using a source such as a laser.
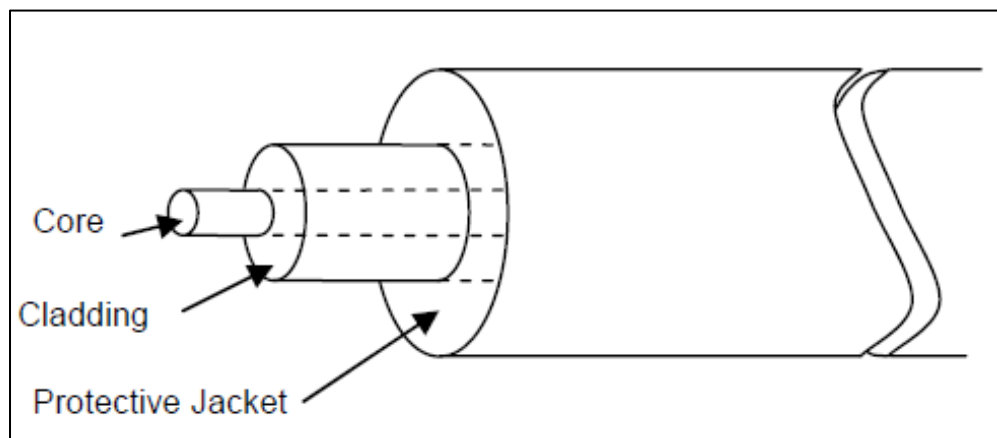
Figure 1: Optical fiber construction. The core is surrounded by the cladding, which is covered by the protective jacket [27].

Total internal reflection is the phenomena that occurs when light in a medium of higher index of refraction hits a boundary between the two media at an angle that is larger than the critical angle and is completely reflected. This effect is what keeps the light contained in the core of the optical fiber. The acceptance cone of the fiber is defined by the range of angles that the light can enter the fiber in such that the light will not leak out. The sine of the maximum angle is called the numerical aperture of the fiber. A fiber with a smaller numerical aperture requires more precise splicing.

A single mode fiber is one that cannot be analyzed using geometric optics and has a core diameter that is less than ~10 times wavelength of the light propagating through the core, typically 8 to 12 microns. Single mode fiber only carry a single mode of light, the transverse

mode. In single mode fiber, a large fraction of the light travels as an evanescent wave in the cladding. Single mode fiber is designed for use in the near infrared and usually for long distance applications. To analyze single mode fibers require using the electromagnetic wave equation reduced from Maxwell's equations since it must be considered as a waveguide structure. A multi-mode fiber is one that can be analyzed by geometrical optics and has a larger core diameter usually from 50-100 microns. Because a multi-mode fiber has a larger core diameter, the maximum length of transmission is more limited than in a single mode fiber.

2.4 Waveguides

A waveguide is a structure that guides electromagnetic waves. Optical fiber is one type of a broader family of waveguides with different applications. Waveguides are classified by their geometry, mode structure, refractive index distribution and materials. Like optical fibers, a waveguide will cause total internal reflection of the light passing through it. The properties of two-dimensional waveguides can be described in closed forms due to their simple nature [28]. Three dimensional waveguides of varying complexity are more difficult to analyze. The basic theory of the propagation of light in a waveguide is derived from the Maxwell's equations. Here, we are denoting E as the electric field amplitude and H as the magnetic field amplitude while D and B are the electric and magnetic fluxes respectively. Assuming a source free ($\rho = 0, J = 0$), linear (ϵ and μ independent of E and H), and isotropic medium [29], the equations are:

$$\nabla \times \vec{E} = -\frac{\partial \vec{B}}{\partial t}$$

Equation 1

$$\nabla \times \vec{H} = \frac{\partial \vec{D}}{\partial t}$$

Equation 2

$$\nabla \cdot \vec{D} = 0 \qquad \qquad \textit{Equation 3}$$

$$\nabla \cdot \vec{B} = 0. \qquad \qquad \textit{Equation 4}$$

Note that ϵ is the electric permittivity of the medium and μ is the magnetic permittivity of the medium. Using these equations, we derive the wave equation:

$$\nabla^2 \vec{E} - \mu\epsilon \frac{\partial^2 \vec{E}}{\partial t^2} = -\nabla (\vec{E} \cdot \frac{\nabla \epsilon}{\epsilon}). \qquad \qquad \textit{Equation 5}$$

For most structures, there is negligible gradient in permittivity of the medium, making the right-hand side of the equation zero. Therefore, the electric field becomes:

$$\nabla^2 \vec{E} - \mu\epsilon \frac{\partial^2 \vec{E}}{\partial t^2} = 0, \qquad \qquad \textit{Equation 6}$$

and the magnetic field becomes:

$$\nabla^2 \vec{H} - \mu\epsilon \frac{\partial^2 \vec{H}}{\partial t^2} = 0. \qquad \qquad \textit{Equation 7}$$

A guided waveguide propagates along the longitudinal direction, along the z coordinate. The characteristics of a waveguide are dependent on the transverse profile (x and y coordinates). Two-dimensional waveguides, or planar waveguides, have optical confinement limited to a single transverse direction, which we will denote as the x direction. On the other hand, non-planar, or 3D waveguides have a two-dimensional optical confinement, where the core is surrounded by cladding on all sides of the transverse directions. Each of these are shown in Fig. 2.
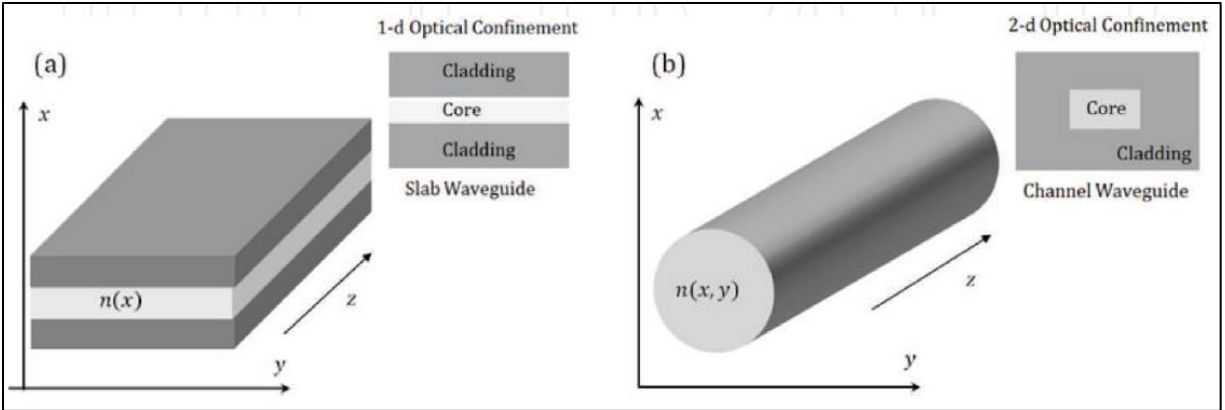
Figure 2: "2D" vs 3D waveguides [29]. Optical confinement in 2D waveguides is limited to a single transverse direction while optical confinement in 3D waveguides have two-dimensional optical confinement.

A waveguide mode is a propagating wave that has a distinct phase velocity, group velocity, cross-sectional intensity distribution, and polarization. A mode can be described by the effective index of the medium and the invariant transversal intensity profile. The phase velocity describes how well the optical power is confined to the core and is defined by the phase velocity $c/n_{effective}$. The effective mode is the refractive index felt by the mode. The following modes exist with an effective index that is higher than the largest cladding index:

1. Guided modes

2. Substrate radiation modes

3. Substrate cover radiation mode

4. Evanescent modes

The possible modes are determined by the dimensions of the waveguide. The single mode is created when the waveguide dimensions are shrunk to a point where the fundamental modes are the sole modes propagating. These modes are the following

1. Transverse electric and magnetic mode (TEM mode)

2. Transverse electric mode (TE mode)

3. Transverse magnetic mode (TM mode)

4. Hybrid mode (only in non-planar waveguides)

There exists a homogeneous wave equation for planar waveguides with any index profile. Non-planar waveguides are a bit more complicated. The most used non-planar waveguides are rectangular waveguides. These include the buried waveguide, diffused waveguide, wire waveguide, strip-loaded, rib waveguide, slot waveguide, ARROW, etc. The wire waveguide consists of a core that sits on top of a cladding of a different material. For the mode to be guided in the waveguide, the effective refractive index must be larger than the cladding's refractive index but smaller than the core index. The rest of the waveguides will not be investigated in this project but are shown in Fig. 3.
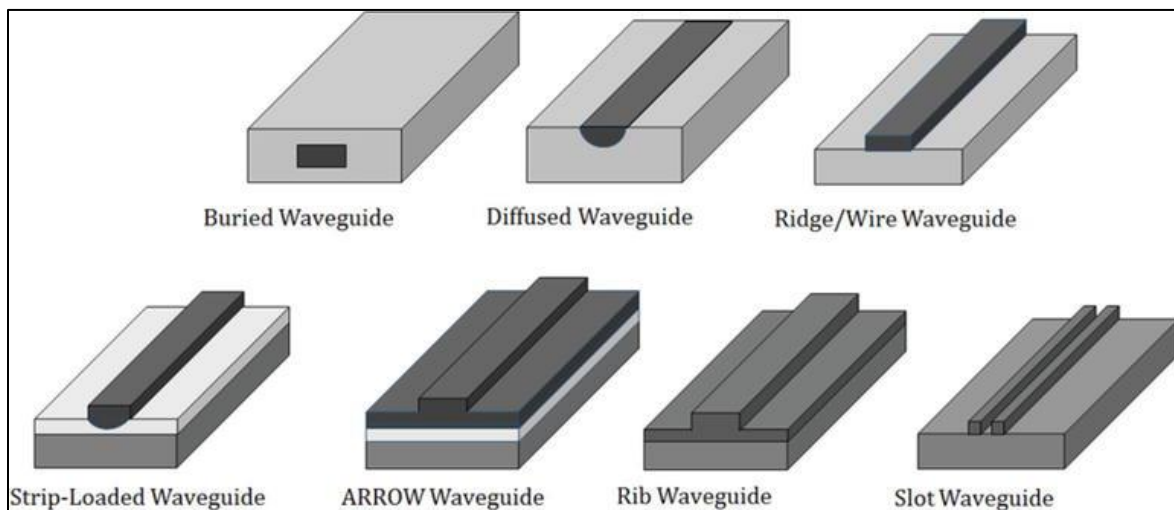
Figure 3: Types of rectangular waveguides [29]. Rectangular waveguides are the most common non-planar waveguides.

Several special types of waveguides exist beyond the ones previously mentioned. These include the diffused waveguide, photonic crystal waveguide, Triplex waveguide, suspended waveguide, pedestal waveguide, augmented waveguide, and hollow waveguide. The ARROW waveguides are anti-resonant reflecting optical waveguides where the waveguide creates a

Fabry-Perot reflector for the transverse component of the wave vector and confines the light. Several ARROW waveguides with a hollow circular core have been designed using the 3D printing method used by this project [30-32]. Pedestal waveguides are waveguides that raise the waveguide thus achieving lower propagation losses than conventional rib or strip waveguides [33]. Subwavelength structures are structures that are smaller than the wavelength of light it is interacting with. In general, this refers to an arrangement of different materials that suppresses the diffraction effects [34]. Subwavelength structured waveguides have been studied [35] to achieve manipulate the optical field and achieve effective index matching for a multitude of devices.

2.5 Photonic Integrated Circuits

The photonics integrated circuits (PICs) are a rapidly growing market with numerous applications. A dominant technology in high-speed communications and an equivalent of microelectronics in the electronics sector, PICs provide many benefits to photonics applications. First proposed by Miller [7] in 1969, PICs have been primarily used in the field of optical communications [4].

Several foundational advances throughout history have made photonic integrated circuits possible, as shown in Fig. 4. These include the invention of the laser, transistor, electronic integrated circuit, and the low attenuation fiber-optic transmission.

Year	Technology Break-Through
1883	Light detection in a semiconductor
1947	Transistor (including the discovery of minority carrier injection)
1959	Electronic integrated circuit (IC)
1960	Invention of the LASER
1961	Light modulation in a III-V semiconductors
1962	Semiconductor injection laser
1962	III-V alloy injection laser
1963	Heterojunction semiconductor laser proposal
1966	Low-loss fiber-optic transmission
1969	Double heterojunction injection laser (RT, cw)
1969	Photonic IC proposal

Figure 4:A timeline of foundational advances enabling PICs [4]. These are fundamental technological advancements that allowed for the PIC to exist.

While the photonic integrated circuit was proposed and its scientific foundations were established, the fabrication technology to manufacture and develop the photonic IC were not. Several fabrication advancements have been made to make photonic ICs a reality (see Fig. 5). These mostly include developments in material science that in conjunction with the development of the building blocks of photonic ICs would result in viable photonic IC decades after Miller's proposal.

Year	Technology Break-Through
1956	Bulk Czochralski crystal growth of III-V materials
1961	Vapor phase epitaxy (VPE) of III-V alloys
1962	Bulk crystal growth of InP
1962	Cleaved optical facets
1970	Viability of III-V quaternary alloys (III-V quaternary alloy injection laser)
1974	DFB injection laser demonstration (integrated mirrors)
1976	InGaAsP / InP laser demonstration (RT, cw)
1977	Viability of Metal Organic Vapor Phase Epitaxy (MOVPE)
1981	Butt-coupled regrowth for photonic ICs
1987	InAlGaAs / InP laser demonstration (RT, cw)
1991	Selective area epitaxy for photonic integration
1992	High-volume MOVPE tools

Figure 5: A timeline of essential new fabrication processes for PICs [4] The processes developed allowed the foundational technological advancements to be applied to the production of the PIC.

The complete, functional, and integrated photonic IC should have sources, modulators, waveguides, and photodetectors in addition to optical amplifiers, multiplexers, demultiplexers, phase shifters, and other tunable devices. These developments are summarized in Fig. 6.

Year	Technology Break-Through
1959	III-V photodetector
1966	III-V electroabsorption (EA) modulator
1971	DFB laser proposal
1974	DFB injection laser demonstration
1975	DFB injection laser (RT, cw)
1975	Self-imaging in planar optical waveguides
1977	Quantum well (QW) injection laser
1979	QW MOVPE injection lasers (RT, cw)
1978	InGaAsP/InP photodetectors
1981	InP-based DFB injection laser (RT,cw)
1984	Strained QW injection laser
1984	III-V Mach-Zehnder modulator
1984	InP-based electroabsorption (EA) modulator
1986	Strained QW laser band-structure engineering
1986	Waveguide photodetector
1988	Phased array waveguides
1989	InP-based Mach-Zehnder modulator
1991	Arrayed waveguide gratings (AWGs)
1992	III-V AWG devices

Figure 6: A timeline of PIC developmental milestones [4]. These events define the creation of the core building blocks of the PIC.

To help the reader understand the basic foundations of photonic integrated circuits, an analogy can be made between the electronic building blocks and the photonic building blocks as shown in Fig. 7. Light has amplitude, phase, and polarization. Using various optical components, these properties can be manipulated using the optical amplifier, a phase modulator, and a polarization converter. An optical amplifier amplifies an optical signal directly and is analogous to the transistor in the electronic circuit. A resistor is analogous to the phase shifter while the capacitor is comparable to the polarization convertor. The waveguide is where the light propagates through, just as the electrical connection is how electricity flows.
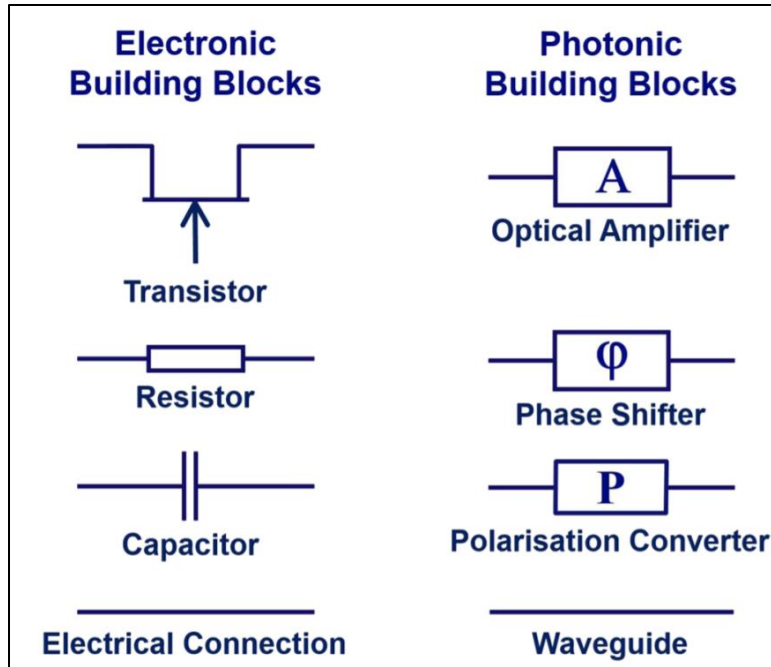
Figure 7: A comparison of the electronic vs photonic integrated circuits [36].
The building blocks of PICs are comparable to the building blocks of the
electronic integrated circuit.

The most commonly used platform for photonic integrated circuits is indium phosphide

(InP), due to its versatility in integrating optically active and passive functions. InP PIC

integration has followed a similar trajectory as the Moore's law for electronic IC [37].

Monolithic integration in InP technology is expected to reduce energy, remove assembly

complexity, and sustain performance increases [38]. Other developments are occurring in InP

photonics technology using sub-micron thick InP membrane [39]. Silicon photonics based on

silicon on insulator (SOI) have also come onto the scene due to the open access nature of silicon

photonics fabs and the reduced overall costs [40] (see Fig. 8). The obvious advantage for silicon

photonics is that it is leveraging the decades of investment put into silicon manufacturing

processing for semiconductors. Silicon is transparent at wavelengths typically used for optical

communications (1270nm - 1625nm) resulting from its intrinsic bandgap ~ 1.1 eV [41]. This

makes it a good candidate for use with optical fibers. To further broaden the use of PICs will

require a large undertaking of research in chip packaging and assembling manufacturing technology [42].

Figure 8: Silicon-on-Insulator chip with a variety of structures including Mach-Zehnder-modulators, Raman-lasers and -amplifiers, Fabry-Pérot modulators, waveguides [41]. Silicon-on Insulator PICs are one of several platforms for PICs.

In his proposal, Miller highlighted economics as a motivating factor for photonic integration. However, since his proposal, there has been limited commercial success of PICs even with much research demonstrations and advancements. Some reasons for why photonic ICs have not been as economically viable as its electronic counterparts, as outlined by Kaminow in 2008 [43] include:

1. The need for a diverse set of semiconductors that are harder to control and manufacture,

2. The larger fundamental size limit of photonic integrated circuits compared with the electronic IC making it less scalable,

3. A larger set of building blocks compared with the electronic IC,

4. The lack of sizeable applications for heavy and continued investment into the technology.

Even so, the photonic IC has been implemented across a variety of applications. The biggest area for photonic integrated circuits is in the field of fiber optic communication. PICs are used as

18

optical transceivers for fiber-optic communications, serving as the interface between the electronic and optical parts of the network [41], and are also used as multiplexers and demultiplexers for high-speed transmission [44]. Beyond communications, PICs are used in biomedical applications [45] and photonic computing. Beyond industrial applications, PICs are a topic of research in defense. For an example, studies have been done on the viability of PICs as biochemical sensors for the Department of Defense [46]. Continuing advancements in photonics is expected to continue to drive growth of the photonics industry across the globe [9]. As a wide range of industries find use for PICs, it will continue to drive demand. Some potential applications include AR, lab-on chip, real-time biosensors, aerospace & defense, and navigation for autonomous vehicles.

2.6 3D Microprinting/Two-Photon polymerization

Direct laser 3D printing, more specifically multiphoton lithography, is a technique used to create intricate three-dimensional nanostructures. It was developed in 2001, when researchers in Germany created a system that used two-photon polymerization [47]. Polymer-based devices are advantageous in their low cost, high transmission, plasticity, and mechanical stability. Direct laser writing using two-photon polymerization allow the user to create prototypes rapidly with high processing resolution. This makes two-photon polymerization direct laser writing very useful in the fields of micro-optics, biomedicine, and microelectronics.

Two photon polymerization is uses a beam emitted from a femtosecond laser and focuses the light into the interior of the material using a high numerical aperture objective lens [48] (see Fig. 9 and 10). It's important that the intensity of the scanning laser is higher than the threshold intensity of the photopolymer resin. The stage controller controls the position and depth of the

polymerization area by controlling the area of the resin being beamed by the laser. The final

structure is obtained by removing to unexposed areas. The photopolymer resin needs to have

photosensitive properties; therefore, the commonly used material is a prepolymer resin

containing a photo initiator such as IP-Dip or SU-8. Additionally, dye molecules may be added

to the substrate as a photosensitizer to make the photopolymerization more efficient.

Figure 1. Schematic diagram of a DLW system.
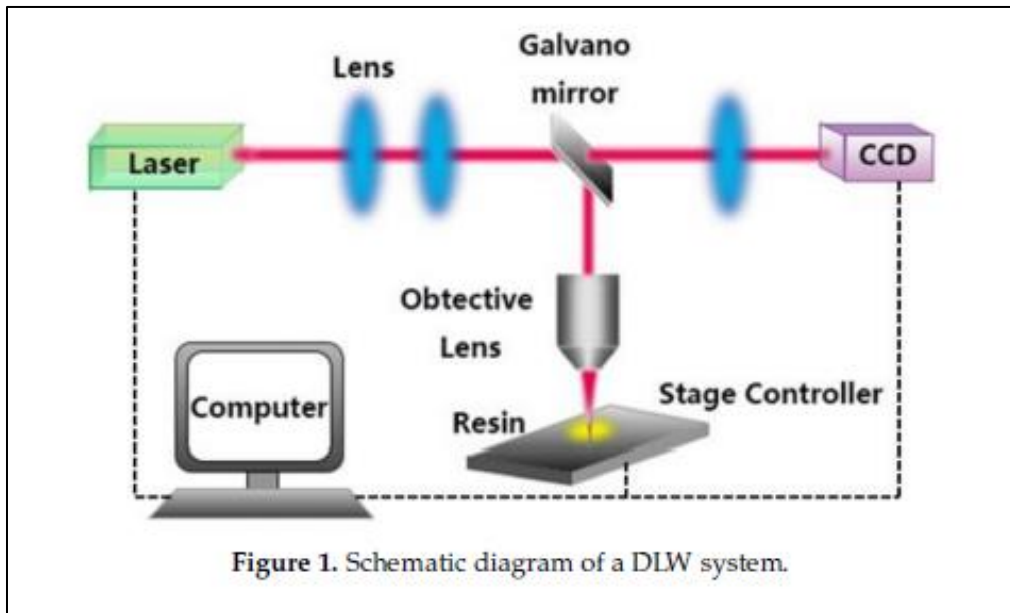
Figure 9: Schematic diagram of a direct laser writing system [48]. Direct laser 3D printing is a technique used to create intricate 3D nanostructures.

The commonly used laser wavelength for fabricating polymer-based printing is 400-800nm and

the power ranges from the milliwatt range to a several hundred milliwatts. The resolution of the

structure is dependent on the chemical reaction that occurs and the chosen parameters of the

system, such as writing speed and power.
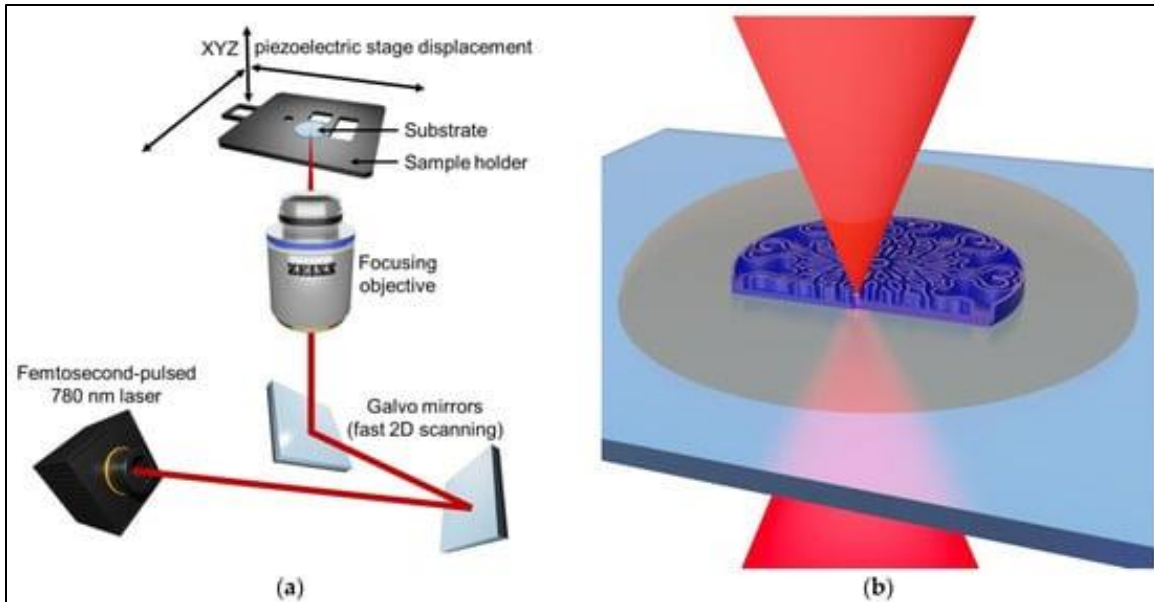
Figure 10: Two photon polymeriztion action in detail [49]. A femtosecond-pulsed laser is directed to the desired location on the stage using the galvo mirror and the piezoelectric stage.

Using two-photon polymerization, polymer fiber gratings, micro resonators, micro lenses, and optical waveguide couplers have been created. Additionally, on the topic of electromagnetics, electronic circuits, PICs, micro capacitors, and electro-optic modulators have also been printed. Thus, two-photon polymerization is a great potential tool for rapid prototyping a variety of PIC applications since many optical elements and circuitry required for PICs can be developed using multiphoton polymerization [50]. Limited research has been done to print waveguides using this method [30, 51-53]. Some notable examples include the hollow light cage ARROW waveguides and pedestal waveguide seen in Fig. 11.
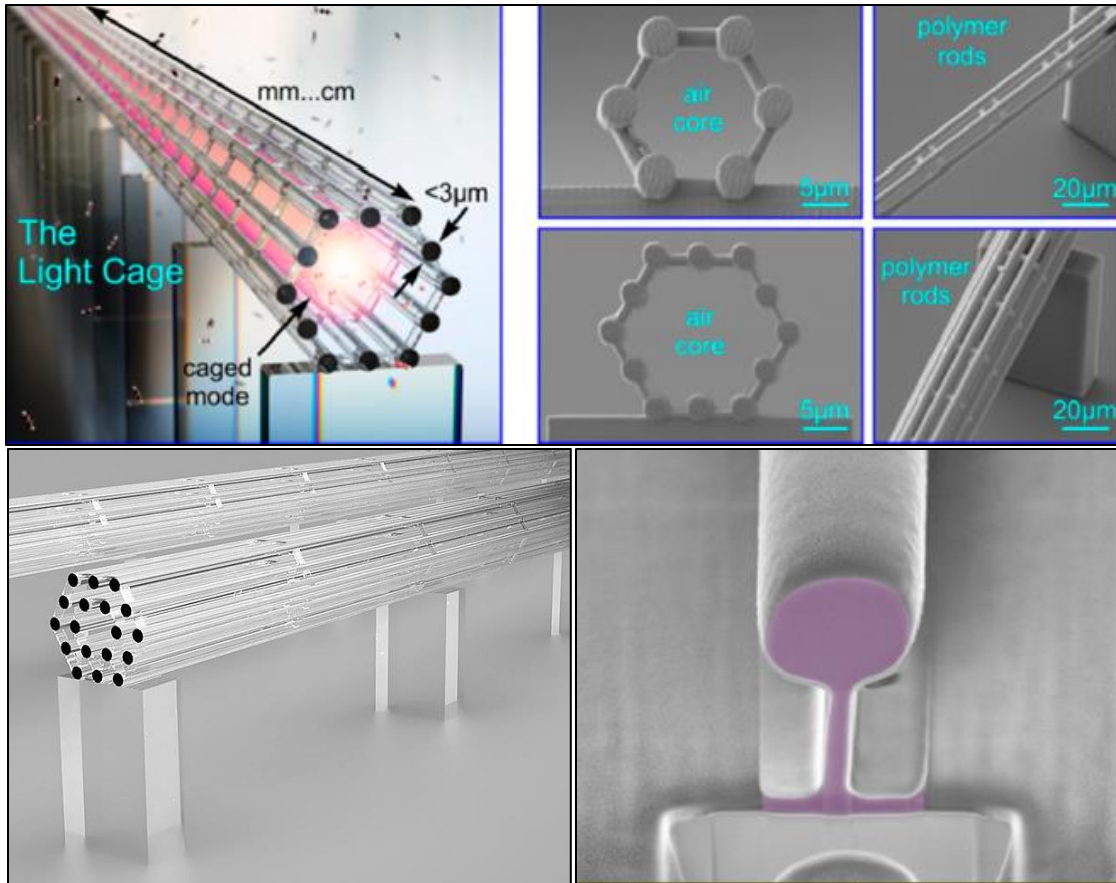
Figure 11: Examples of waveguides fabricated using two-photon polymerization. The upper left, upper right, and lower left figures all are hollow light cage ARROW waveguides [30, 53]. The figure on the bottom right is an example of a pedestal waveguide [52].

2.7 Research Tools

2.7.1 COMSOL Multiphysics

COMSOL Multiphysics or COMSOL is a physics simulation software used in engineering, manufacturing, and scientific research fields to model and simulate systems. It is often used by scientists and engineers to simulate real-world situations that are very costly to test. In addition to the possibility of exploring more extreme conditions while maintaining safety and product integrity, COMSOL allows us to evaluate and predict entities not directly measurable in experiments. There are two components of the COMSOL Desktop environment:

the Model Builder and the Application Builder [54]. The Application Builder allows the user to create an application based on a model created with the Model Builder with a specialized user interface. The Model Builder, the primary focus of this review, allows the user to define a model, specify ways to solve it, and analyze the simulation result. The Model Builder works by building a model tree which reflects the model object, which stores various settings relevant to the state of the model. Fig. 12 show the COMSOL user interface for the Model Builder.

COMSOL uses different modules with predefined physics of several different categories, simplifying the modeling of device geometry, governing equations, boundary conditions, etc. These include modules relating to Electromagnetics, Fluid Flow & Heat Transfer, Structural Mechanics & Acoustics, Chemical Engineering, and other Multipurpose and Interfacing Modules. For the purpose creating a waveguide simulation, the Wave Optics module under the Electromagnetic category was used.
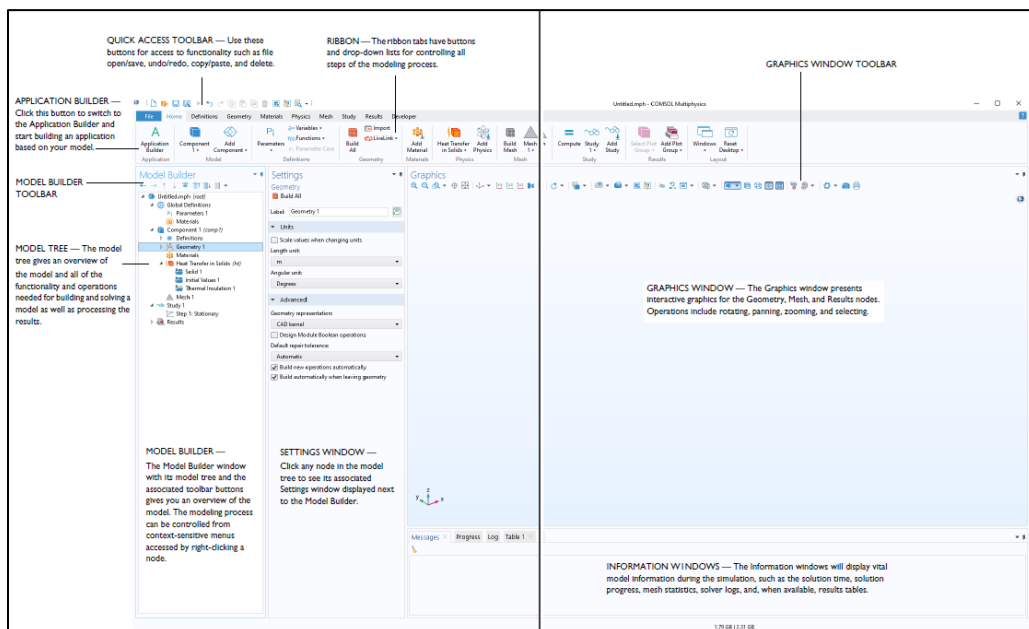
Figure 12:COMSOL Model Builder user interface [54].

2.7.1.1 Wave Optics Module

The Wave Optics Module is used to simulate electromagnetic wave propagation and resonance effects in applications relating to optics in both two-dimensional and three-dimensional designs [55]. It can predict electromagnetic field distributions, transmission, reflection coefficients, and power dissipation in design. The modeling is based on Maxwell's equations and material propagation laws. The wave optics module is often used to simulate the propagation and coupling of electromagnetic fields and waves in different optical structures. Wave optics module is useful in E&M problems at optical frequencies, corresponding to nano to micrometer wavelength range [56]. Using the Wave Optics Module, the user can solve problems with high frequency E&M simulations. It is very useful in simulations that involve domains that are much larger than the wavelength. Thus, the module can solve problems that involve optical phenomena and typical waveguide simulations without huge computer memory needs. The applications of the wave optics module include just about any optical applications such as optical fiber, photonic waveguides, photonic crystals, nonlinear optics, laser resonator design, and active devices in photonics. Material properties can range from inhomogeneous and fully anisotropic materials, complex valued material properties, and medium with gains or losses. The simulations can directly compute S-parameters and far-field radiation patterns and simulation can have ports with specified power and mode with perfectly matched layers to simulate unbounded domain.

The Wave Optics Module works with several physics interfaces that cover across different types of electromagnetic field simulations. They handle problems involving time-harmonic, time-dependent, and eigenfrequency & eigenmode problems. Analysis of in-plane, axisymmetric, and full 3D electromagnetic propagation and full vector mode analysis in 2D and

3D can be done. The following predefined wave optics interfaces allow the setup of electromagnetic models (see Fig. 13 for details):

- Electromagnetic Waves, Frequency Domain

- Electromagnetic Waves, Time Explicit

- Electromagnetic Waves, Beam Envelopes

- Electromagnetic Waves, Transient

PHYSICS INTERFACE	ICON	TAG	SPACE DIMENSION	AVAILABLE STUDY TYPE
Optics				
Wave Optics				
Electromagnetic Waves, Beam Envelopes		ewbe	3D, 2D, 2D axisymmetric	adaptive frequency sweep; boundary mode analysis; eigenfrequency; frequency domain; frequency domain, modal; wavelength domain; frequency domain source sweep
Electromagnetic Waves, Frequency Domain		ewfd	3D, 2D, 2D axisymmetric	adaptive frequency sweep; boundary mode analysis; eigenfrequency; frequency domain; frequency domain, modal; mode analysis (2D and 2D axisymmetric models only); wavelength domain; frequency domain source sweep
Electromagnetic Waves, Time Explicit		teew	3D, 2D, 2D axisymmetric	time dependent; time dependent with FFT
Electromagnetic Waves, Transient		ewt	3D, 2D, 2D axisymmetric	eigenfrequency; time dependent; time dependent, modal; time dependent with FFT

Figure 13:Overview of Wave Optics interfaces [56].

Interfaces formulate and solve the differential form of Maxwell's equations with initial and boundary initial and boundary conditions using the finite element method with numerically stable edge element discretization and algorithms for preconditioning and solution of resulting sparse equation systems. The results are displayed using plots of electromagnetic fields,

reflectance, transmittances, diffraction efficiencies, S-parameters, power flow, and dissipation. The result presentation is customizable as well if the default plots are not sufficient. The steps for creating a simulation are as follows:

1. Define geometry
2. Select materials
3. Select wave optics interface
4. Define boundary and initial conditions
5. Define fine element mesh
6. Select solver
7. Visualize results

There are more than a thousand prepared materials for use in the built-in material libraries, but a custom material can be created with user defined properties. The mesh creation and solver selection are tuned for each interface specifically and often done automatically with default settings.

In an environment with time variations, there are two approaches the user can take. One is to calculate change for each time step by using the Time Dependent study through the Electromagnetic Waves, Time Explicit and Electromagnetic Waves, Time Explicit interfaces. One downside of this approach is that it can be time intensive depending on the size of the time steps. The alternative approach is to use the Frequency Domain study through the Electromagnetic Waves, Frequency Domain and the Electromagnetic Waves, Beam Envelopes interfaces. By assuming that all time variations occur sinusoidally, the problem becomes time harmonic and in the frequency domain. This simplifies the problem and applies to all periodic signals in conjunction with Fourier analysis.

In the Frequency Domain interface, the total electric field is the dependent variable. As long as the mesh size is small enough relative to the wavelength, the Frequency Domain interfaces are very efficient for solving propagation and scattering simulations. As mentioned earlier, the wave optics module is often used for simulations involving high frequency electromagnetic waves. For many optical applications, the length of propagation is much longer than the wavelength. For example, the wavelength may be around 1 micron and the propagation length may be on the millimeter scale. While this would necessitate a huge amount of memory resources, the beam Envelopes interface can simplify this problem by assuming a slowly varying amplitude factor and a rapidly varying phase factor. Fig. 14 gives an overview of the different interfaces and their governing equations.

	Interface	Governing Equations
Time-dependent	Time Explicit	$\epsilon_0\epsilon_r\dfrac{\partial E}{\partial t} - \nabla \times H + \sigma E = 0$ $\mu_0\mu_r\dfrac{\partial H}{\partial t} + \nabla \times E = 0$
	Transient	$\nabla \times \mu_r^{-1}(\nabla \times A) + \mu_0\sigma\dfrac{\partial A}{\partial t} + \mu_0\dfrac{\partial}{\partial t}\left(\epsilon_0\epsilon_r\dfrac{\partial A}{\partial t}\right) = 0$
	Frequency Domain	$\nabla \times \mu_r^{-1}(\nabla \times E) - k_0^2\left(\epsilon_r - \dfrac{j\sigma}{\omega\epsilon_0}\right)E = 0$
Stationary	**Beam Envelopes**	$(\nabla - i k_1) \times \mu_r^{-1}((\nabla - i k_1) \times E_1) - k_0^2\left(\epsilon_r - \dfrac{j\sigma}{\omega\epsilon_0}\right)E_1 = 0$

Figure 14: Governing equations for Wave Optics module interfaces [57]. The Beam Envelopes interface was the interface used for the simulations in this project.

2.7.1.2 The Electromagnetic Waves, Beam Envelopes Interface

The Electromagnetic Waves, Beam Envelopes interface is used to model systems that need solutions on one or two frequency-domain wave equations for the electric field envelope. As mentioned above, the interface computes electric and magnetic field distributions for simulations where the amplitude factor is varying slowly, and the phase factor is varying rapidly.

See Fig. 15 for a more detailed description of the theory of the Beam Envelopes interface. The Beam Envelopes interface is best suited for uni and bidirectional propagation. This interface supports the Frequency Domain and Eigenfrequency studies, and Boundary Mode Analysis and Wavelength Domain studies that find resonance frequencies and the respective eigenmodes.
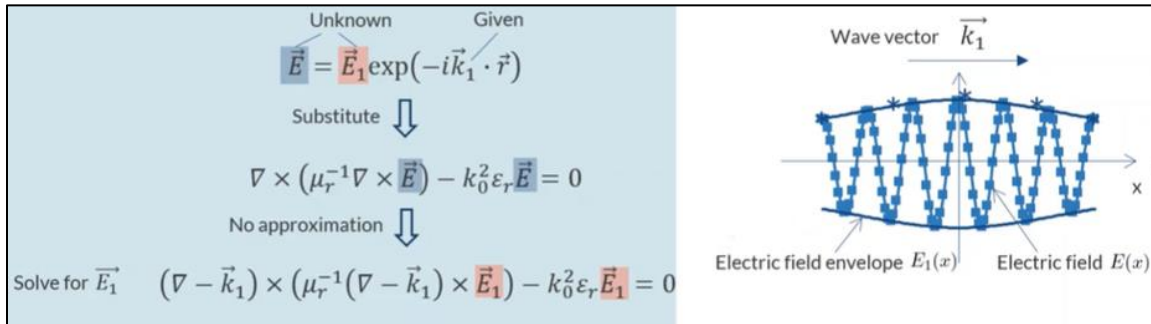
Figure 15: Beam Envelopes interface theory [57]. The interface computes electric and magnetic field distributions for simulations where the amplitude factor is varying slowly, and the phase factor is varying rapidly

2.7.2 Nanoscribe

2.7.2.1 Nanoscribe Photonic Professional GT+

The Nanoscibe Photonic Professional GT+, equivalent to the Nanoscribe Photonic Professional GT2 [49], is a high resolution two-photon polymerization 3D printer designed for microfabrication. The device is capable of creating a variety of 3D structures including crystal lattices, porous scaffolds, sharp edges, contours, and nearly any imaginable designs [58] (see Fig. 16). The printer is versatile with numerous substrates, materials, and options, while its galvo-based system allows for high-speed submicron precision in nano, micro, and mesoscale fabrication. More than 1200 research projects have been used for state-of-the-art research in over 30 countries. The 3D printing workflow from the CAD file to the printed product is straightforward through Nanoscribe's proprietary printing software, DeScribe.

Figure 16: The figure on top is the Nanoscribe Photonic Professional GT2 [58]. The GT2 model is equivalent to the GT+. The bottom figure is a set of sample structures printed using the Nanoscribe printer. Note the intricate shapes and sizes.

The Photonic Professional GT+ has broad applications as it has been designed for use in microfluidics, micromechanics, biomedical engineering, micro-electro-mechanical systems, mechanical metamaterials, photonic metamaterials and plasmonic, micro-optics, nanostructures. In one application, the this printer was used to create a polymer micro-ring resonator integrated with a fiber ring laser for ultrasound detection [59] (see Fig. 17).
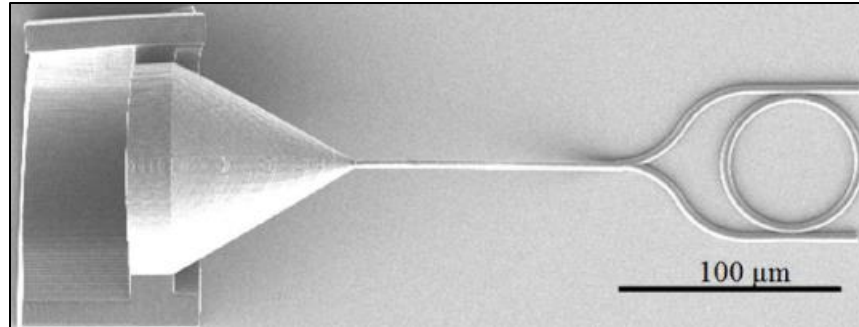
*Figure 17: Polymer micro-ring resonator sensor [59]. The Photonic Professional GT+
has broad applications as it has been designed for use in microfluidics,
micromechanics, biomedical engineering, and more.*

By using two-photon polymerization, the Nanoscribe Photonics Professional GT2 printer

is capable of 400nm XY resolution, and 1-micron vertical resolution. The combination of two-

photon polymerization with additive manufacturing allows for high-speed 3D Microfabrication

and sub-micrometer precision. See the full technical details in Fig. 18.

TECHNICAL SPECIFICATIONS

Printing technology	Layer-by-layer Two-Photon Polymerization
Minimum XY feature size	160 nm typical; 200 nm specified*
Finest XY resolution	400 nm typical; 500 nm specified*
Finest vertical resolution	1,000 nm typical; 1,500 nm specified*
Layer distance	0.3−5.0 μm*
Maximum object height	8 mm*
Build volume	100 x 100 x 8 mm³*
Minimum surface roughness R_a	≤ 20 nm*
Max. scan speed	from 100 to 625 mm/s*

Values may vary depending on the Solution Set, objective or photoresin in use

Figure 18: Nanoscribe Photonic Professional GT2 technical specifications [60].

The print job allows for different printing modes, called Dynamic Precision Printing

(DPP) modes. These modes are designed to optimize balance between precision and speed

depending on the needs of the application. The solid mode, the base mode, is the highest

precision mode with the slowest print time. The shell/scaffold mode creates inner support

structures instead of printing at full volume to maintain same shape accuracy and increase print

speed by a factor of five. This can be useful if the internal structure of the print is not important

for the application. The pure shell mode increases the print speed 7x but has no internal structure at all. The swift mode prints 10 times faster than the solid mode and is the fastest print mode of all the structures. However, its precision is the lowest out of the five. Lastly, the balanced swift mode prints at 6x the speed of the solid mode with higher precision than the swift mode. Fig. 19 shows the different DPP modes on a precision vs speed scale.
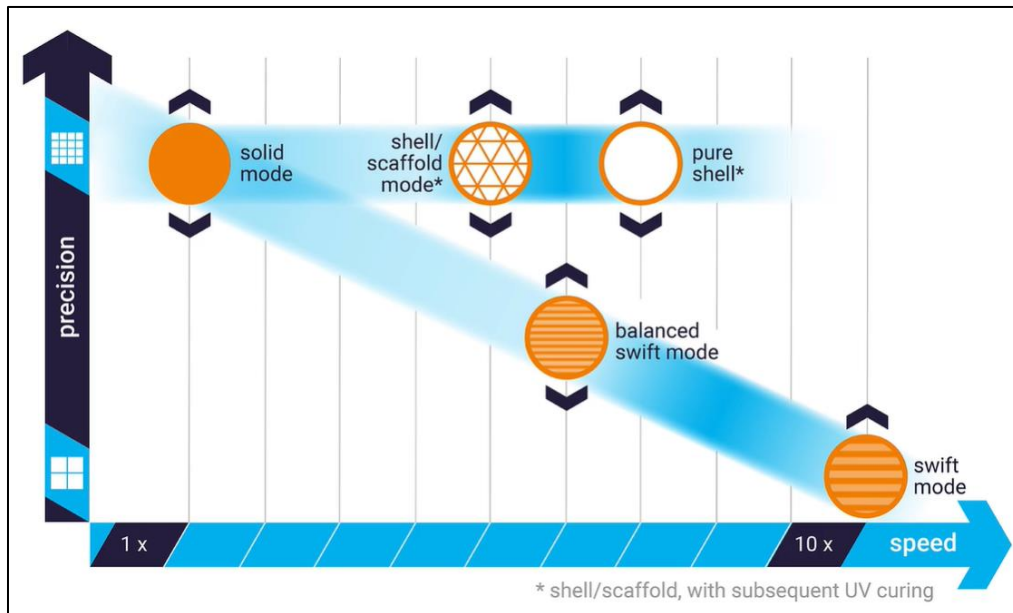
Figure 19: Dynamic Precision Printing modes [58]. These odes are designed to optimize balance between precision and speed depending on the needs of the application.

2.7.2.2 DeScribe

DeScribe is Nanoscribe's proprietary print job development software for Nanoscribe Photonics Professional systems. It imports 3D STL (CAD) files and generates print jobs for Nanoscribe printers. The streamlined import wizard takes the 3D CAD model and prepares it for printing. Some benefits of the software are the intuitive workflow, a balance between detail controllability through the IDE and simplicity of ready to use preset parameters, and the ability to use different Dynamic Precision Printing modes for optimizing precision and speed (see Fig. 20).

Key feature	Benefits
3D CAD model import wizard	Intuitive workflow generates suitable print job files from standard STL files
Printing modes with field-proven print parameter presets	Ready-to-use preset parameters to achieve optimal printing results right out of the box
Dynamic Precision Printing modes	Find optimized balance between precision and speed
Adaptive slicing	For improving shape accuracy
Parameter sweep	Find perfectly matching print parameter for new materials and applications easily
Integrated Development Environment (IDE)	Experts can generate and modify print files (GWL) for customized and really advanced print tasks
3D preview and printing simulation	What you see is what you print! DeScribe displays parameters such as print time, scan speed or laser power and simulates the whole printing process in detail

Figure 20: DeScribe features and benefits [58].

The workflow of a print job is the following. The 3D CAD model is imported into DeScribe

software and the user selects the applicable parameters (slicing distance, hatching distance, print

mode, etc) and output the print job file. From there, the print job is loaded to the NanoWrite, the

printer's user interface, and the NanoWrite executes the job maintaining all the parameters the

user selected throughout the print. The live camera allows the user to monitor the print process in

real-time. The simple workflow process is described in Fig. 21.
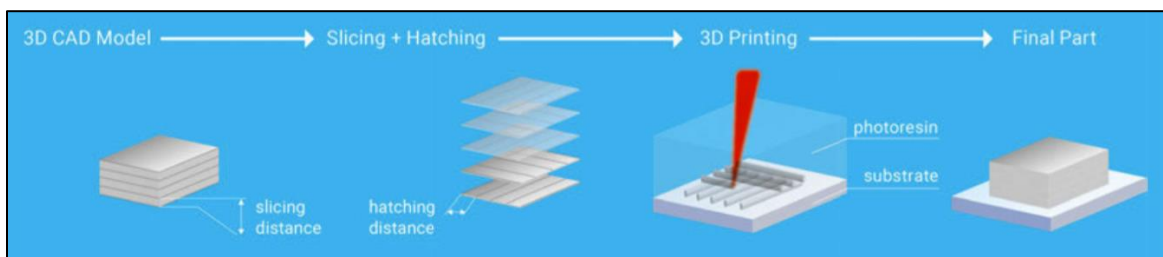
Figure 21: Nanoscribe printing workflow [60]. A 3D CAD model can be imported into the DeScribe to be processed into a print job file. From there, the print job is loaded onto the printer user interface.

The interface for DeScribe is intuitive. Once the 3D CAD model is imported, the

DeScribe graphical user interface displays a high-quality rendition of the model and displays

what the print will look like according the parameters that the user selects. Once the print job is

created, the user can view the 3D Preview of the print job that simulates the actual print. The

preview also allows the user to estimate how long the print will take to finish. See Fig. 22 to see

an example of this 3D Preview.
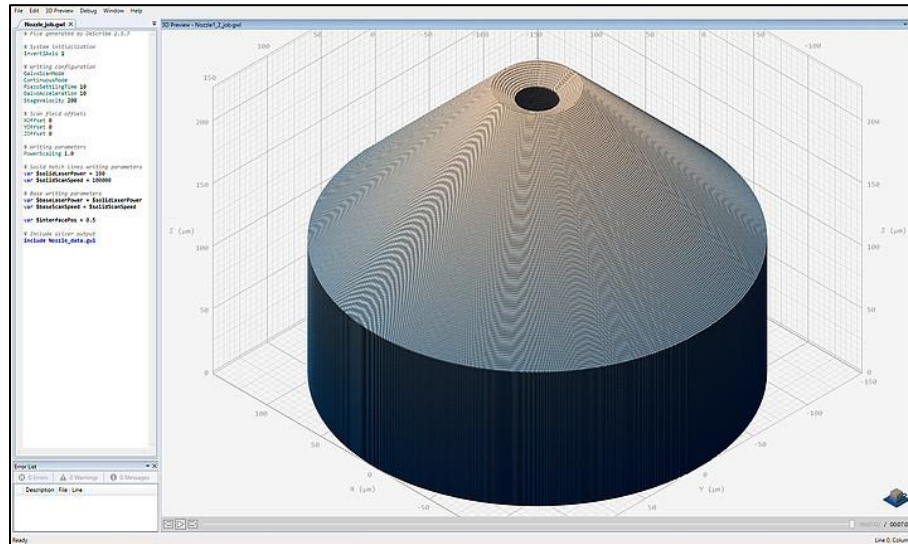
Figure 22: 3D Preview of the finished print job in DeScribe [58]

2.7.3 Probe Station

Probe stations are used to characterize and test devices, usually with external stimulus of

electrical, optical, or RF. The probe station is used to position the device being tested and other

equipment required for the analysis. Probing is used often in semiconductor failure analysis to

improve quality and it is used for characterization of integrated circuits for engineers. Optical

probe stations work in similar ways for photonic integrated circuits. The MD-100 Optical Probe

Station by Maple Leaf Photonics is a multi-die probe station that is capable of characterizing

multiple dies in a single test run with automatic optical alignment [61] (see Fig. 23). Its fotonica

software suite provides specialized alignment routines, instrument controls and test routines,

while providing intuitive control of motion. The probe station features automatic optical

alignment, application specific aligners driven by motorized stages, and multi-vendor instrument

support that allows users to use existing equipment in conjunction with the station. The MD-100 is also capable of multi-die handling for chips ranging in size from $1 \times 3 \ mm^2$ to $5 \times 8 \ mm^2$ in addition to the $25 \times 25 \ mm^2$ single die mount.
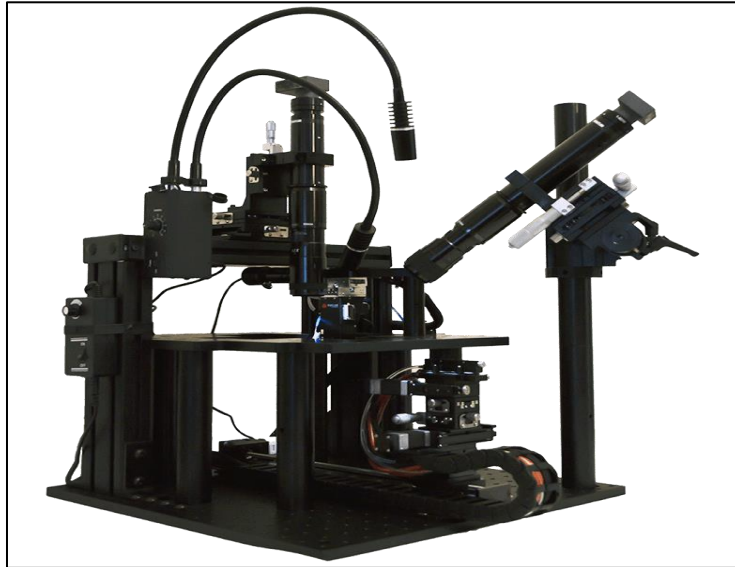
Figure 23: Maple Leaf Photonics Multi-Die Probe Station [62]. A probe station assists in testing and characterization of photonic integrated circuit.

The fotonica software suite provides a GUI that connects instruments, registers the chip selects devices, executes complex tests, and log results. Fig. 24 shows the user interface for the sensor instrument control, which allows the user to control the laser and detector. The script interface gives the user more control, and alternatively, the fotonica API allows integration into existing environments. Fotonica provides the necessary motion control, routines, and instrument settings that are needed for automated testing. The routines could involve wavelength sweeps, fiber alignments, etc. The first light and Fiber Alignment Algorithms allows the software to get first light quickly and allows the user to quickly set up a coordinate system. The automated testing feature gives users the ability to test hundreds of devices in a single run or run a parametric test.

34
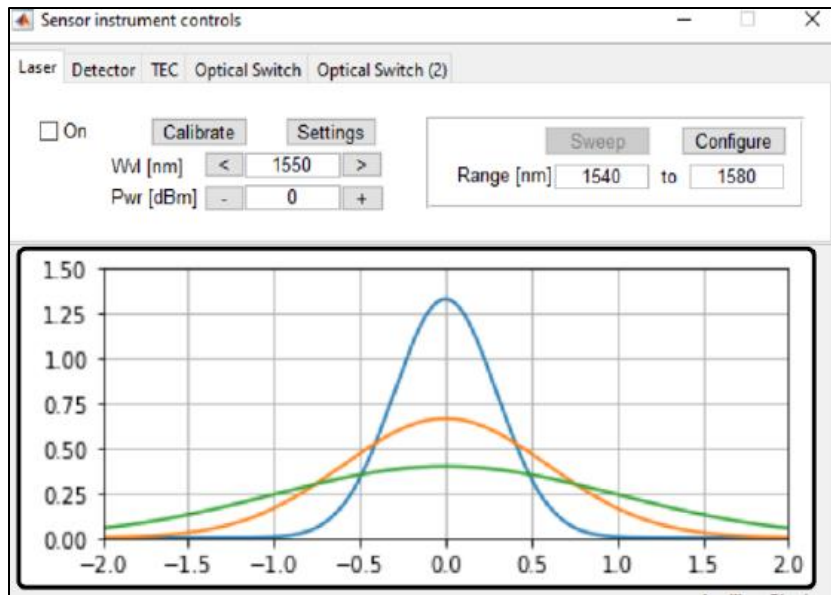
*Figure 24: Sensor instrument controls on Maple Leaf's fotonica software [61]. This
interface allows the user to control to laser and detector.*

2.7.3.1 Laser and Power Meter

The probe station uses the laser as a light source when testing photonic devices. For this

project, we used the Keysight 8164B Lightwave Measurement System (see Fig. 25). The

Keysight 8164B mainframe is a basis platform for optical component tests that hosts a tunable

laser source [63, 64]. The device we had at the facility had a range of $1450\ nm - 1650\ nm$.

*Figure 25: Our Keysight 8164B lightwave measurement system holds a laser
source with a range of 1450 nm – 1650 nm [64].*

Often for optical component tests, a power meter is used in addition to the laser source to measure power changes across a component. The Keysight n7744a optical multiport power meter is a 4 channel power meter with 1 μs minimum average time and 1250 nm - 1650 nm wavelength range [65, 66] (see Fig. 26). The power uncertainty is ±2.5% and it has a low polarization dependence $< \pm 0.01$ dB

Figure 26: Keysight N7744A optical multiport power meter with the range 1250 nm -1650 nm [66]. This is used to measure transmitted power.

The ThorLabs PM100D is also a power meter console that reads power measurements independent of beam shape, beam uniformity, divergence angle, or entrance angle (see Fig. 27). This is a useful tool for working with fiber sources and off-axis free space sources without connectors.

Figure 27: ThorLabs PM100D compact power and energy meter console [67]. This is used to obtain power measurements through optical fiber when a connector is not available.

2.7.4 Microscope and Optical Profilometer

Microscopes and optical profilometers are often used in realms of photonics due to its small nature. Profilometry is a technique used to read topographical data from a surface. Optical profilometers are a non-contact (probe less) method of profiling a surface. Modern microscopes have become digitized and more complex and many functionalities that were not available in the past. The Keyence VHX-7000 is the world's first 4K ultra high accuracy microscope that view, capture, and measure in an all in one system [68, 69] (see Fig. 28). The microscope delivers images with a fully automated digital microscope system that offers a depth of field that is 20 times greater than a conventional optical microscope and provides the user with the ability to easily perform 2D and 3D measurements. Examples include roughness, contamination, grain size, and other measurements. Its Optical Shadow Effect Mode combines high resolution lenses, a 4K CMOS, and high-performance lighting to provide the user with minute surface details for analysis. The magnification ranges from 20x to 6000x.

Figure 28: The Keyence VHX is the world's first 4K ultra high accuracy microscope that view, capture, and measure in an all in one system [68].

2.8 Stakeholders and Beneficiaries

The stakeholders of this project are:

- Photonics-Industry

- LEAP facility

- Future MQP Research Teams

Traditionally, businesses and research teams start with the product or development and work on making whatever it is that they produced fit into the existing system by marketing and advertising. While this works, it is not the most efficient way to deliver value. In business, it is much more difficult to force a product onto the market than it is to develop something that the market wants. In research, it is much more beneficial to research topics that will provide the most value than it is to work on an obscure topic with not much benefit to anyone. This is not to say that the traditional method isn't useful. In fact, some of the most incredible breakthroughs

happen by mistake and without grand planning and people generally find a use for almost anything. However, more often than not, it's more efficient to start with finding value needs. The value delivery system [70] focuses on starting with an analysis into the needs of the market, choosing the value, providing the value, then communicating the value to the world. Refer to Fig. 29 for a comparison of the value delivery system vs. the traditional model.
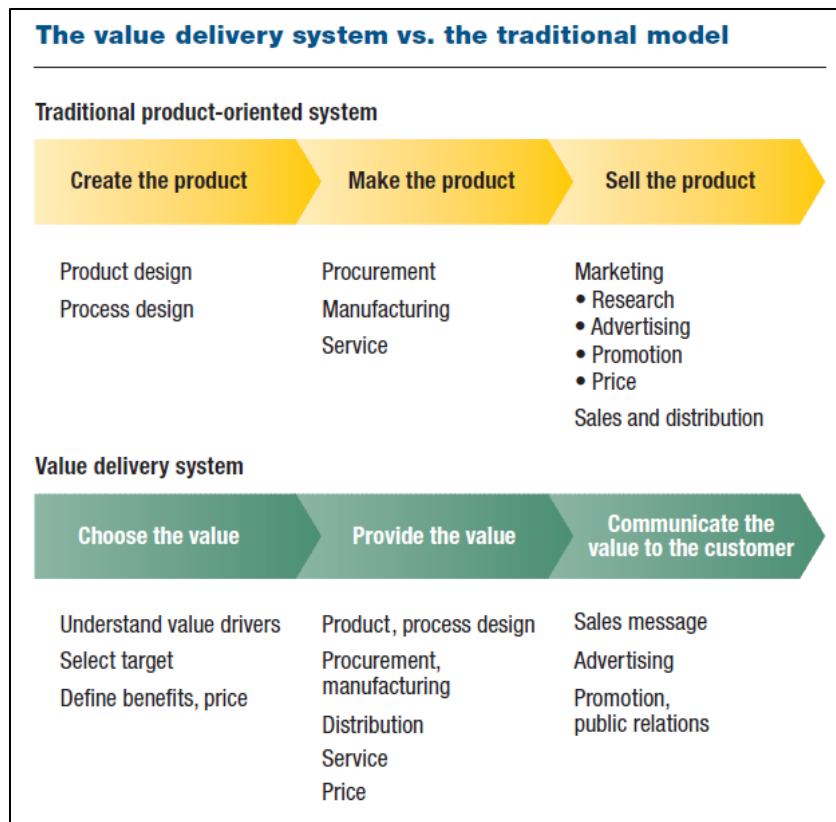
Figure 29: Value delivery system vs. the traditional model [70]. The value delivery system emphasizes starting by choosing the value rather than the traditional product-oriented system which creates the product first. The value delivery system is a more efficient way to deliver value to the stakeholders.

In this section we look at the variety of stakeholders of this project and analyze the potential impacts of this project on them. This analysis informed the project strategy.

2.8.1 Photonics Industry

The photonics industry developed after the development of the laser in the 1960s. With the first widely commercialized lasers entering the market, their primary use was in high cost applications like advanced research and cutting edge medicine [8]. Some applications include DNA sequencing, semiconductor manufacturing, surgery, and many other research applications. Since then, the market has slowly grown but innovation has been stagnant. As the core technology advanced, low-cost products entered the market and average sales price for high volume end products felt the squeeze. With recent developments on integrated optics and demand for more sophisticated optical devices, the laser market could return to high growth and innovation.

Since the 1990s, laser technology moved from laboratory to commercial sphere, raising the laser market to a valuation of $17 billion in 2020. While this is a good sign for the market, there are some worrying signs. For example, Fig. 30 shows the drop in the number of new laser related patents since 2011. From the 1960s through the 2000s, the number of new patents in this area doubled each decade. The years from 2011-2020 show a massive deviation from this trend with a drop in about 5000 patents compared to the previous decade. It's possible that this is due to the Telecoms crash in the early 2000s. In addition to the drop in patent applications, the focus of technology is changing for fiber, diode, solid state, carbon dioxide, excimer, and quantum cascade lasers. Fiber lasers account for more than 45% of all patents. Its ability to focus the beam down to the micro level and generate more power in a smaller than the CO_2 makes it attractive for metal and welding applications in addition to precision medical applications such as dermatology. Quantum cascade lasers have opened new opportunities in communications and industrial process monitoring due to its efficiency and wavelength. It has seen more rapid growth

than fiber in recent years. Part of the reason why laser patents are declining is that research and development in lasers can be very expensive and once a solid solution is found, companies are hesitant to spend more for continued innovation in the sector.
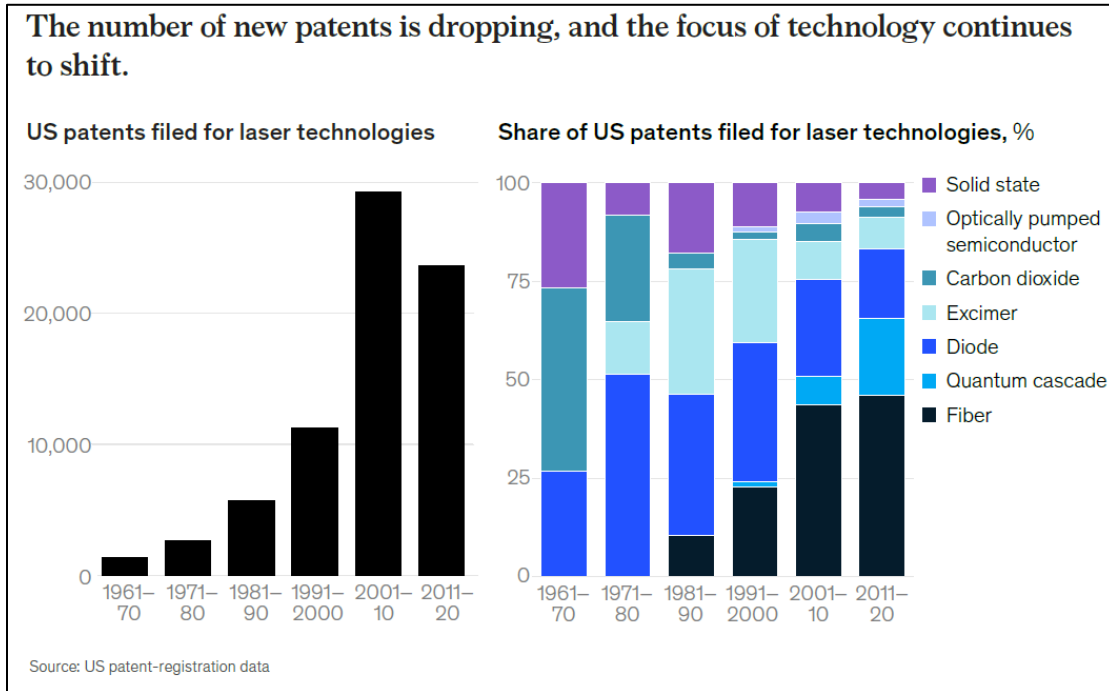
Figure 30: US laser patents filed by decade since 1961 [8]

Even with lower applications for laser technologies, the laser device market is expected to grow 10 percent annually through 2025, a very strong growth potential that will reach a market value of nearly $28 billion by 2025 (see Fig. 31). The aerospace and defense sector is expected to have the highest growth of 24% per year due to increasing need for high performance sensing and tracking. Industries with the highest growth are those where lasers are combined with other advancing technologies. These include optics and photonic sensors, whose combination can enhance the performance of lasers. The integration of optic, laser, and sensor technologies show exceptional promise in future applications.
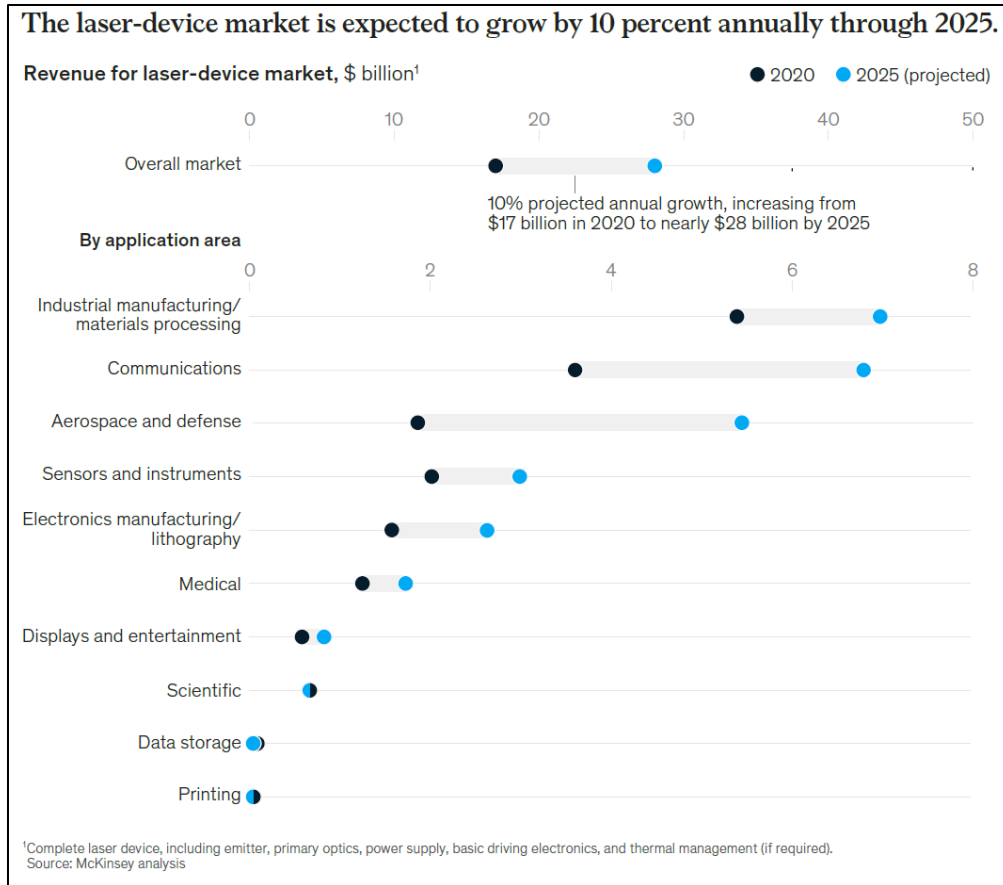
Figure 31: Projected revenues for the laser device market [8]

The optics market includes components such as filters, lenses, selective mirrors, beam splitters, prisms, and adaptive optics. Precision optics, making up nearly two-thirds of the overall optics market with a value of $20 billion, is expected to grow at 8% annually through 2025 (see Fig. 32). This will be driven mostly by consumer applications such as LiDAR, biosensing and security. Additionally, the automotive, space, and semiconductor sectors will provide strong revenue.

Most segments of precision optics are growing significantly.

Revenue for optical components by type in 2020, %

Total: $33 billion

Precision optics[1]	Standard optics and optical components	
62	36	2

Silicon photonics

Revenue for precision optics, $ billion   ● 2020   ● 2025 (projected)

Overall market

8% projected annual growth, increasing from $20 billion in 2020 to nearly $28 billion by 2025

By application area

Consumer
Aerospace and defense
Semiconductor
Automotive
Bio-instrumentation
Medical
Industrial

[1]Precision optics is defined by tighter manufacturing tolerances (eg, thickness, diameter, centering, curvature, surface, and coating uniformity) 2–10x higher than those of standard optics, at a minimum.
Source: McKinsey analysis

Figure 32: Projected revenues for the precision optics market [8]

The photonic sensor market is a $29 billion market, 16% of the $180 billion general sensor market. The photonic sensor market is expected to see 9 percent growth annually through 2025, amounting to $44 billion in revenues in 2025 (see Fig. 33). The automotive application of the photonic sensor market is expected to grow by 21 percent a year due to increased interest in autonomous driving systems that require high precision sensors. Infrastructure applications will see a demand rise by about 14% as building measurement technology advances. The energy sector has potential to grow by 15 percent a year with a changing landscape of the energy sector and the incorporation of fiber optic sensor technology for monitoring and measuring. Aerospace and defense sector is expected to see 8 percent growth as automated applications and other remote sensing tools increase demand.

Photonic sensors are expected to experience 9 percent annual growth through 2025.

Revenue for the photonic-sensor market, $ billion   ● 2020   ● 2025 (projected)

Overall market

9% projected annual growth, increasing from
$29 billion in 2020 to $44 billion by 2025

By application area

Consumer
Automotive
Industrial
Healthcare
Medical/pharmaceuticals
Aerospace and defense
Energy
Infrastructure

Source: McKinsey analysis

Figure 33: Projected revenues for the photonic-sensor market [8]

The laser device industry is currently fragmented, with many smaller companies specializing in small segments of technology. Thus, there are many opportunities for synergistic combinations. As lasers, sensors, and optics continue to become integrated, it becomes imperative that stakeholders position themselves for the disruption on the value chain. Photonics is a high-tech sector and requires constant innovation to survive. Development of laser technology is slowing down. However, new devices that integrate lasers, sensors, and optics onto a smaller package is a new area of opportunity. By providing a way to rapidly prototype photonic devices at a facility that is a part of a larger photonics development network (LEAP), we help advance the integration of photonics.

2.8.2 LEAP facility and WPI (MQP)

The Lab for Education & Application Prototypes (LEAP @ WPI/QCC) is a collaboration between WPI and QCC, located at WPI's Gateway Park. The goal of the LEAP facility in Worcester in to collaborate with industry affiliates and advance the growing field of integrated photonics [71]. Designed to be the intersection of industry, government, and academia, LEAP promises collaboration without barriers to develop technology for mass production. The laboratory was built by joint efforts from WPI and Quinsigamond Community College (QCC) as part of the national American Institute for Manufacturing Integrated Photonics (AIM Photonics) and funded through the Massachusetts Manufacturing Innovation Initiative (M2I2). The facility contains state of the art equipment to develop photonic integrated devices and support the integrated photonics manufacturing sector in central Massachusetts. The LEAP Network, consisting of organizations and government entities at the community, state, and national level is illustrated in Fig. 34.

The LEAP facility in Worcester has a highly flexible membership model that allows all types of organizations ranging from startups to large corporations to incorporate integrated photonics into their business. With state-of-the-art equipment and strong network, the facility is well positioned to be a hub for innovation in the photonics sector. Beyond the industry, the LEAP facility benefits the students at WPI, who will have the opportunity to gain experience with cutting edge technology while contributing to variety of ongoing research.
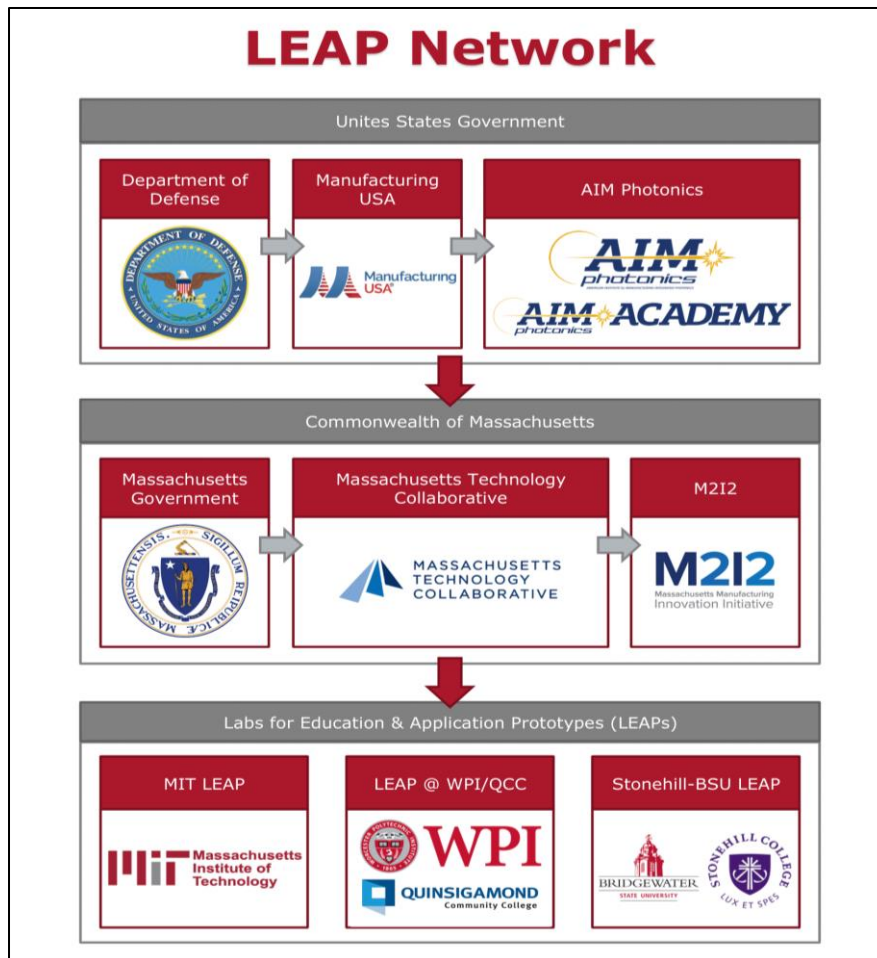
Figure 34: LEAP Network [71]

The Major Qualifying Project (MQP) is a critical part of WPI's unique signature education. The WPI Plan, implemented in 1970 as a bold experiment, sets its graduates apart in the world with its emphasis on project-based learning and real-world problem-solving experiences (see Fig. 35). The equivalent of a traditional senior capstone project, the MQP is a team-based, professional level design or research experience that answers the question, "once you graduate, what will you be able to DO?" [72]. As the final part of WPI's project-based education, the MQP is the final test that pushes students to put theory into practice by tackling a real-life situation.

The Elements of the WPI Plan

The pioneering elements of a WPI education set the footing for a personal journey—yours. Here you'll be encouraged to chart your own path and do things you've only imagined.

PURSUE YOUR PASSION

LEARN HOW TO LEARN

PROJECT-BASED LEARNING

GLOBAL IMMERSION

BEYOND THE CLASSROOM

PERSONAL IMPACT

Figure 35: The Elements of the WPI Plan [73]

This project is one of the first to make use of the new LEAP facility's research equipment. Thus, this paper sets a baseline for which future projects can refer to as a reference point when attempting to tackle a similar problem.

Chapter 3: Project Strategy

The goal of this project was to showcase the capabilities of the new photonics laboratory at WPI and set a foundation for future projects at the laboratory. The following objectives guided the project:

Objective 1: To develop basic waveguides using two-photon polymerization;

Objective 2: To provide recommendations for similar future projects at WPI.

The objectives and methods used to complete this project are illustrated below in Fig. 36.
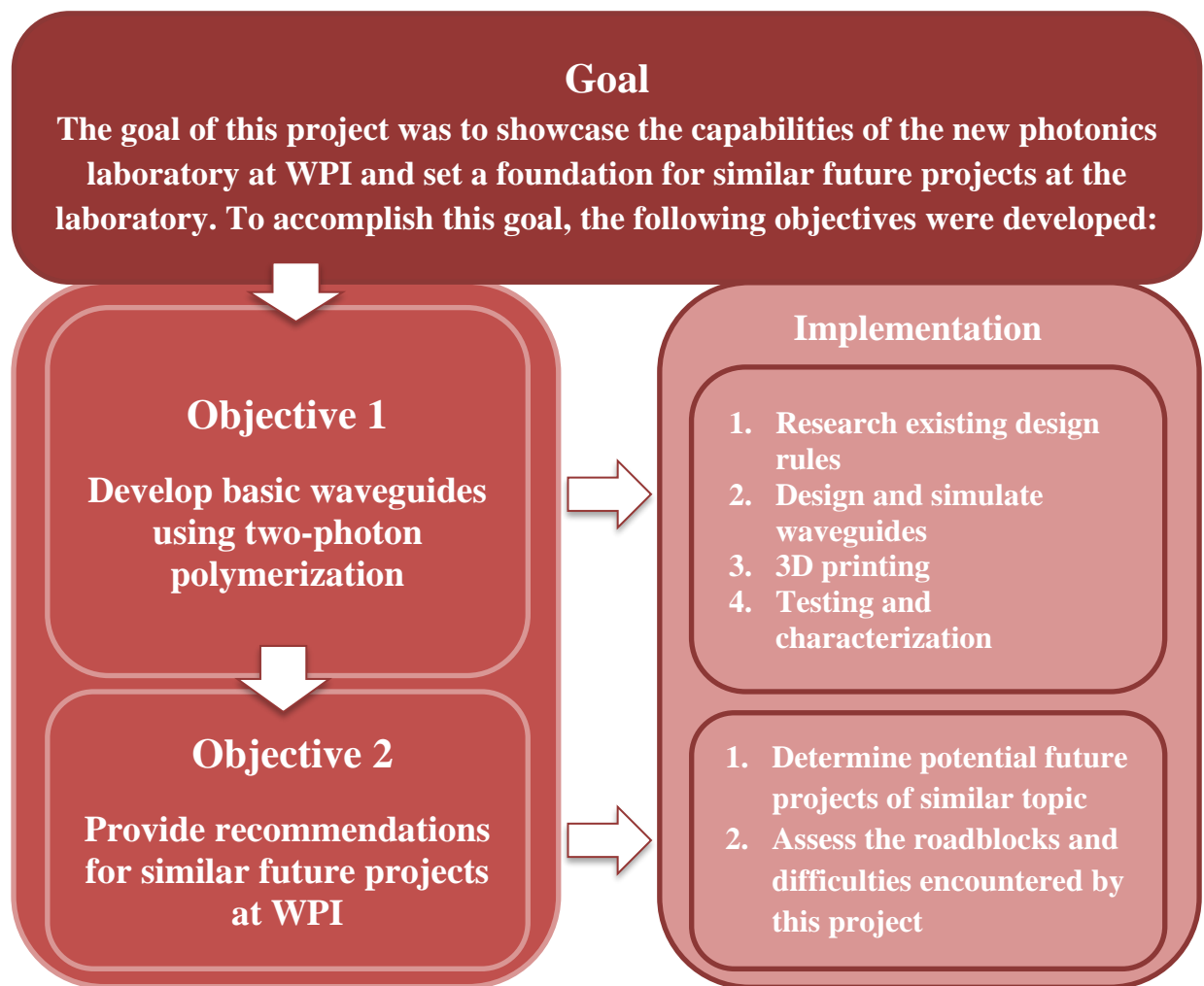
Figure 36: Project Strategy Overview

The following sections lay out the methods that were used to complete these objectives.

3.1 Objective 1: Develop Basic waveguides using 2PP

In order to showcase the capabilities of the new photonics laboratory at WPI, it was essential that a photonic building block component was produced and tested in the facility. Thus, the first objective of this project was to develop basic waveguides in the laboratory using two-photon polymerization rapid prototyping capabilities. To achieve this objective, we first researched existing design rules that could guide this project and provide direction. Then, using the research, we designed and simulated a set of waveguides in COMSOl. Next, using the Nanoscribe Photonic Professional GT+, we printed the waveguide design. Lastly, to test the quality of the waveguides printed and further illustrate the capabilities of the laboratory, we tested and characterized the waveguides using a variety of equipment available.

3.2 Objective 2: Provide Recommendations for future projects

Ultimately, the aim of this project was to provide a foundation for similar future projects at WPI. By microfabricating a set of waveguides, we gave a physical and tangible foundation for other projects to build upon. Beyond the physical deliverable, the background review, research of design rules, and the development process inspired some exciting future potential projects and informed us of numerous improvements to our approach. Using this experience, we propose some potential future projects of similar topic and provide recommendations on things to consider when attempting to tackle a project such as this one.

The timeline for this project was 25 August 2021 through 28 April 2022.

Chapter 4: Results & Analysis

This chapter presents the results and analysis of this project. This chapter covers the results and analysis that were obtained while completing Objective 1, which was to develop basic waveguides using two-photon polymerization. The following results led to the completion of Objective 2, which will be covered in the next chapter.

4.1 Existing Design Rules/Requirements

Design rules are a set of guidelines that assist a developer fabricate the intended product. When it comes to printing waveguides using two photon polymerization, established design rules don't exist due to its relatively recent emergence. Several attempts to develop design rules and 3D print using 2PP have been made [51, 74, 75] with general positive results. There were several things we considered as we worked through the design process. These included the refractive index of the resin and substrate used by the Nanoscribe printer, coupling/fiber alignment challenges, and printing parameters.

To simulate the the waveguides, it was necessary to understand the refractive index of the materials in question. This required us to first make a decision on the printing parameters. Nanoscribe provides a set of standard printing parameters called process recipes. These recipes differ in print time, resolution, and applications. For micro-optics and photonic applications, process recipes using the photoresist resins IP-DIP and IP-S are the best to use. See Fig. 37 for resin and process recipe information. Refer to Appendix A for more data on both photopolymers.

	Properties	Application areas	Key Features
IP-Q	High-speed fabrication of mesoscale structures with print volumes > 10 mm³, designed for Dip-in Laser Lithography (DiLL)	‣ 3D Microfabrication on the mesoscale ‣ Biomedical engineering ‣ Mechanical components	‣ Refractive index matched material for Nanoscribe's large features set
IP-S	Smooth surfaces for micro- and meso-scale fabrication with smooth surfaces and shape accuracy in optical quality, designed for Dip-in Laser Lithography (DiLL)	‣ 3D Microfabrication on the mesoscale ‣ Microoptics ‣ Integrated photonics ‣ Microfluidics	‣ Refractive index matched material for Nanoscribe's medium features set ‣ Biocompatible
IP-Dip	Finest submicron features and high aspect ratio structures, designed for Dip-in Laser Lithography (DiLL)	‣ 3D Microfabrication on the submicron scale ‣ Microoptics ‣ Micromechanics & MEMS ‣ Integrated photonics	‣ Refractive index matched material for Nanoscribe's small features set ‣ Biocompatible
IP-L	Finest submicron features and low shrinkage, designed for oil immersion configuration	‣ 3D Microfabrication on the submicron scale ‣ Material engineering ‣ Integrated photonics	‣ Refractive index matched material for Nanoscribe's small features set ‣ Biocompatible

Recipe	Solution Set	Application examples	Print time per mm³	Availability
Process recipes for Microfabrication Solution Sets				
IP-Dip 63x Fused Silica (3D SF)	3D SF	photonic meta-materials, rheology microfilters	~25 days/mm³ (estimated)	
IP-Dip 63x Fused Silica Swift (3D SF)			10 h/mm³	
IP-S 25x ITO Solid (3D MF)	3D MF	microoptics, microfluidics	10 h/mm³	integrated in DeScribe
IP-S 25x ITO Shell (3D MF)			2.5 h/mm³	
IP-S 25x ITO balanced Swift (3D MF)			1.7 h/mm³	
IP-S 25x ITO Swift (3D MF)			1 h/mm³	
IP-Q 10x Silicon Solid (3D LF)	3D LF	Microtools (tweezers, clamps), microfluidic chips, molds for electroplating, MEMS	0.6 h/mm³	
IP-Q 10x Silicon Shell (3D LF)			0.2 h/mm³	
IP-Q 10x Silicon Swift (3D LF)			~0.1 h/mm³	

Figure 37: Overview of Nanoscribe resins available shown on top [76]. An overview of Nanoscribe process recipes is shown on the bottom [77]. Each process recipe has a specific resin it must use and has different print times and resolutions.

Each process recipe uses a solution set that defines the objective, resin, substrate, substrate holder, and other materials needed to use the recipe. Many applications of the Nanoscribe Photonic Professional GT+ in the photonic field have used IP-Dip because of its higher resolution [51, 74, 75]. However, the print time per mm^3 for the IP-Dip 63x Fused Silica recipe is around 60 times that of the IP-S 25x ITO Solid recipe (see Fig. 38). Recognizing the reality of

potential errors and missteps in the first few prints as a first of its kind at the new laboratory, we

decided to use the the IP-S 25x ITO Solid process recipe for our prints to reduce time lost in case

of failures and to test the IP-S as a viable resin for a waveguide. The solution set that

supplements the recipe is the 3D medium feature (MF) solution set. The 3D MF includes the 25x

NA 0.8 objective lens, IP-S resin, ITO-coated substrate, multi-Dip-in Laser Lithography (DiLL)

substrate holder. See Fig. 38 for an overview of the MF solution set and the ITO coated

substrate. When printing with the ITO-coated substrate, it's important to use an ohmmeter to test

for the ITO coated side, which will have resistance and will be the side the printer will print on.

Material	Description	Comment
Objective	25x NA 0.8	scan mode: galvo/piezo
		working distance: 380 µm
		printing field (Ø): 400 µm
		adjustment ring set on 'Glyc'
2PP resins	IP-S	1.478 @ 780 nm, 20°C
Substrate	ITO-coated substrate (3D MF DiLL)	dimensions: 25 × 25 × 0.7 mm^3
		1.624 @ 780 nm ITO; coated side facing objective
Substrate holder	multi-DiLL	
Recipes	IP-S 25x ITO Solid (3D MF)	hatching distance: 0.5 µm
	IP-S 25x ITO Shell (3D MF)	slicing distance: 1 µm
Other material	felt ring	30 mm or 32 mm inner diameter (depending on objective version)

Property	Value	Comments
Material	soda lime glass	
Refractive index	• 1.624 @ 780 nm ITO • 1.518 @ 780 nm soda lime	
Dimension	25 mm x 25 mm x 0.7 mm	
Thickness variation	± 60 µm	
Surface finish	polished on both sides	
Coating	indium-tin oxide (ITO)	
ITO film thickness	18 nm ± 5 nm	
ITO surface resistance	100 - 300 Ω	
Transmittance	≥89%	

Figure 38: 3D MF Solution Set (shown on top) and ITO coated substrate (shown on bottom) [77]. The MF solution set is used by the IP-S 25x ITO Solid process recipe, a medium feature recipe.

The refractive index of the IP-S resin is outlined on the nanoscribe website for wavelengths between 405-950 nm (see Appendix A). For the waveguide, we wanted to use 1550 nm laser because it is the most common wavelength for optical fiber due to its low loss in optical fiber. To find the refractive index of IP-S at 1550 nm required us to look through the literature for experimental data on Nanoscribe resins. IP-Dip has a refractive index of around 1.53 at 1550 nm [78, 79]. The relationship of the refractive index and wavelength can be described by Cauchy's equation:

$$n(\lambda) = A + \frac{B}{\lambda^2} + \frac{C}{\lambda^4}.$$ *Equation 8*

The Cauchy parameters are shown in Fig. 39.

Cauchy parameters	A	B (μm^2)	C (μm^4)
Nanoscribe IP-S	1.4915	$4.8486 \cdot 10^{-3}$	$1.3694 \cdot 10^{-4}$
Nanoscribe IP-L	1.5003	$3.6771 \cdot 10^{-3}$	$3.5288 \cdot 10^{-4}$
Nanoscribe IP-G	1.5008	$4.3331 \cdot 10^{-3}$	$1.9364 \cdot 10^{-4}$
micro resist OrmoComp	1.5049	$5.5461 \cdot 10^{-3}$	$-3.3369 \cdot 10^{-5}$
Nanoscribe IP-Dip	1.5273	$6.5456 \cdot 10^{-3}$	$2.5345 \cdot 10^{-4}$

Figure 39: cauchy parameters from various photoresists [79]

Using this equation, IP-S has a refractive index of around 1.49 at 1550 nm.

Beyond the materials used and the printing parameters, it was clear that one of the challenges of this project would be coupling light from the fiber into the printed waveguide. The fiber we used is TPMJ-X-1550-8/125-0.4-10-2.5-14-1-AR fiber [80] (see Fig. 40). Since the stripped fiber diameter is at 125 μm, it was important that we make the structure tall enough such that the fiber could couple into the waveguides with no obstruction from the substrate. The core itself is 8 μm thick and the stripped length is 10 μm. Since the fiber is tapered, the spot diameter at the working distance of 14 ± 2 μm is 2.5 ± 0.5 μm.
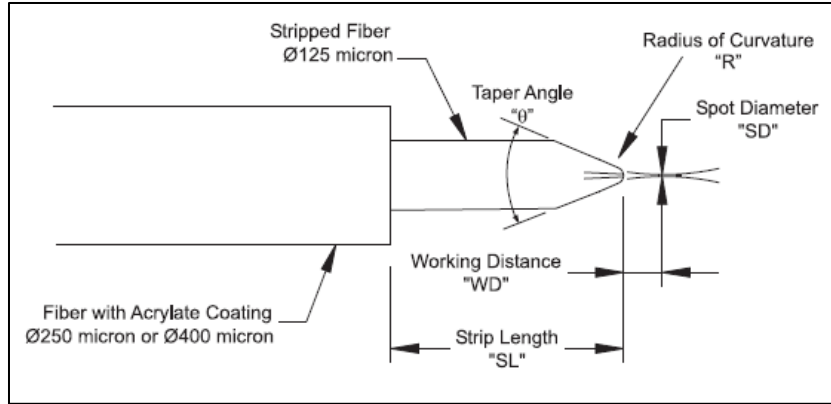
Figure 40: Tapered Lensed Fiber (End Detail of TPMJ-X-1550-8/125-0.4-10-2.5-14-1-AR fiber) [80].

During the research process, we discovered a paper published in the *Journal of Physics: Photonics* [51] that attempted a similar project based on the IP-Dip resin and the 63x objective lens. The paper describes a design that raises the waveguide onto a support such that the waveguide's center is positioned at a height of 62.5 μm to align with the center of the single mode fiber's core due to its 125 μm diameter. In addition to the support, the design includes a ridge that sits between the waveguide and the supporting structure that is narrow enough to not affect the waveguide's guiding properties. The simulations of these structures found that the best mode matching, thus best coupling for a square waveguide for IP-Dip to be a $14 \times 14 \ \mu m^2$ square waveguide (see Fig. 41).
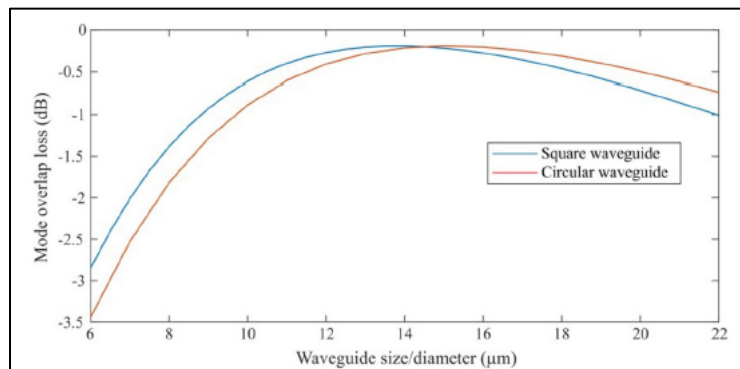
Figure 41: Simulation of mode overlap loss as a function of waveguide cross section dimension for IP-Dip [51].

To find the ideal dimensions for their ridge, the research team fixed the height of the ridge to 3 μm and simulated results for varying ridge width from 0 to 8 μm. The paper found that ridge width up to 4 μm has a negligible effect on the mode overlap loss (see Fig. 42).
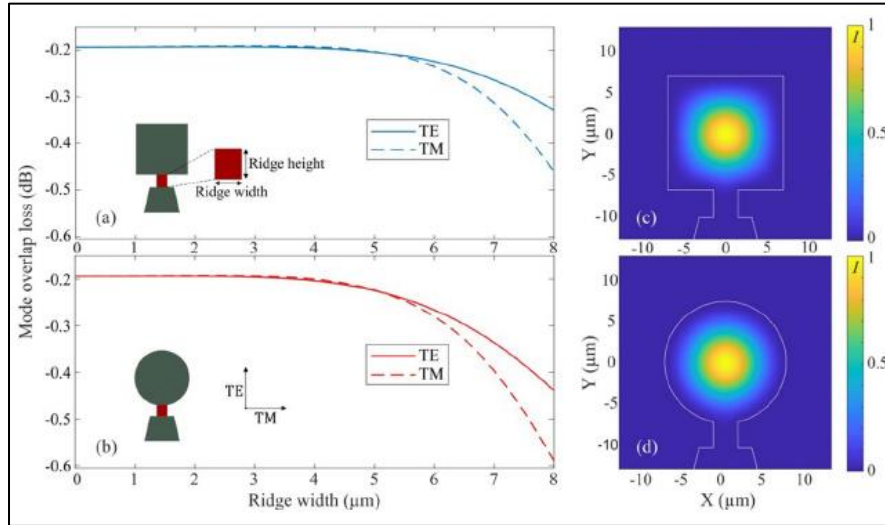
Figure 42: Simulation of mode overlap loss as a function of ridge width between waveguide and supporting structure for IP-Dip [51].

4.2 Designs, Simulations, & Prints

This section of the chapter contains the process taken to print the waveguides that were tested in the next section. The first part briefly describes the simulation process, the second part delves into the first two designs that failed, and the last part addresses the final design which was successful.

4.2.1 Simulation Settings

Because of the costs associated with microfabrication and to optimize time use during the project, we first used COMSOL to simulate our waveguides. To simulate waveguides in COMSOL, there were some properties of waveguides to consider:

1. Bounded fields

2. Known propagation directions

3. Length of waveguides are long compared with the wavelength.

The length of the waveguide relative to the wavelength greatly increases the amount of mesh during the simulation process, which can easily overload the memory. However, the Beam Envelope interface of the Wave Optics module reformulates the electromagnetic equations using the first two properties above and makes it easier to simulate waveguide systems [57]. To model the simulation, we did the following. In the Physics settings, we first determined the number of wave directions in our model, which in this case, was unidirectional. Then we defined the wave vector of the electromagnetic wave as *ewbe.beta_1*. This is a built-in variable in COMSOL that represents the propagation constant for wave 1 (1 in case of bidirectional models). COMSOL calculates the boundary mode transverse propagation constant first, then calculates *ewbe.beta_1*, the longitudinal propagation. Next, we defined the ports with the *Numerical Port Boundary* condition and allowed port excitation on the input port. Moving onto the Study settings, we added a *Boundary Mode Analysis* study step for each Port before adding the main step and configured them to search for modes around the core index. Lastly, we added the main study step, the *wavelength domain study* and set the wavelength to 1550 nm, our desired input wavelength.

4.2.2 Failed Designs

Design 1 (No Prints)

The project started out with designing and simulating waveguides using the information gathered in the previous section. The design process started with several parameters. First, the refractive indices of the ITO coated substrate, IP-S resin, and air were obtained. Then, for the

actual dimensions of the waveguides, we referred to the experiment done using IP-Dip described in the previous section. Because the difference between the refractive indices of the two polymers are low, we expected coupling effects to be similar. Therefore, we modeled a 14×14 μm^2 square waveguide on top of a $3 \times 3 \ \mu m^2$ ridge that sits upon a rectangular structure $14 \times 2.5 \ \mu m^2$ that is designed to raise the center of the waveguide to a height of 62.5 μm. When considering the constraints set for coupling, it's helpful to understand the room for error on the side of entrance angle of the light by calculating the acceptance angle of the waveguide, which is the maximum angle with the axis of the waveguide at which the light can enter for it to propagate through it. The acceptance angle can be calculated as follows:

The numerical aperture of an optical system is given by

$$NA = n \ sin\theta.$$

<div align="right">Equation 9</div>

For a multi-mode waveguide with a step-index profile, the numerical aperture is given as

$$NA = \sqrt{n_{core}^2 - n_{cladding}^2}.$$

<div align="right">Equation 10</div>

Then, rearranging the equation

$$Acceptance \ Angle = sin^{-1} \frac{NA}{n_{core}}.$$

<div align="right">Equation 11</div>

Using the refractive index of IP-S we calculated earlier (1.49), and the refractive index of air (1), the acceptance angle of our waveguide is 0.835 radians or 47.8 degrees. We felt that this was enough wiggle room for our coupling needs. The simulation for this design showed very good optical confinement for this design (see Fig. 43).
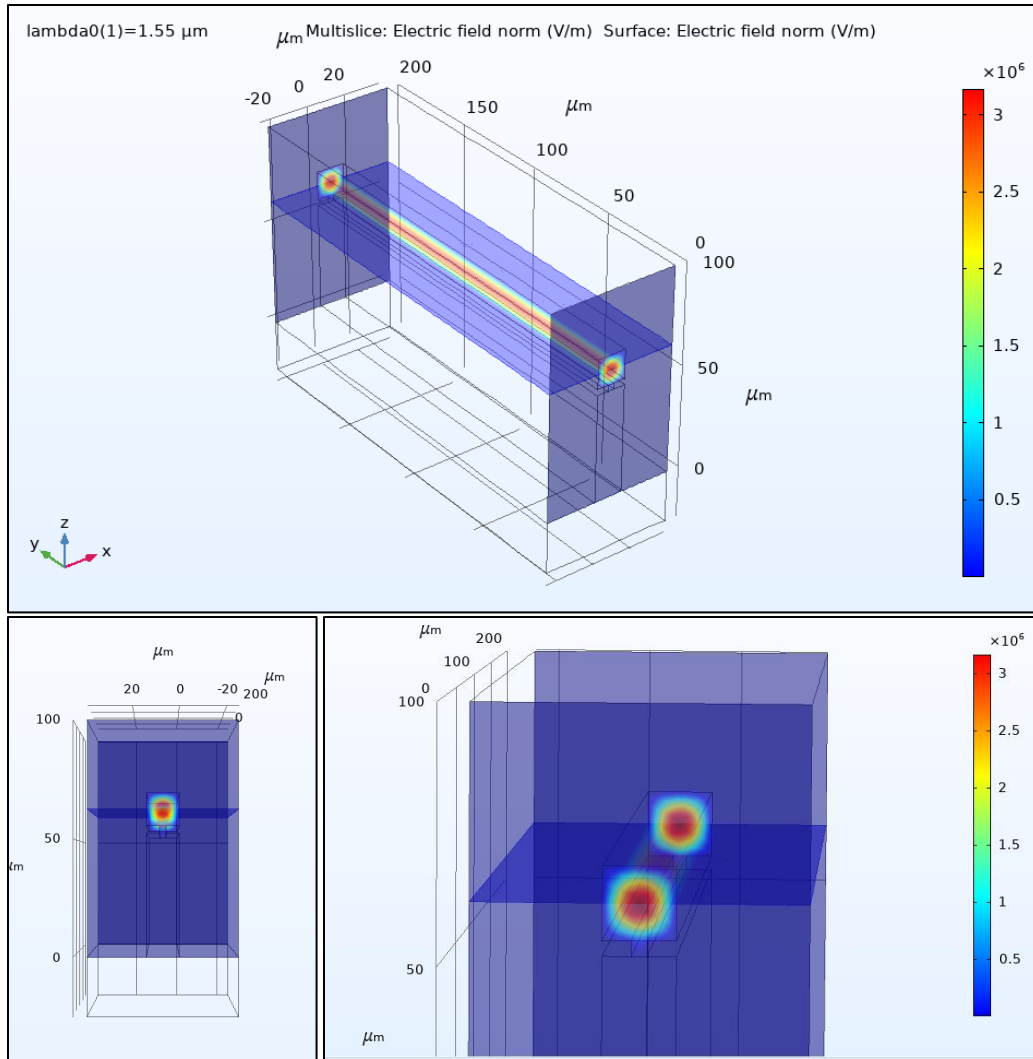
Figure 43: Waveguide simulations for Design 1 & 2. Note that the electric field is well confined in the waveguide. The waveguide cross section is a 14 x 14 µm² square and the waveguide is centered at 62.5 µm from the substrate. The cross-section dimensions for the ridge between the waveguide and pedestal is 3 x 3 µm².

In addition to the straight waveguide, we designed a waveguide with an S-bend that offset the waveguide axes with respect to each other. Our approach to designing this shape was based on two basic circular section curves. Other methods of creating S-bends exist, but we leave the exploration of the alternative shapes for future research.

Lastly, for absolute certainty that the light is being guided by the waveguide, two 90-degree curved waveguides were designed. Thus, for the first print design, there were five straight waveguides with the lengths ranging from 200 μm to 1 mm in 200 μm increments, two S-bend

waveguides, and two 90-degree curved waveguides (see Fig. 44). The cross section of all the structures were the same: $14 \times 14 \ \mu m^2$ square waveguide on top of a $3 \times 3 \ \mu m^2$ ridge on top of a $14 \times 52.5 \ \mu m^2$ pedestal.
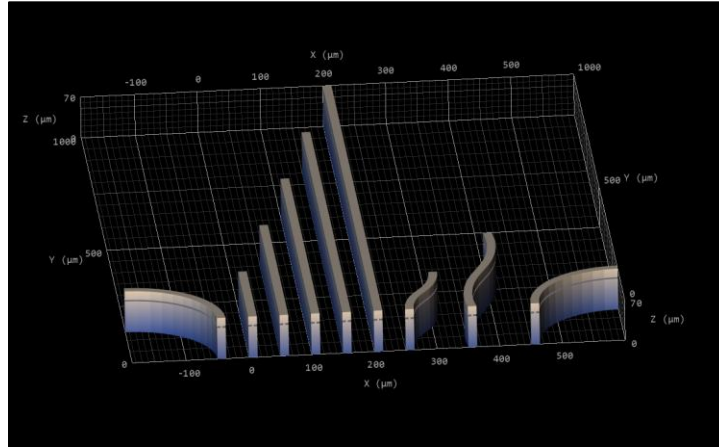
Figure 44: Design 1 model. There were 5 straight waveguides in this design of increasing length, two 90-degree curved waveguides, and two S-bend waveguides. Testing challenges of having the 90-degree waveguides led us to move to a newer design.

Before this print was loaded onto the Nanoscribe, we realized the 90-degree curved waveguides would increase testing time and create additional coupling challenges by forcing us to make modifications to our probe station during the testing. Coupling would be much easier to keep waveguide inputs and outputs on opposite sides of each other. Because of this realization, we decided to replace the 90-degree curved waveguides with additional S-bend waveguides.

Design 2 (Print 1&2)

For design 2, we maintained the cross section of the waveguides and the five straight waveguides with lengths ranging from 200 μm to 1 mm. The four S- bend waveguides, each with increasing curvature, replaced the previous S-bends and 90-degree bends (see Fig. 45).
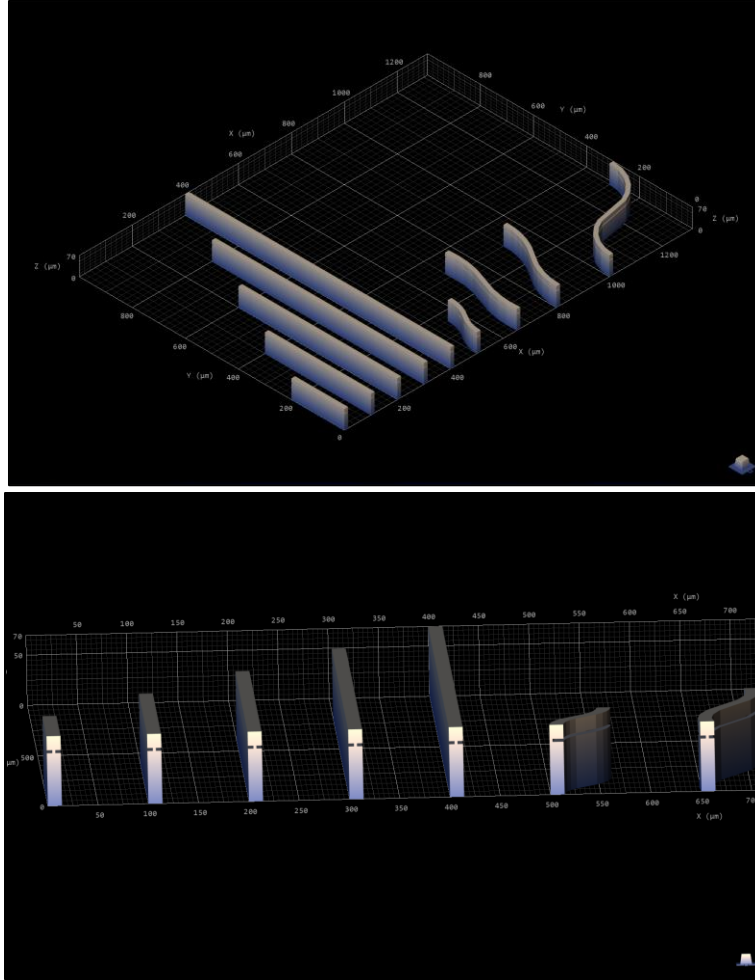
Figure 45: Design 2 model. In this design, we modified the 90-degree curved waveguides into S-bend waveguides, so in this design, we had 4 S-bend waveguides and 5 straight waveguides.

4.2.2.1 Print 1: Printed on March 30th, 2022

In an attempt to increase the precision of the prints, we reduced the typical slicing and hatching distances of 1 μm and 0.5 μm respectively by half. When printing with the Nanoscribe Photonic Professional, there are three positioning scanning modes in decreasing accuracy: PiezoScanMode, GalvoScanMode, and StageScanMode. The PiezoScanMode results in the highest resolution positioning accuracy in the range of 10 nm within a writing area of 300×300 μm^2. Our first design's dimensions were too large for this mode and the DeScribe software set the positioning mode to GalvoScanMode. GalvoScanMode's positioning accuracy and printing

field depends upon the objective in use. In the case of IP-S 25x ITO Solid recipe, the objective in use is the 25x NA0.8, which give a printing field of 400 μm in diameter or $285 \times 285 \ \mu m^2$ (see Fig. 46). We did not catch this limitation in time and proceeded to print the design without any block splitting and stitching parameters that would allow for stage movement.

Property	Value	Comments
Objective	25x NA0.8	see also objective overview
Immersion (DiLL) mode	yes	
Immersion media	oil/glycol/water/2PP resin	Most IP resins from Nanoscribe are safe to use with this objective
Working distance WD	380 µm	
Objective opening angle a	31°	
Objective lens diameter D	5.2 mm	
Felt ring size	30 mm / 32 mm	depending on objective version
Printing field (Galvo Ø)	400 µm	stage movement allows for a larger printing field
Theoretical lateral (a_{xy}) and axial resolution (a_z);[ref] [aspect ratio]	$a_{xy} = 595$ nm, $a_z = 3313$ nm; 5.6	for 780 nm laser wavelength, IP-S and 25°C; voxel size and line width depend on solution set and print parameters
Standard 2PP resin	IP-S	IP-Visio, IP-L, IP-n162 and IP-PDMS are also suitable
Solution set	3D MF	
Δn required @ 830nm	>0.1	
Typical slicing distance	1 µm	standard recipe for IP-S
Typical hatching distance	0.5 µm	
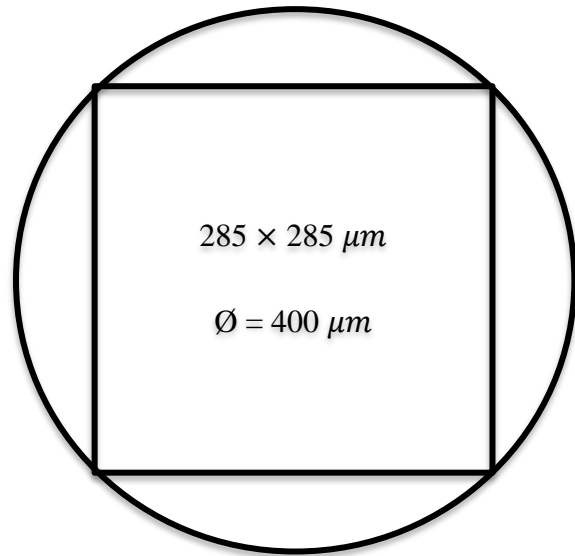
Figure 46: 25x NA0.8 Properties (shown on left) and its Galvo Writing Field (shown on right). The writing field is defined by the objective lens used and will limit the size of the structure that can be printed without stage movement. Stage movement is less precise and can cause discontinuous structures.

Thus, our first print attempt resulted in an incomplete print of waveguides.

4.2.2.2 Print 2: Printed on March 30th, 2022

For the second print, we modified the block splitting and stitching parameters such that the print would be split between several blocks within the galvo printing field and stitched together after all of the blocks were developed. After this modification, the print was successful in producing the complete structure. However, when we attempted to test the waveguides on the probe station, we realized that we didn't provide enough clearance for the optical fibers needed for testing. In a perfect situation, the design that we created would have worked with exact precision. What we didn't consider was the amount of room for error that would be required due to several factors.

4.2.3 Design 3 (Print 3)

The goals for this design and print were the following:

1. Increase the height of the ridge,

2. Provide more height clearance for our testing tools to interact with the waveguide,

3. Keep print block within the printing range for contiguous printing.

We wanted to raise the height of the ridge because after our initial visual inspection, the ridge structure wasn't very clear. If it was the case that the ridge didn't do its job of separating the waveguide from the pedestal, then there was no reason for including it in the design. Since the theoretical resolution of the objective lens is $a_{x,y} = 595 \ nm$ and $a_z = 3313 \ nm$ (see Fig. 46), it is very possible that the height of the ridge design was too small for a proper ridge to print. Thus, to make sure there is a gap between the waveguide and the pedestal, we increased height of the ridge from 3 μm to 10 μm and created simulations with varying width. To make sure that our input and output optical fibers are able to interact with the waveguides with no obstructions, we had to provide more height clearance for the waveguide. Part of the reason for this was that we didn't give any room for error when it came to the fiber alignment. The print could be slightly off the intended design, the input/output fibers may be slightly off axis, and the probe station does not have the level of precision required to make sub-micron adjustments. Additionally, the length of the waveguide is so short that when printed on our substrate which is $25 \times 25 \ mm^2$, the optical fiber's stripped length of 10 mm is not enough to reach within the working distance. Therefore, we had to provide enough clearance for any potential problems in addition to the 400 μm coating jacket. Raising the height of the pedestal also meant increasing the width such that it would have less chance of falling over. Lastly, to reduce structural defects of the printed

waveguide, we limited the size of the print to the printing field allowed by the 25x NA0.8

objective. It is likely possible to produce a larger working waveguide with block splitting and

stitching parameters using the 25x ITO Solid recipe. However, judging from the second print, it

will likely cause additional limitations to the design, and we leave this to be investigated by

future research.

To investigate the optimal ridge width, we simulated varying ridge sizes to see how well

different ridge widths would affect optical confinement. We simulated three ridge widths, 3 μm,

5 μm, 10 μm. The simulation showed that a ridge width of 10 μm would not confine the electric

field. A ridge width of 3 μm showed best optical confinement in the waveguide but worries

about the structural strength of a ridge of those dimensions led us to look deeper (see Fig. 47).
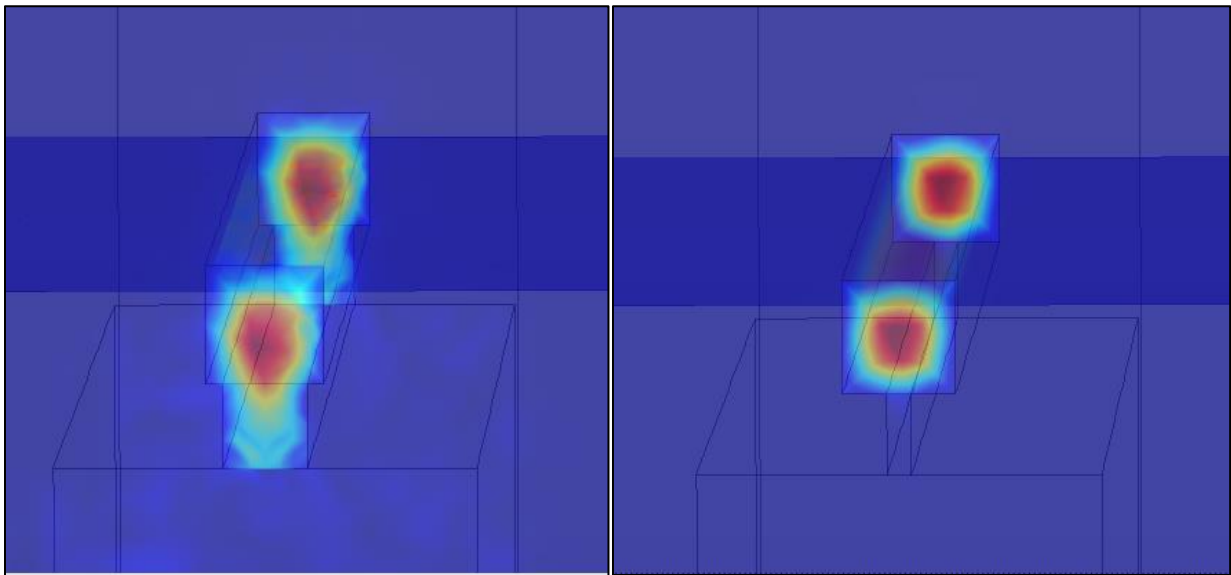
Figure 47: The left figure shows the simulation of a ridge with the dimensions 10 x 10 μm^2. Notice how the electric field couples into the ridge and will cause higher loss. The right figure is a simulation of a ridge with the dimensions 3 x 10 μm^2. Notice the excellent optical confinement.

The 5 × 10 μm^2 ridge waveguide showed good optical confinement while improving upon the

structural integrity of the design (see Fig. 48).
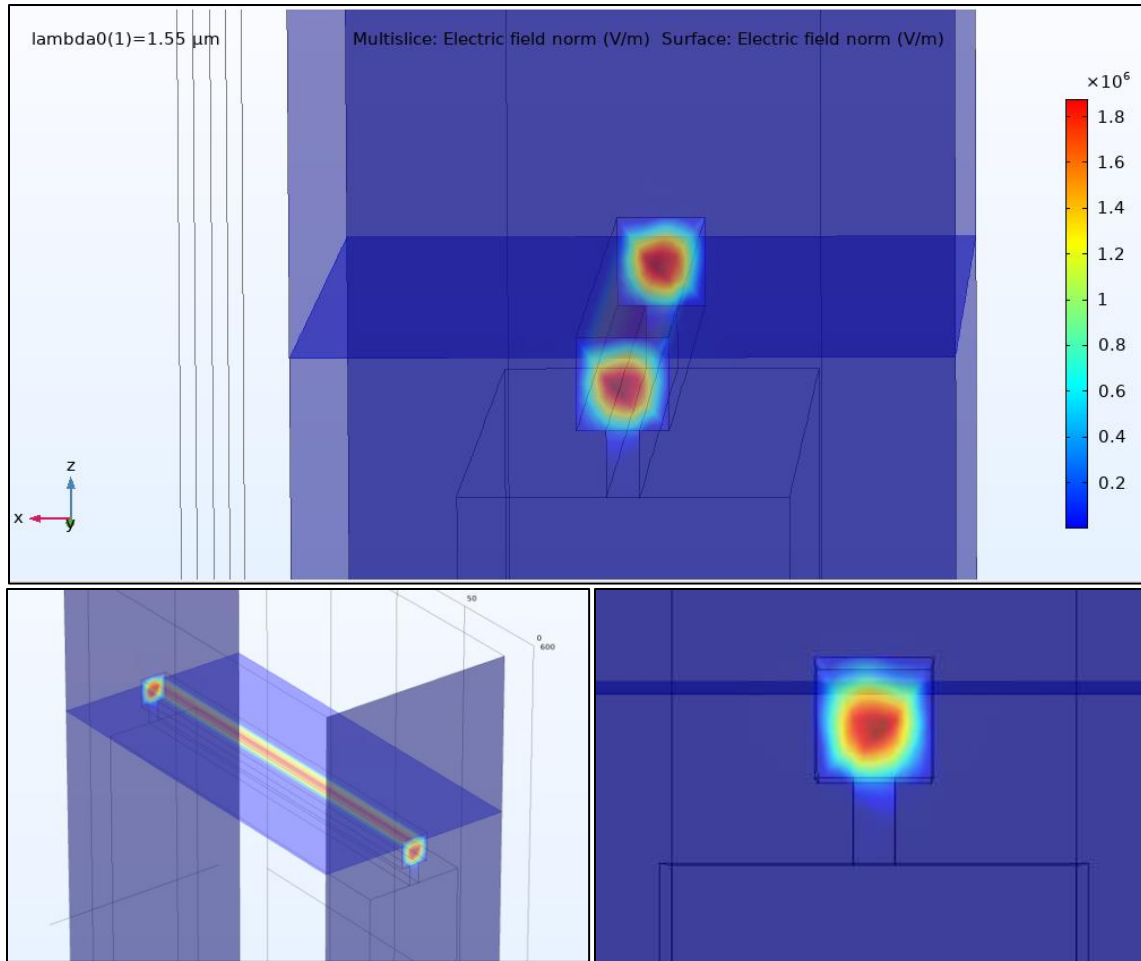
Figure 48: Waveguide simulations for Design 3. Note that the electric field is well confined in the waveguide. The ridge has the dimensions 5 x 10 μm^2 and the waveguide is maintained at its 14 x 14 μm^2 cross section.

The final design resulted in two waveguides within the printing field of the 25x ITO Solid recipe and consisted of one straight waveguide and one S-bend waveguide. Both waveguides had a length of 200 μm (see Fig. 49). The cross section of the structures was the following:

- $14 \times 14\ \mu m^2$ square waveguide

- $5 \times 10\ \mu m^2$ ridge

- $50 \times 500\ \mu m^2$ pedestal

The S-bend waveguide was offset by 50 μm and created using two circular section curves with a radius of 140 μm.
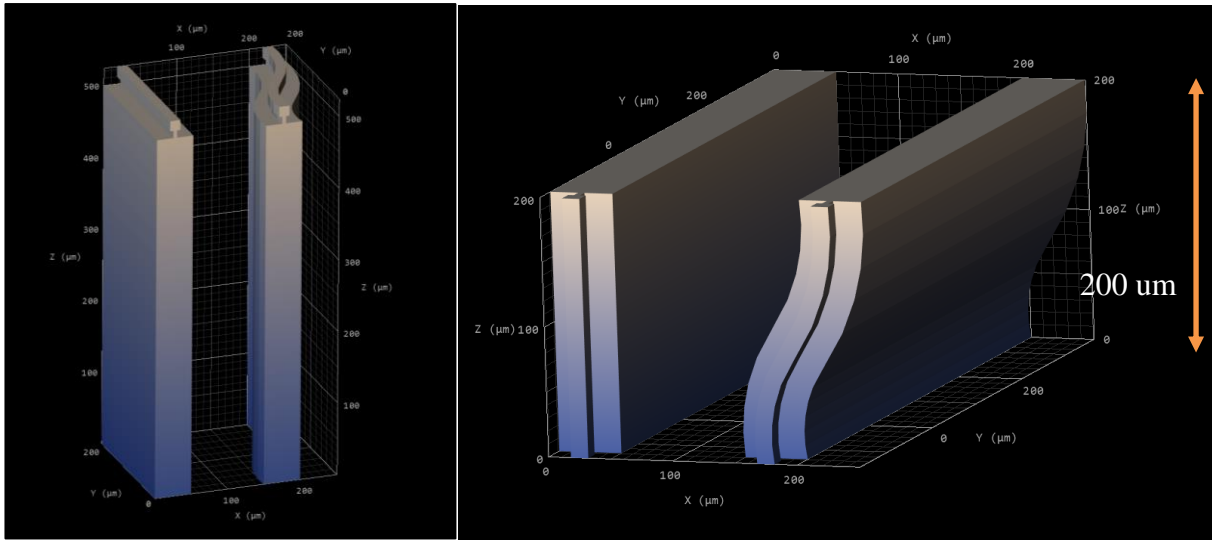
Figure 49:Design 3 model. In this design we confine the dimensions into the writing field of the objective lens for continuous printing and increase the height of the pedestal for higher clearance.

4.2.3.1 Print 3: Printed on April 5th, 2022

The final print of the project took 28 minutes and 54 seconds to print. Immediately after the print was developed, it was brought to the testing station for quality inspection. During this inspection, we checked to see that the waveguide, ridge, and pedestal were all printed and didn't have any breaks or discontinuities. Satisfied with the quality, structural integrity and seeing that it would be suitable for our needs, we proceeded with the testing and characterization of the waveguides.

4.3 Testing and Characterization

The testing and characterization are critical parts of the waveguide development and manufacturing process. The objective of testing and characterization is to evaluate the resulting characteristics and properties in comparison to the intended properties of the design. For a

waveguide, the major key characteristics include surface and sidewall roughness, refractive index, thickness, structural integrity, resolution quality, optical coupling, optical loss, and nonlinear properties [81].

For the purpose of this project, we characterized the waveguides through geometrical inspection and testing optical insertion loss. We conducted the geometrical inspection on all three prints, but the optical insertion loss was only carried out on the final print as it was not possible to test the previous prints.

4.3.1 Geometrical Inspection

Waveguides confine and guide electromagnetic waves in a region of higher refractive index than its surrounding medium. Additionally, the structure, thickness, and its other topological and physical qualities are important in its ability to confine and guide light. Using the VHX-7000 microscope, we looked at the quality of the prints and made an attempt to optically profile the waveguides using the 3D mapping software of the VHX-7000.

The first print was too large to print without block splitting parameters and resulted in an incomplete print. The edges if the incomplete seem to outline a circular path which we assume to be the limits of the galvo printing field of the 25x objective used (see Fig. 50). For reasons that are unclear, the edges that were cut off due to the printing limits seem to have been burnt during the process.

Figure 50: Print 1. Notice the circular path outlined by the edges near the bottom of the figure in addition to the seemingly burnt edges for the left three waveguides. This print failed due to improper block stitch settings.

The second print resulted in the full intended structure but had some serious block stitching issues (see Fig. 51). The height between the stitched blocks were mismatched as noticed when we were trying to focus on the microscope lens on the waveguides. Additionally, it was unclear whether or not the ridge had been printed to achieve its goal, to create a gap between the pedestal and the waveguide.
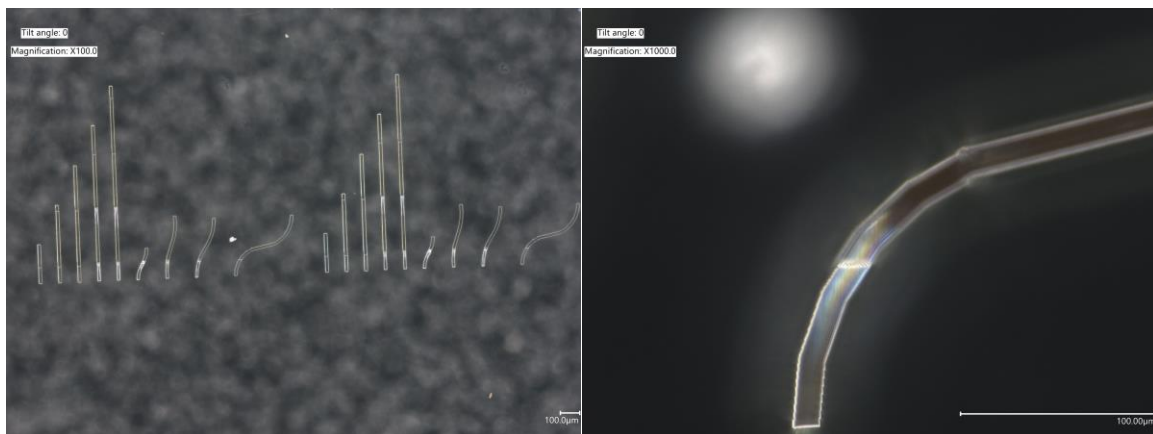
Figure 51: Print 2. Notice the fully printed structures in this print compared to Print 1. This print failed due to the block stitches that were significantly mismatched in height. The block stitch can be seen in the right figure at the line between the two segments of the waveguide. The height difference is realized when both segments do not come into focus in the same image.

The modifications made between the second and final prints made a substantial difference in the print quality. We had initially worried about the very large height to width ratio for both the pedestal and ridge, but the geometrical inspection revealed a sound structure with clear view of the ridge. In this final print, there were no block stitches, and the waveguide was continuous with less structural defects (see Fig. 52).

Figure 52:Print 3. The top view (left figure) shows that the waveguide has no heigh mismatch and the full structure was printed. The side view (right figure) shows that all three parts of the structure (pedestal, ridge, waveguide) are all printed and seem to be without significantly noticeable errors.

With the final print, we explored the use of optical profilometry to obtain the surface topography of the cured polymer structure. However, it became apparent that this would not be possible with the equipment that we had (see Fig. 53). One of the challenges we faced in visually inspected the waveguides was the low difference in refractive index between the substrate and the cured polymer. While we overcame this challenge using different lighting and background methods, the 3D mapping software found it near impossible to single out the structure.
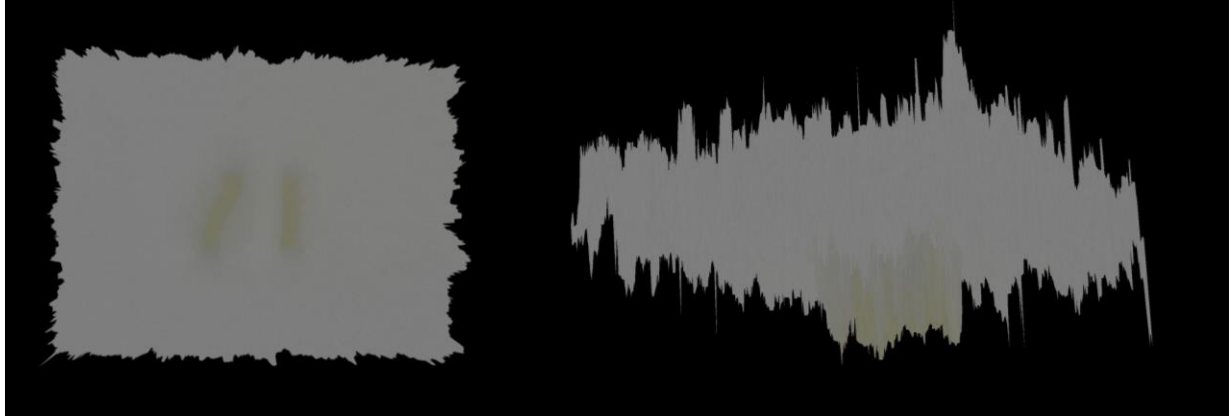
Figure 53:3D mapping attempt using the VHX-7000 microscope. The 3D mapping software was not able to map out the structure due to the similar refractive indices of the cured polymer and substrate.

See Appendix B for more photographs from the VHX-7000 microscope.

4.3.2 Attenuation/Insertion Loss

To truly test the effectiveness of a waveguide, we need to test its ability to confine and guide light through itself. One way to do this is by testing for the insertion loss of the waveguide, that is, the loss of signal power resulting from the signal traveling through the waveguide. When discussing power levels in waveguides, dBm is often used as the unit of level with reference to one milliwatt:

$$P_{dbm} = 10 \, log_{10} \frac{P_{mW}}{1mW}.$$

Equation 12

Our coupling/fiber alignment method was carried out using the probe station and visual fault detector. The visual fault detector is a $650 \, nm$ (red) laser that allows the user to visually test fiber optic cables for breaks, bad splices, bends, etc. The visual fault detector assisted us in getting a general sense for alignment and waveguide coupling. Fig. 54 shows this in practice. The difference between misalignment and coupling of light into the waveguide is subtle on the infrared camera, but much clearer on the side camera of the probe station. The visual fault

detector's effectiveness is best shown at the bottom of Fig. 54 where it is clear that the light is being guided through the S-bend waveguide from one end to the other.
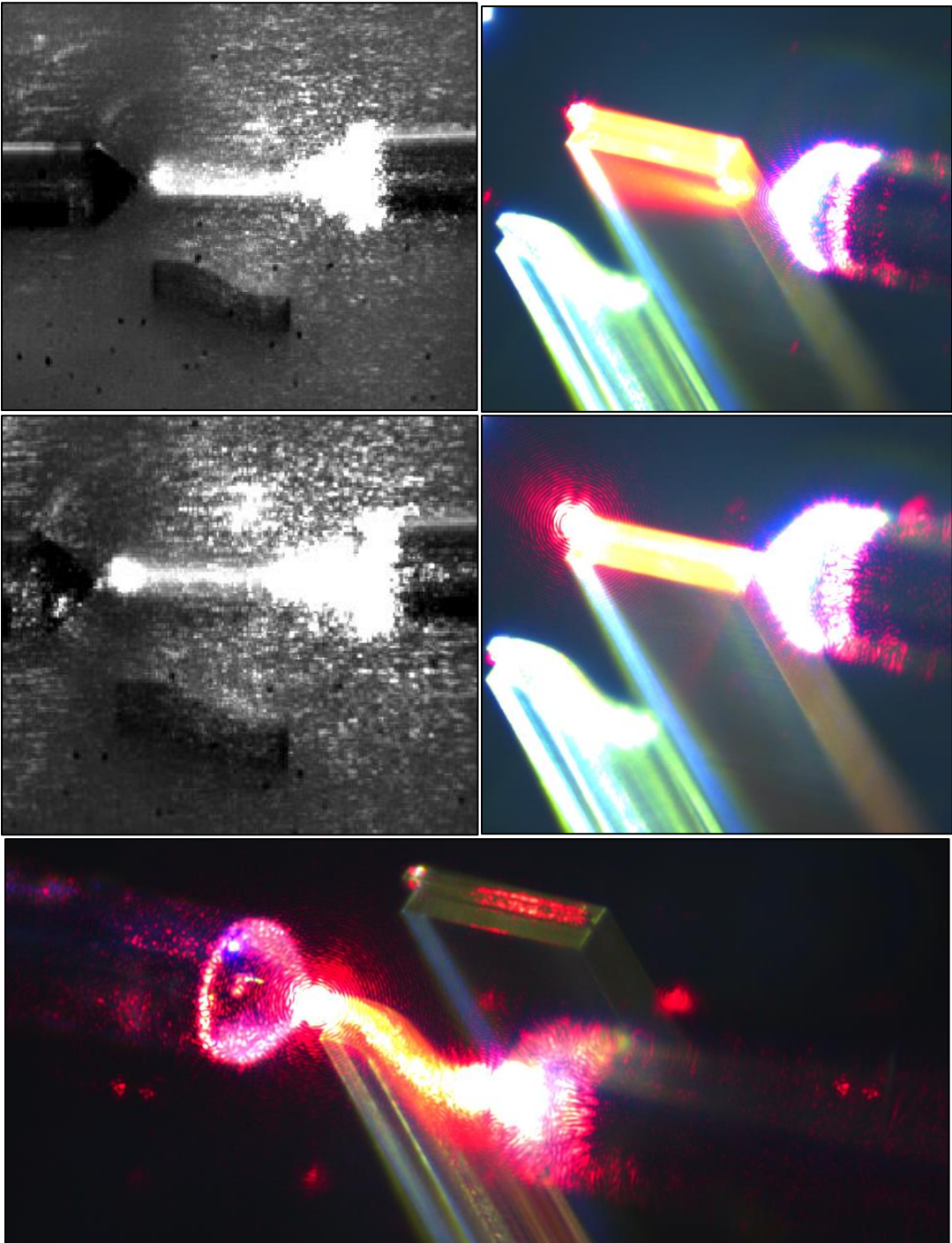
Figure 54: The fiber alignment process shown through the infrared (gray) and probe station cameras (color). The top two photos show the light coupling into the supporting pedestal. The middle two photos show fiber alignment and light coupling into the waveguide itself. The bottom photo shows the light being guided through the S-bend waveguide. See Appendix C for additional probe station photos.

To maximize coupling, we conducted a raster scan which scans the transverse plane to find the zone with the highest power transmission (see Fig. 55).
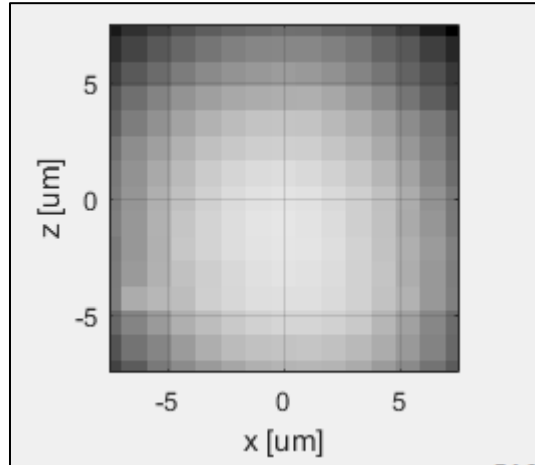
Figure 55: Raster scan display on the probe station software. The darker the color of the box, the higher the power transmission.

After the raster scan, we proceeded with the fine alignment function of the probe station's software which finds the location with the highest power with even greater detail than the raster scan.

We performed our insertion loss calculations by first taking the reference optical power measurement M0, using the PM100D power meter. The total reference power measurement (M0) was measured at -2.33 dBm (-1.28 dBm for transmitter fiber and -1.05 dBm for receiver fiber). The reference power measurement's insertion loss is most likely due to the fusion splice that had to be created to connect the pig tail fiber to the lensed fiber used for the probe station. After aligning the input and output fibers with the polymer waveguide using the method above, we took the second transmission power measurement (M1). We then calculated the insertion loss of the device as M0-M1. To reduce scattering, the power output on the laser was kept low at 0.1 dBm. We carried out insertion loss calculations for wavelengths 1550-1560 nm in 0.0003 nm

increments. Three trials were carried out for each measurement and were averaged together for

analysis. The results of the analysis are shown in Fig.56.
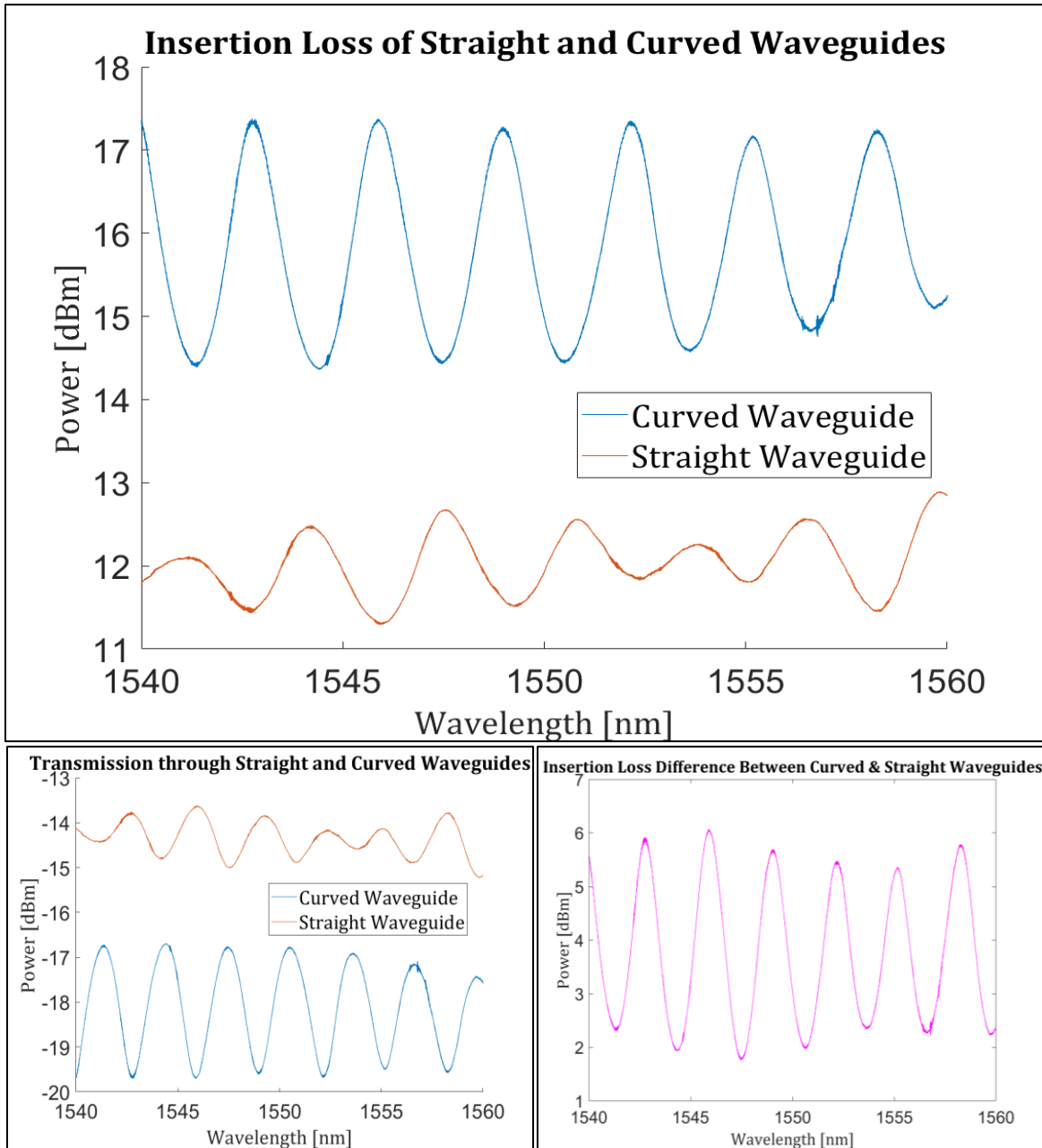
Figure 56: The top figure shows the insertion loss of straight and curved waveguide and is the result of taking the reference optical power measurement to adjust the transmission spectrum displayed at the bottom left. The difference in the insertion loss of the two waveguides is shown in the bottom right. The periodic oscillations which have a peak to peak spacing of approximately~ 3 nm are the result of a phenomenon that occurs when a multimode waveguide is placed in between two single-mode waveguides (optical fibers) and produces multimode interference. One point of interest is that the curved and straight curves are 180 degrees out of phase. We leave the exploration of this effect for future research.

The first thing that is noticeable in the spectral transmission and insertion loss spectra for both waveguides are the periodic oscillations. These oscillations are the result of a phenomenon that occurs when a multimode waveguide is placed in between two single-mode waveguides (optical fibers) and produces multimode interference [51, 82, 83]. The interference arises from the excitation of the closest higher order mode of the waveguide and the oscillation period depends on the length of the waveguide. Some potential causes for the oscillations include surface roughness and low-quality coupling of light from the fiber into the waveguide. While we did not explore this further, we encourage future research into these effects for polymer waveguides.

As expected, the straight waveguide showed lower loss than the curved waveguide. The insertion loss across the spectrum of 1540-1560 nm ranged from 11.29 dB to 12.90 dB and was 11.93 dB at 1550 nm. For the curved waveguide, the insertion loss ranged from 14.36 dB to 17.38 dB and was 14.98 dB at 1550 nm. The similar project using IP-Dip found the mean insertion loss value of their $14 \times 14\ \mu m^2$ square waveguide at $200\ \mu m$ to be around -0.6 dB [51]. Insertion loss should always be a positive number since a passive waveguide would never amplify the power level. It is possible that the authors of this report meant an insertion loss of 0.6 dB. Regardless of the intent of the authors of this paper, the magnitude of this value is very small and implies a much smaller insertion loss through their waveguide compared to ours. Similarly, the paper mentions a mean insertion loss of their S-bend waveguide to be -1.69 dB. While their design included a taper for better coupling and had a slightly different shape, the reported performance is much better than our waveguide.

There are several reasons why our insertion loss was so high. One reason is that our coupling method was imprecise. While we did our best to use the tools available, our fiber

alignment was less than perfect. There is also likely to be some reflection off the surface of the waveguide which would cause there to be insertion loss. Additionally, lower quality of print due to the lower level of resolution of the IP-S printing recipe could increase sidewall roughness of the material which could increase insertion loss. Lastly, further loss is likely to come from the free space coupling method which leads to Fresnal reflections and potentially Fabry Perot etalon created by the air gap [84].

Supplementary air coupling transmission data was collected by raising the input and output fibers after collecting transmission data on the waveguides. It was unclear how beneficial this data will be, but it may be of interest to the reader to see how much power can be transmitted through the air at the same displacement as the waveguides. See Appendix D for this data in addition to the raw transmission data graphs.

Chapter 5: Recommendations & Conclusions

The final chapter includes the second objective of this project, which was to provide recommendations for similar future projects at WPI.

5.1 Recommendations

The recommendations for future projects are illustrated below in Fig. 57.

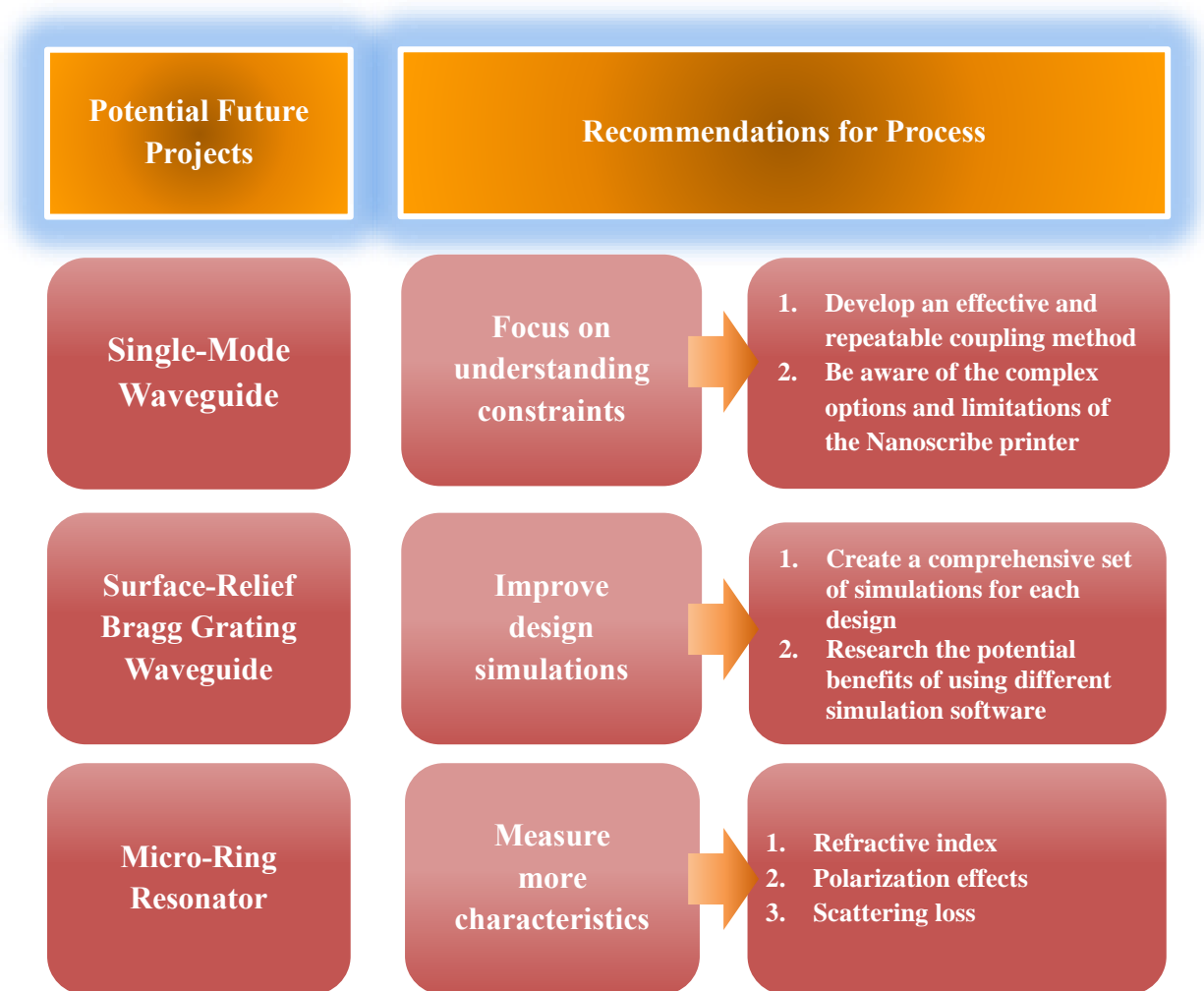| Potential Future Projects	Recommendations for Process	
Single-Mode Waveguide	Focus on understanding constraints	1. Develop an effective and repeatable coupling method 2. Be aware of the complex options and limitations of the Nanoscribe printer
Surface-Relief Bragg Grating Waveguide	Improve design simulations	1. Create a comprehensive set of simulations for each design 2. Research the potential benefits of using different simulation software
Micro-Ring Resonator	Measure more characteristics	1. Refractive index 2. Polarization effects 3. Scattering loss

Figure 57: Recommendations Overview

5.1.1 Potential Future Projects

The first set of recommendations pertain to similar potential future projects. To select these projects, we looked at the broad set of applications of two photon polymerization in the photonics field and separated them by difficulty levels. As a foundational project for the new laboratory, we've fabricated a proof-of-concept waveguide, and we propose future teams some project ideas that could realistically build upon this project without significant challenges:

1. Single-mode waveguide

2. Surface-relief Bragg grating waveguide

3. Micro-ring resonator

Fabricating a single-mode polymer waveguide should be a relatively manageable project for anyone attempting to build upon this project. Developing a single-mode waveguide will require redesigning the waveguide's cross section to make it smaller and potentially move away from the square waveguide. Beyond the higher focus on the fundamental modes, most of the work done in this project should apply to creating a single-mode polymer waveguide. A Bragg grating is a modified waveguide that reflects certain wavelengths of light and transits all others. This is done by periodically varying the refractive index of the core to create a wavelength specific dielectric mirror. A Bragg grating can used to lock certain wavelengths, which can be useful in sensing applications. A polymer surface-relief Bragg grating waveguide has been studied using IP-Dip [74]. The design is similar to a regular waveguide except that there are surface relief gratings on the waveguide. Brief research into Bragg gratings in addition to this report should provide enough guidance to put this project on the right path. The micro-ring resonator is an important photonic component used in sensing and filtering applications. It consists of a set of waveguides

where one is a close loop that couples to an input and an output. When a resonant wavelength propagates through the loop, the constructive interference will increase the intensity of light. Because only certain wavelengths are at resonance within the loop, the micro-ring resonator acts as a filter. A polymer micro-ring resonator has been studied for ultrasound detection [59] and this could be an interesting application to explore.

Several other applications of direct laser writing (2PP) in micro-optics, waveguides, and optical micro-cavities exist, each with its own challenges [85] and there is no doubt an endless number of potential future projects. This list is not intended to be exhaustive by any means and are only suggestions to guide the future research team in deciding. An important thing to consider when picking a similar project is to watch that the proposed project does not pose too many new and extreme challenges from the beginning where the team needs to fully start from scratch. The recommended projects are not at the cutting edge of research in the field of photonics. However, they are the steppingstones for the LEAP facility to gain expertise in this area to conduct cutting edge research in the future. We recommend that project teams think big but be aware of the challenges that come with it.

5.1.2 Recommendations for Process

The second set of recommendations delves into the approach and process of future similar projects at the LEAP facility. After analyzing the roadblocks and difficulties encountered by the project, we found several improvements and considerations for the project process and approach:

1. Focus on understanding constraints
2. Improve design simulations

3. Measure more characteristics.

5.1.2.1 Focus on understanding constraints

A project that requires very high precision (micron or submicron level) has many constraints either in the design, fabrication, or testing. These constraints are very important in the design process because a lack of understanding of these constraints can lead to serious problems for the project. Two key constraints that posed the greatest challenges were in fiber alignment for maximum coupling into the waveguides and the complexity of options and limitations of the Nanoscribe printer. We recommend that an effective and repeatable coupling method be developed and to be aware of the complex options and limitations of the Nanoscribe printer.

Fiber alignment and maximizing coupling is a difficult challenge with any project dealing with photonics due to the incredibly small nature of the structures in addition to need for high precision. For a project using two-photon polymerization, it's important to remember that the structures will be printed on a substrate that will hinder the ability for fiber to couple in directly into the waveguide without raising it in some way. If the structure is small enough, then the clearance needed will increase because it may become necessary to get farther down the fiber where the coating jacket is. The type of fiber being used to test the waveguides matter when determining these design constraints. The type of fiber will determine how far the fiber must be from the waveguide and how high the clearance should be. A potential way of getting around the issue of the substrate would be to find some way to have a custom substrate that is smaller, or to find a way to cut off the substrate after the prints are complete. These options should only be considered after a cost analysis of these modifications. An improvement in the actual method of fiber alignment could be very beneficial for future research. The method that we used involves general coupling using the visual fault detector, raster scanning, and fiber alignment. While this

method works, it is unclear how effective it was in maximizing the coupling and it took a very long time to get through. As we increase the number of inputs and outputs on future projects, a faster, reliable, and effective method of fiber alignment is necessary. One possible way to separate the loss to coupling and loss because of poor waveguide design could be to print different lengths of waveguides. Additionally, automating fiber alignment for many fibers will be very helpful for the testing process, and could be a worthwhile investment. Some ways that other projects have solved this problem is by using tapers and v grooves [51]. There are many interesting ways to couple light into waveguides, and we encourage the reader to explore the many options.

Beyond the issues with coupling, the complexity of options and limitations of the Nanoscribe Photonics GT+ can be both exciting and frustrating. Our first two prints suffered from serious printing issues that in addition to lack of clearance for the fiber, did not make it to the testing phase of the project. A few key things stand out when attempting to use the Nanoscribe printer. Resolution depends on the process recipe used that determines the objective and resin used in the print in addition to the different printing modes selected. The print time can be very substantial when using high resolution settings and every effort should be made to avoid high print times unless the user is highly certain of the design. Each resin has a slightly different refractive index, and these values change based on the temperature, state of resin, and the wavelength propagating through. The substrate's properties also change depending on the process recipe/resin used. When designing larger prints, a critical setting to understand is the block splitting/stitching modes. If done incorrectly, it can cause serious structural problems including mismatched heights of stitched parts and incontiguous structures. It seems that using a higher objective

reduces these effects [51] but it's unclear how to optimize the setting to create large structures without significant defects.

5.1.2.2 Improve design simulations

Simulations are very useful in getting a general sense in design performance without the costs and time associated with an actual experiment. This project used COMSOL to simulate the straight waveguide's ability to confine the electric field from one end to another and kept the same waveguide cross section design for a curved waveguide. However, a more detailed and exhaustive set of simulations will be beneficial for larger, more complex projects. With the increasing complexity, some may find COMSOL not adequate for their needs. We recommend future projects create a more comprehensive set of simulations for each design and to research the potential benefits of using different photonics simulation software.

For the purpose of this project, we did not conduct a comprehensive set of simulations that covered all the waveguides printed and we did not attempt to collect data beyond electric field confinement in the waveguide. As projects get more complex and the aim turns towards optimizing performance of the application at hand, this data becomes increasingly important. As the designs become more complicated with bends and complex coupling techniques, creating the simulation can itself be burdensome.

While COMSOL is a very useful tool for general Multiphysics simulations, it may not be the best platform for complex photonics design simulations. Several photonics specialized simulation software platforms currently exist. One such platform is called Ansys Lumerical, a photonics simulation solution that models light's interactions for designing photonic systems [86]. Ansys Lumerical has a set of photonics simulation and analysis tools called suites. The suites together offer component and system level simulations with enhanced design flows that

enable designers with models that are calibrated to leading foundry processes. The suites work together with flexible interoperability to model and solve complex problems in photonics design for optical, electrical, and thermal effects. Two suites worth mentioning are the DEVICE Suite and SYSTEM Suite (see Fig. 58). The two suites combine device multiphysics and system level photonic circuit simulation with third party productivity tools. Python based automation combine device multiphysics and system-level photonic circuit simulation with h Python-based automation further increases interoperability.

Figure 58: Ansys Lumerical's DEVICE and SYSTEM Suites [87]

We do not support any specific software for future research. Ansys Lumerical is but one of many tools that exist for numerical simulations. It is up to the future project teams to decide which software will best suit their needs and understand the costs and availability of that software.

5.1.2.3 Measure more characteristics

Our last recommendation for future projects is to measure more characteristics during the testing phase. In this project, we conducted geometric inspection and insertion loss characterization for the waveguides that we printed. As mentioned previously, there are many characteristics of a waveguide-based system. We recommend measuring the following characteristics for future projects:

1. Refractive index

2. Polarization effects

3. Scattering loss.

The refractive index is one of the most important characteristics of an optical component. Refractive index can be used to calculate insertion loss, cutoff wavelengths, and more. Several techniques exist for measure the refractive index of waveguides including reflectometry and ellipsometry, surface plasmon resonance, incoherent light transmission the refracted near field technique, prism coupling, as well as the propagation-mode near-field method [81]. The refractive index of the different polymer resins has been studied but it would be beneficial for future projects to conduct their own measurements of the refractive index of their structures as it is a crucial property of any optical component.

Another characteristic to considering measuring is the effects of using polarized light on other variables such as insertion loss. While our research used unpolarized beams in our insertion loss measurements, it would be interesting to see the impact of polarized beams on waveguide performance.

The last characteristic to consider is scattering loss. There exists many methods to measure scattering: the sliding prism method, three-prism method, out-of-plane scattering measurement, pyroelectric absorption loss measurement, direct temperature measurement, Fabry Perot resonance method, photothermal deflection, and the Coblentz mirror method [88]. Scattering loss measurements can also be used to calculate the propagation loss of a waveguide assuming that the amount of light scattered from the surface is proportional to the light propagation inside the waveguide [81]. If nothing else, scattering loss measurements would provide feedback on where the losses are coming from.

One of the most difficult things about working with waveguides is that they are very small structures requiring high precision. Beyond the design constraints that they create, the equipment that we use has an impact on what we can measure. Using equipment such as the atomic force microscope, electron scanning microscope, and the Zygo optical profilometers could improve the geometrical inspection of the prints and higher resolution cameras on the probe station can improve fiber alignment.

5.2 Conclusions

The goal of this project was to showcase the capabilities of the new photonics laboratory at WPI and set a foundation for similar future projects at the laboratory. The final set of deliverables included the air clad polymer waveguides and recommendations for future projects.

By using COMSOL, we modeled and simulated our waveguide based on similar work done by other research teams. We fabricated one straight waveguide and one curved waveguide using the IP-S 25x ITO Solid process recipe on the Nanoscribe Photonics Professional GT+ printer. Using the VHX-7000 microscope we conducted geometrical inspections and attempted to 3D map the surface of the polymer waveguide. We also measured the insertion loss of the waveguides across the wavelengths 1540-1560 nm using a laser source, power meter, lensed fibers, and a probe station. While the insertion loss of our waveguides was higher than those in open literature, we found that the curved waveguide has higher insertion loss than the straight waveguide as expected.

After going through the process and analyzing the various challenges, roadblocks, and successes, we made recommendations on future work. For potential future project we believe that an air-clad polymer single mode waveguide, surface-relief Bragg grating waveguide, and

micro-ring resonators are all reasonable projects that can build upon this project without significant challenges. Our recommendations on the process of a similar project are based around design constraints, design simulations, and testing characteristics. Understanding the constraints set by the equipment and tools that we have are critical to the design process. We recommend that an effective and repeatable coupling/fiber alignment be developed. Our method was cumbersome, time consuming, and possibly imprecise. As designs become more complex, it will be important to have a reliable method of coupling the input/output fiber with the component. We also recommend that future teams make every effort to fully understand the options and limitations of the Nanoscribe printer. The complexity of the Nanoscribe printer can be turned into an advantage but can also cause structural flaws as it did in our project. Design simulations are important for understanding the likelihood of success of a design. It is a cost effective and time efficient method of getting a basic idea of how the component will perform in an experiment. We recommend that a comprehensive set of simulations for each component and design be created to get a deeper understanding of the design's potential. We also recommend researching different simulation software specializing in photonics as they may provide more functionality. Lastly, we recommend that future teams measure more characteristics such as the refractive index, polarization effects, and scattering loss of the photonic device. Our focus was to provide a proof-of-concept waveguide and we did not delve into the different characteristics to test. As projects become more advanced, properties to test and characterize the designs will also need to increase.

We hope that this work can serve as a starting point for future research teams at WPI attempting similar projects.

Appendices

Appendix A: IP-Dip and IP-S Data Sheets

All data in Appendix A is sourced from the nanoscribe support website at support.nanoscribe.com

IP-Dip

General Info

Property	Description	Comments
Reactive group	acrylate	
Curing mechanism	free radical polymerization (FRP)	
Cured Polymer	thermoset	
Polarity	hydrophobic	cured flat resin structures are slightly hydrophilic[ref][ref][ref]; see printing non-stick surfaces article
Hazard class	refer to the MSDS supplied with the shipment	
Expiration date/shelf life and storage	warranted shelf life of 12 months from production	store at 4-8°C
Chemical resistance	polymerized resin does not melt and cannot be dissolved	polymerized resin can be degraded using harsh conditions,[ref] see removal/stripping article
Biocompatibility		see biocompatibility article

Process Info

Property	Description	Comments
Resist tone	negative	
Polymerization	designed for 2PP	
Solution set	3D SF	further information on the usage of IP-Dip can be found in the application article
Development/washing	12 min Mr-Dev/30 s Novec	see sample development article
Pre/post bake	not required	
Spin coating	not required	see sample preparation article
Removal/stripping		see removal/stripping article

Physical Properties

Property	Value			Comments
Degradation temperature	Recipe	Degradation temperature [°C]	95% Material loss [°C]	info
	IP-Dip solid custom[graph]	371	585	
Color	yellow fluorescent (liquid; polymerized)			
Fluorescence	yes			fluorescence is observable between 400-700 nm; see also[ref][ref]
Refractive index (liquid)	1.521 @ 589 nm, 20°C			more data, graph
Refractive index (2PP polymerized)	1.552 @ 589 nm, 20°C			more data; see also[ref][ref]; refractive indices of 1-photon polymerized (1PP) resin[ref][ref]
Transmittance (polymerized)	>95% @ at 633 nm and essentially transparent up to 2.4 µm with two local transmission minima at 2.9 µm and 3.4 µm			see[ref]; 1PP spectrum[ref]
Extinction coefficient				graph
Dielectric constant (relative permittivity)/loss tangent	1.8/0.12			info; see also[ref]
Young's modulus	2.91 GPa			used recipe: IP-Dip 63x Fused Silica (3D SF); more info; see also[ref][ref][ref]
Vickers Hardness	12.05 HV0.0025			
Hardness	130.13 MPa			
Storage modulus	3.17 GPa			
Loss modulus	0.24 GPa			
Poisson's ratio (estimated)	0.3			
Expansion coefficient (2PP polymerized)	$5\text{-}8 \cdot 10^{-5}$ K^{-5}			[ref]
Shrinkage after polymerization	5-17%			see shrinkage article
Density (liquid)	1.170 g/cm³ @ 20°C			
Viscosity η (liquid)	2420 mPas @ 20°C			

Refractive Index Liquid Phase

T [°C]	Wavelength [nm]							Abbe number
	405	479.3	546.1	589.3	643.8	780	950	
10	1.553	1.538	1.529	1.525	1.521	1.516	1.511	32
15	1.551	1.536	1.527	1.523	1.519	1.514	1.509	32
20	1.549	1.534	1.525	1.521	1.517	1.512	1.508	32
25	1.547	1.532	1.523	1.519	1.515	1.510	1.506	32
30	1.545	1.530	1.521	1.517	1.513	1.508	1.504	32
35	1.543	1.528	1.519	1.515	1.511	1.506	1.502	32
40	1.541	1.526	1.517	1.513	1.509	1.504	1.500	32
45	1.539	1.524	1.515	1.511	1.507	1.502	1.498	32
50	1.537	1.522	1.513	1.509	1.505	1.500	1.496	32
55	1.535	1.520	1.511	1.507	1.504	1.498	1.494	32
60	1.532	1.518	1.509	1.505	1.502	1.496	1.492	32
65	1.530	1.516	1.507	1.503	1.499	1.494	1.490	32
70	1.528	1.514	1.505	1.501	1.498	1.492	1.488	32
75	1.526	1.512	1.503	1.499	1.496	1.490	1.486	32
80	1.524	1.510	1.501	1.497	1.494	1.488	1.484	32

Refractive Index 2PP Solid

Print set	T [°C]	Wavelength [nm]							Abbe number
		405	479.3	546.1	589.3	643.8	780	950	
Custom	20	1.579	1.564	1.556	1.552	1.548	1.543	1.539	36

IP-S

General Information

Property	Description	Comments
Reactive group	methacrylate	
Curing mechanism	free radical polymerization (FRP)	
Cured Polymer	thermoset	
Polarity	hydrophobic	cured flat resin structures are slightly hydrophilic[ref][ref]; see printing non-stick surfaces
Hazard class	refer to the MSDS supplied with the shipment	
Expiration date/shelf life and storage	warranted shelf life of 12 months from production	store at 4-8˚C
Chemical resistance	polymerized resin does not melt and cannot be dissolved	polymerized resin can be degraded using harsh conditions, [ref] see removal/stripping
Cytotoxity	after 72 h incubation, 2.0% inhibition of L929 mouse fibroblast cell growth by a UV-cured IP-S sample; UV-cured IP-S is therefore considered to be non-cytotoxic according to ISO10993-5	see biocompatibility

Process Information

Property	Description	Comments
Resin tone	negative	
Polymerization	designed for 2PP; UV flood curing is possible	see UV curing article
Solution set	3D MF	further information on the usage of IP-S can be found in the application article
Developer/washing	20 min Mr-Dev/30 s Novec	see sample development
Pre/post bake	not required	
Spin coating	not required	see sample preparation
Removal/stripping		see removal/stripping

Physical Properties

Property	Value			Comments
Degradation temperature	Recipe	Degradation temperature [°C]	95% Material loss [°C]	info
	IP-S 25x ITO Solid (3D MF)[graph]	300	552	
	IP-S 25x ITO Shell (3D MF)[graph]	286	549	
Color	colorless (liquid); greenish (solid printing); yellowish (shell and scaffold printing)			the structure will develop a more distinct color upon UV curing or exposing the printed structures to white light for longer time periods
Fluorescence	yes			fluorescence is observable between 400-700 nm, see also[ref][ref]
Refractive index (liquid)	1.486 @ 589 nm, 20°C			more data, graph
Refractive index (2PP polymerized)	1.515 @ 589 nm, 20°C			more data; see also[ref][ref]; refractive indices of 1-photon polymerized (1PP) resin[ref][ref]
Transmittance (polymerized)	2PP Transmittance >95% from 633 nm to 2.4 μm. Two local transmission minima at 2.9 and 3.4 μm.			see[ref]; 1PP spectrum[ref]
Extinction coefficient				graph
Young's modulus	5.11 GPa			used recipe: IP-S 25x ITO Solid (3D MF); more info; see also[ref][ref]
Vickers Hardness	20.68 HV0.0025			
Hardness	223.33 MPa			
Storage modulus	5.33 GPa			
Loss modulus	0.26 GPa			
Young's modulus	4.68 GPa			used recipe: IP-S 25x ITO Shell (3D MF); more info; see also[ref][ref]
Vickers Hardness	20.29 HV0.0025			
Hardness	219.11 MPa			
Storage modulus	5.03 GPa			
Loss modulus	0.27 GPa			
Poisson's ratio (estimated)	0.3			
Expansion coefficient (2PP polymerized)				see[ref]; related to data from IP-Dip[ref]
Shrinkage after polymerization	2-12%			see shrinkage
Density (liquid)	1.111 g/cm³ @ 20°C			
Swelling	Solvent	Weight increase [%]		info
	purified water	1.5		
	isopropanol	2		
	PGMEA	1		
	acetone	9.5		
Viscosity η (liquid)	13600 mPas @ 20°C			

Refractive Index Liquid Phase

T [˚C]	Wavelength [nm]							Abbe number
	405	479.3	546.1	589.3	643.8	780	950	
10	1.511	1.498	1.492	1.489	1.487	1.483	1.480	45
15	1.509	1.496	1.490	1.488	1.485	1.481	1.478	45
20	1.507	1.494	1.488	1.486	1.483	1.479	1.476	45
25	1.505	1.493	1.487	1.484	1.481	1.477	1.474	45
30	1.503	1.491	1.485	1.482	1.480	1.475	1.473	45
35	1.501	1.489	1.483	1.480	1.478	1.474	1.471	45
40	1.499	1.487	1.481	1.479	1.476	1.472	1.469	45
45	1.498	1.485	1.480	1.477	1.474	1.470	1.467	45
50	1.496	1.483	1.478	1.475	1.473	1.468	1.466	45
55	1.494	1.482	1.476	1.473	1.471	1.467	1.464	45
60	1.492	1.480	1.474	1.472	1.469	1.465	1.462	45
65	1.490	1.478	1.472	1.470	1.467	1.463	1.460	45
70	1.488	1.476	1.471	1.468	1.466	1.461	1.459	45
75	1.486	1.474	1.469	1.466	1.464	1.460	1.457	45
80	1.484	1.473	1.467	1.464	1.462	1.458	1.455	45

Refractive Index 2PP Solid

Print set	T [˚C]	Wavelength [nm]							Abbe number
		405	479.3	546.1	589.3	643.8	780	950	
25x Solid (ITO)	20	1.535	1.522	1.517	1.514	1.511	1.507	1.504	48
25x Shell (ITO)	20	1.538	1.522	1.516	1.515	1.512	1.507	1.503	48

Appendix B: Photos from VHX-7000 Microscope

Print 1

Taken on April 14th, 2022

Print 2

Taken on April 14th, 2022

Tilt angle: 0
Magnification: X1000.0

100.00μm

Tilt angle: 0
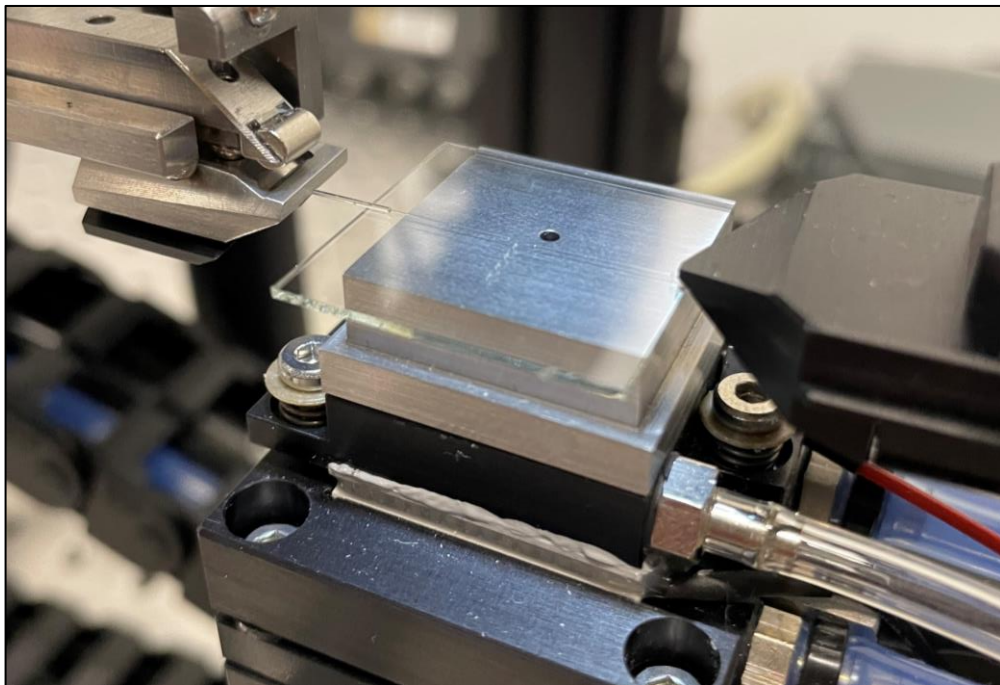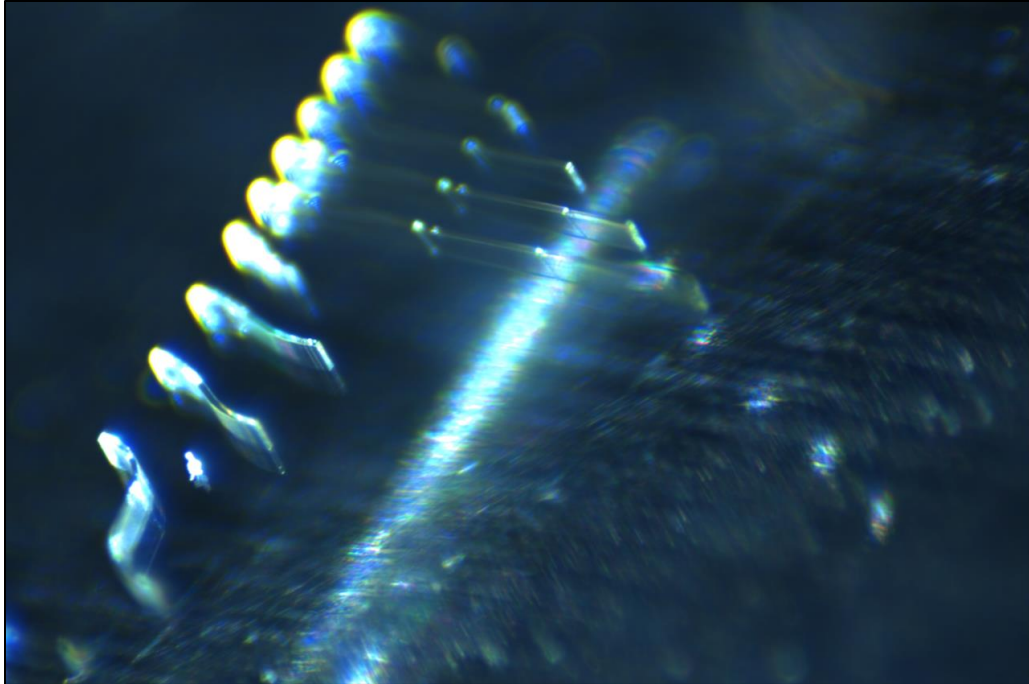Magnification: X2500.0

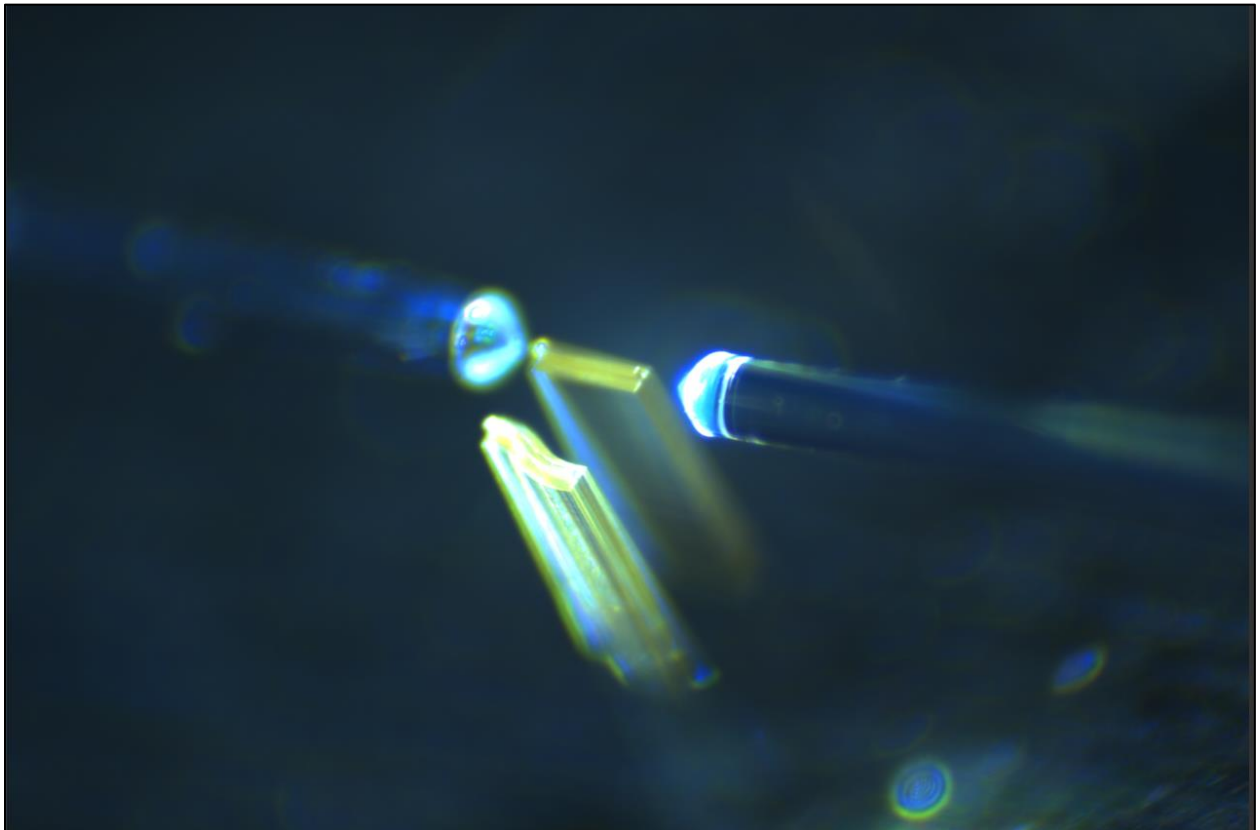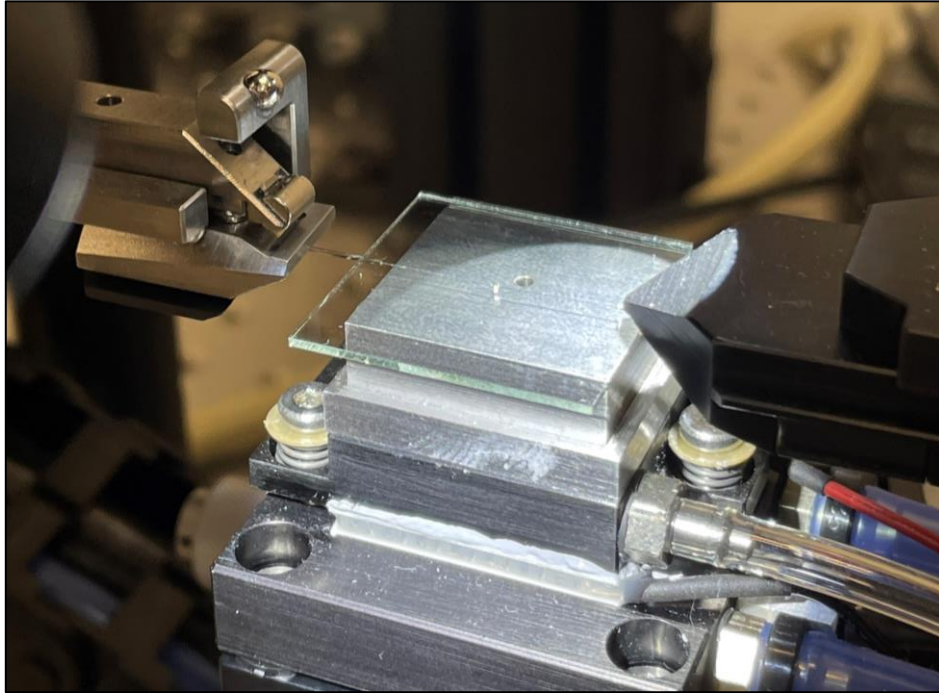10.00μm
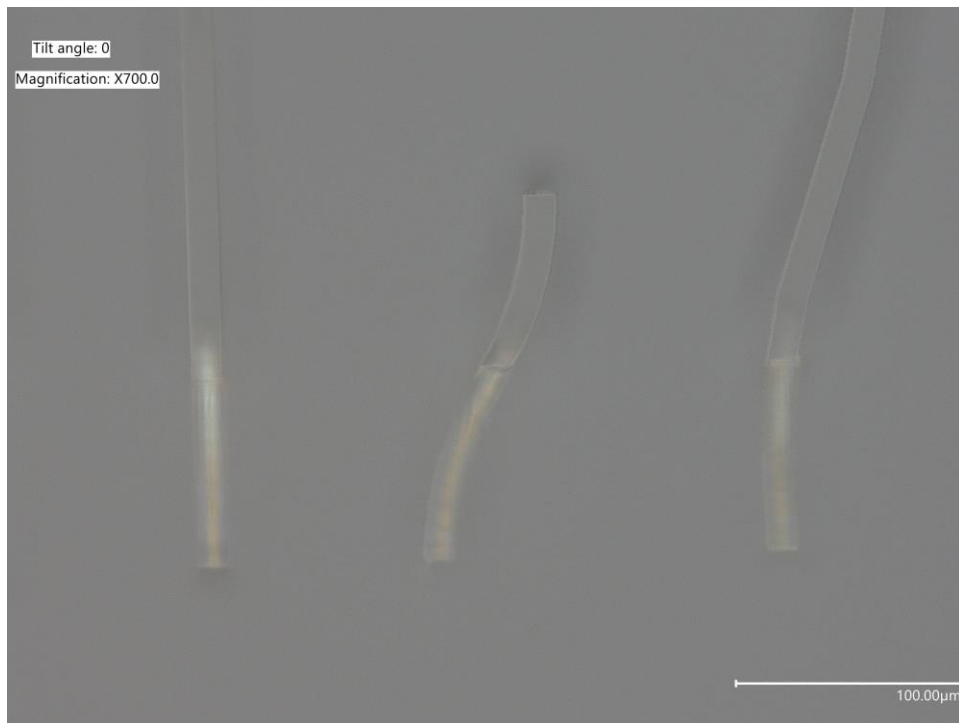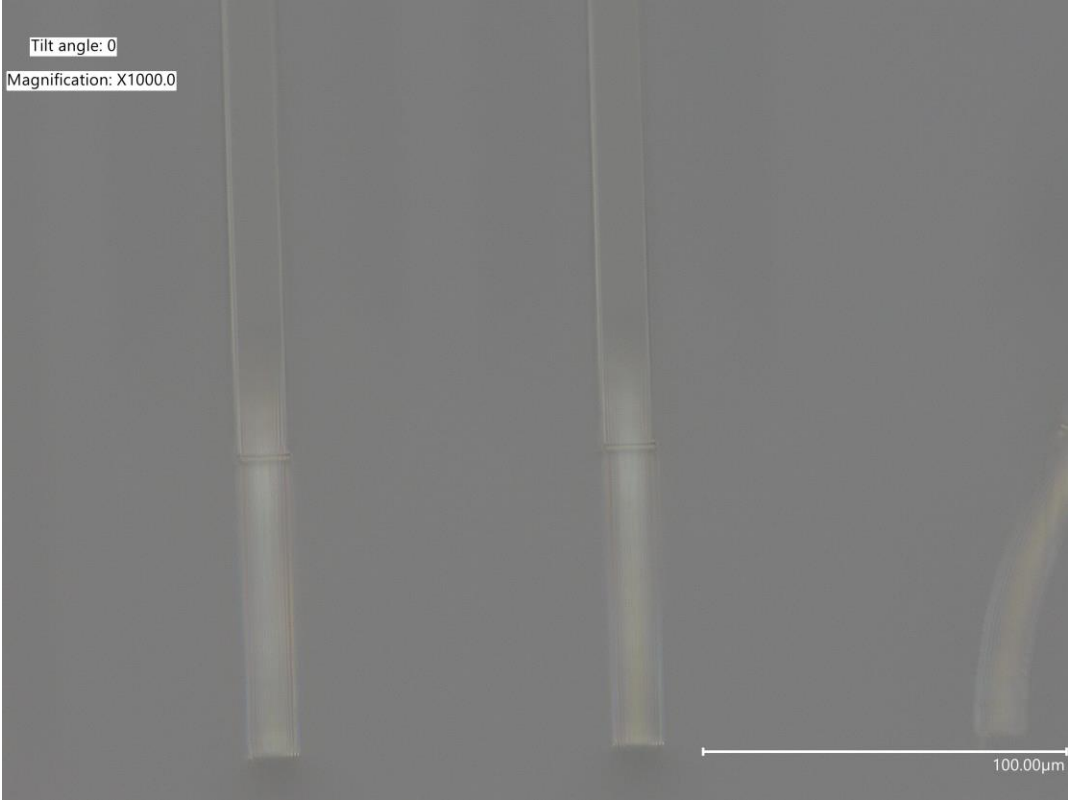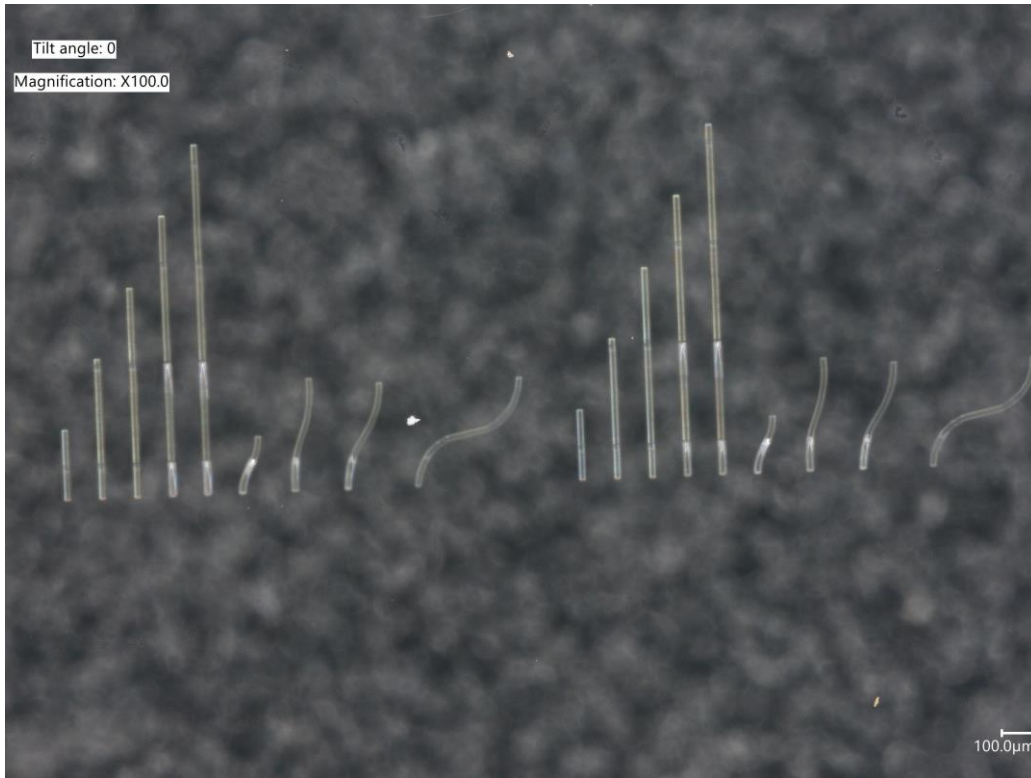
Print 3

Taken on April 7th, 2022
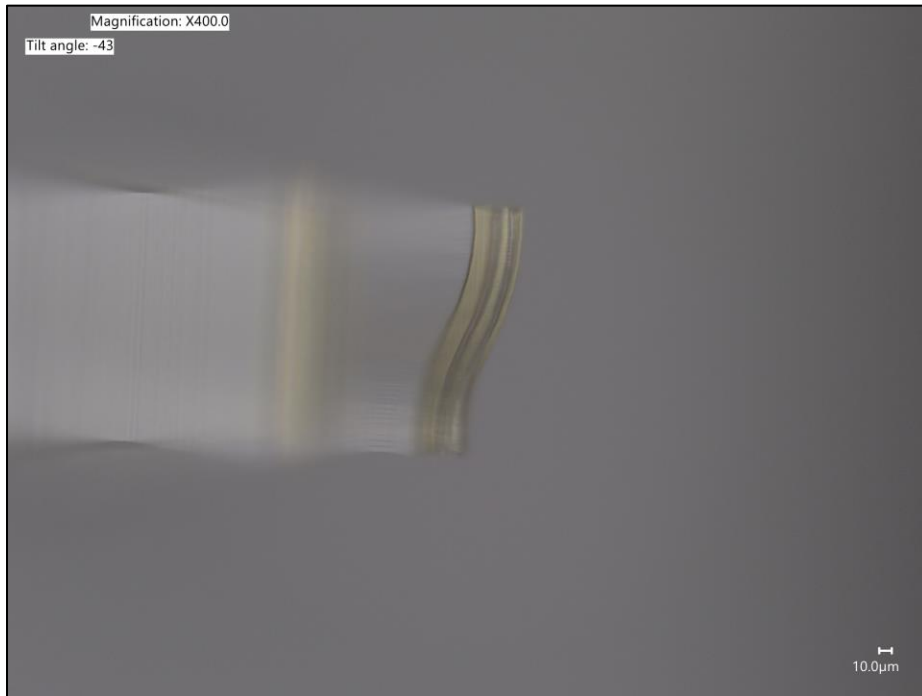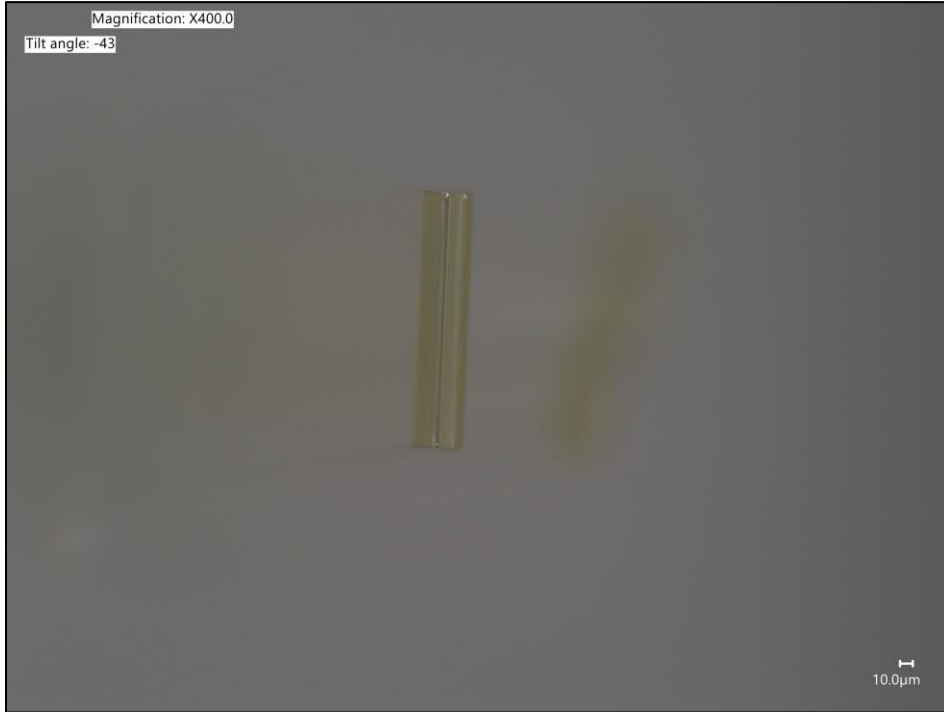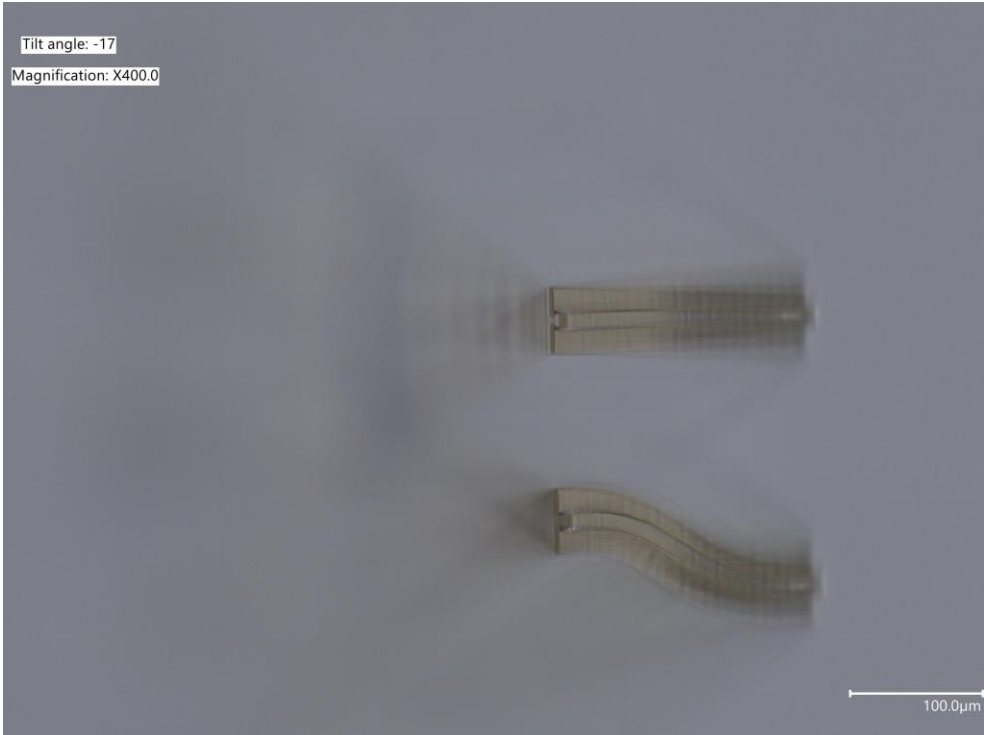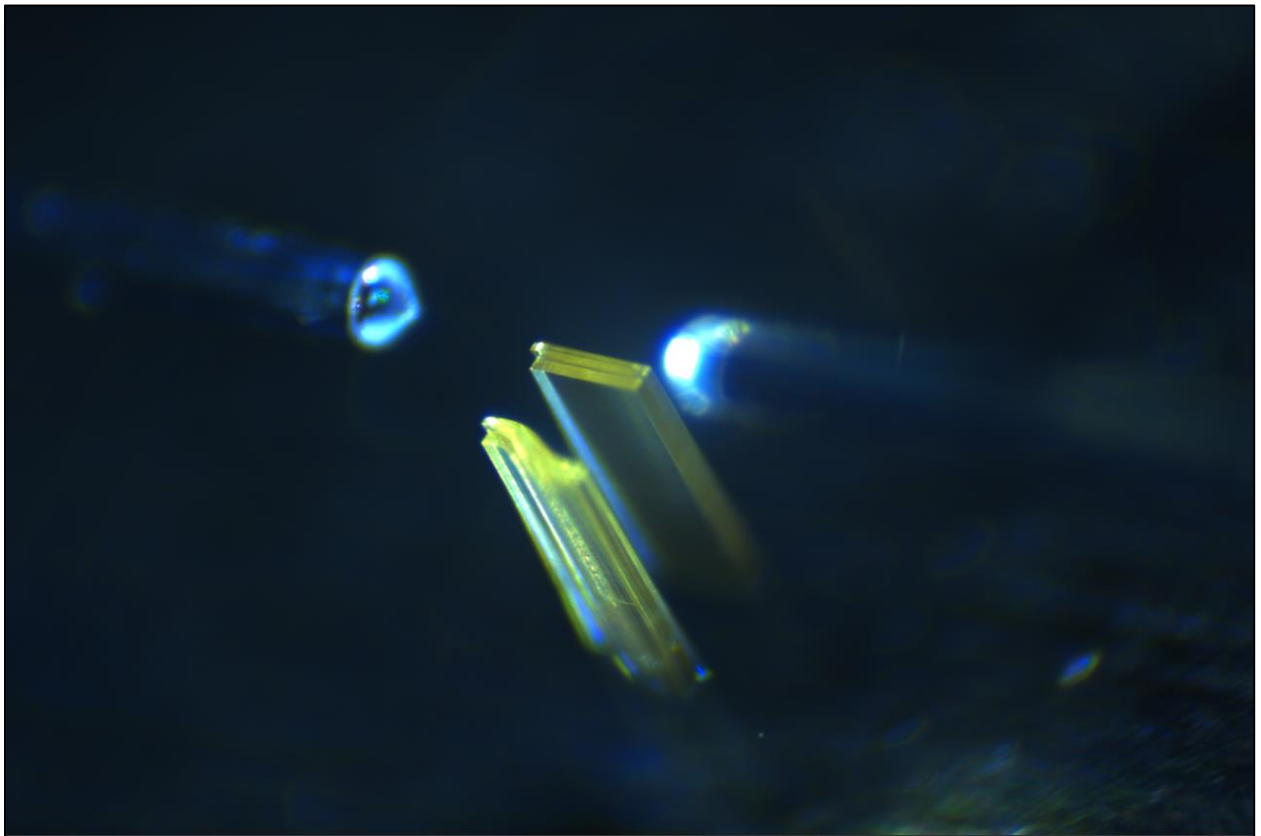
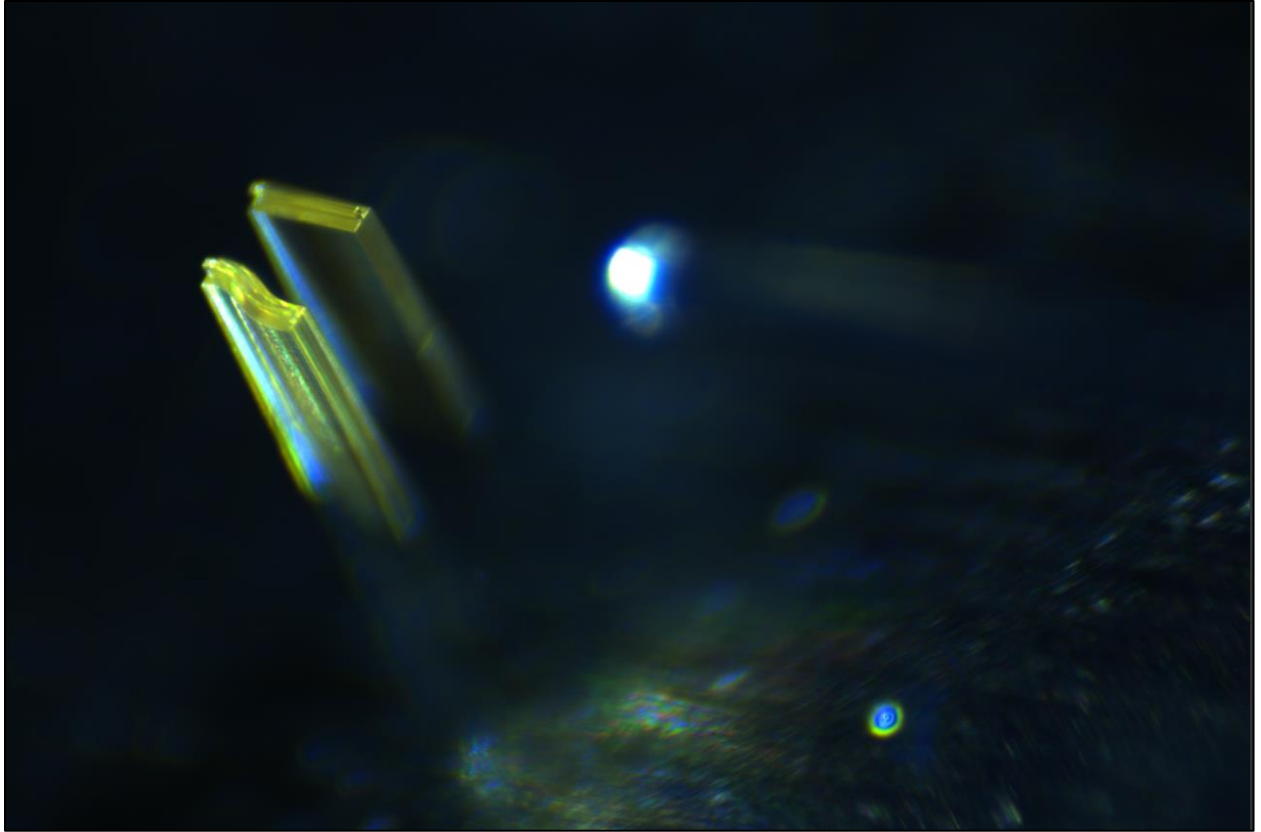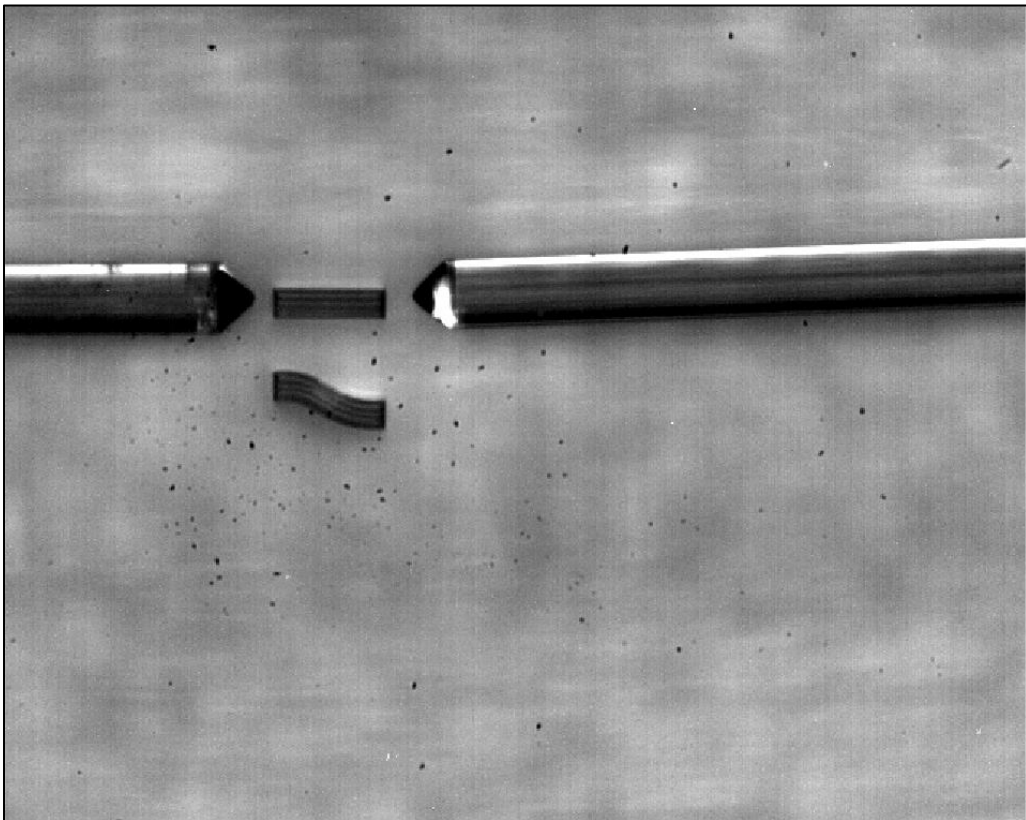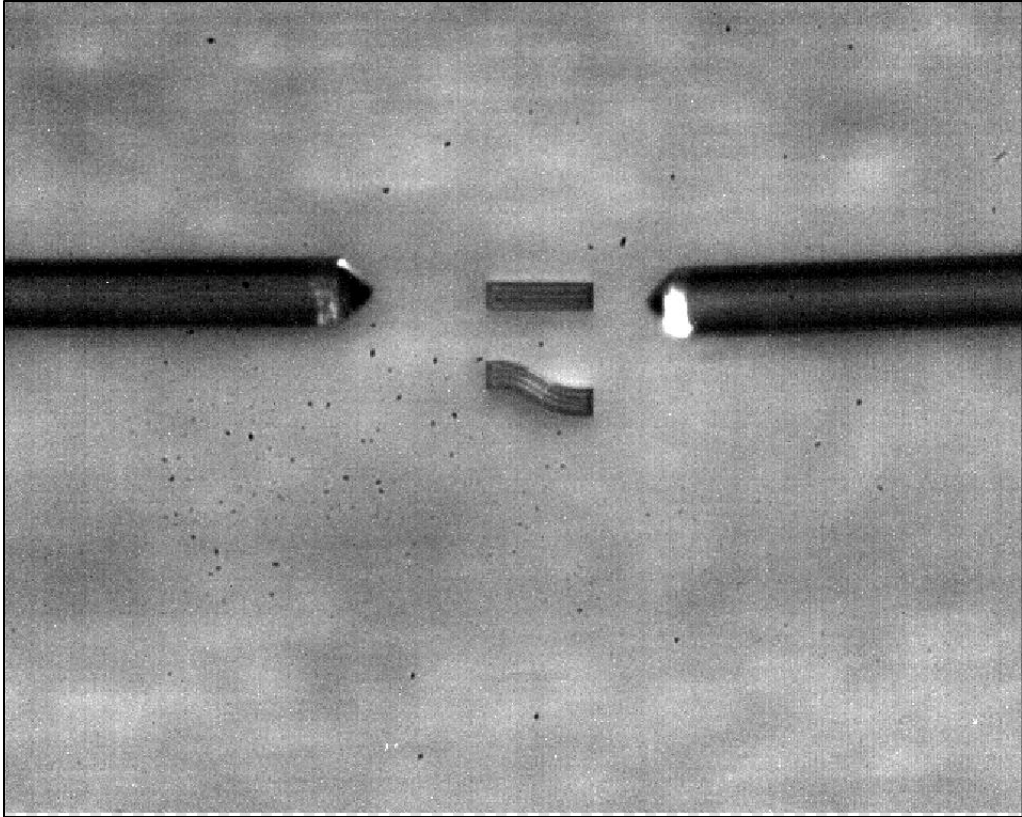# Appendix C: Gallery of 3D Print Photos on Probe Station
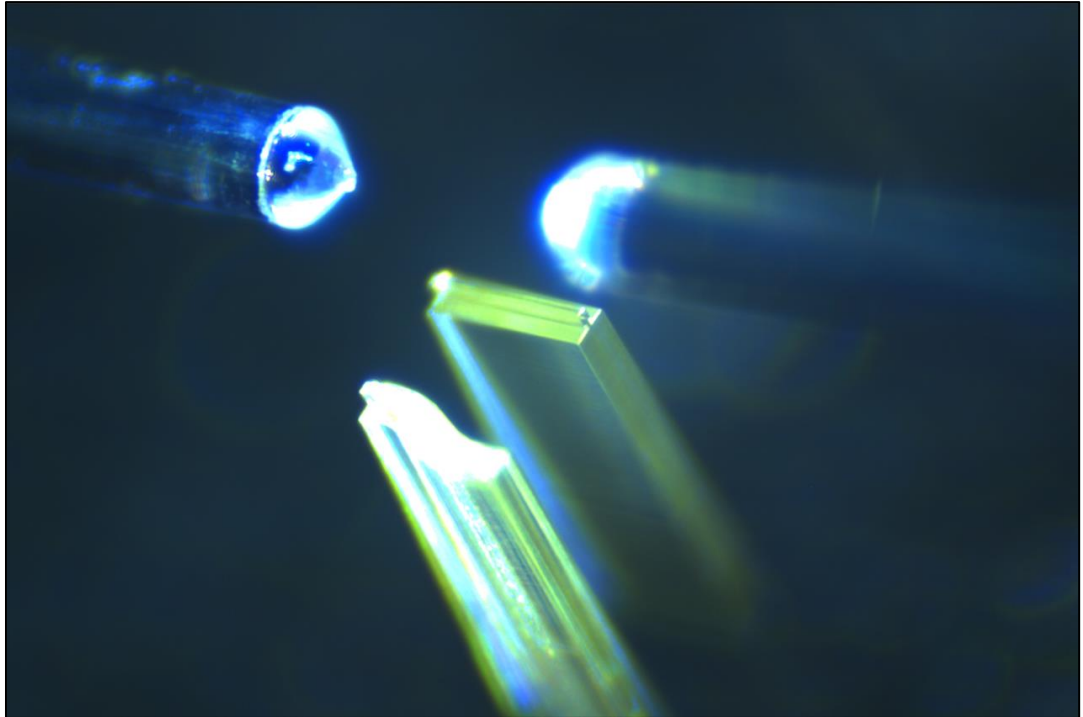
Print 2

Taken on March 31st, 2022
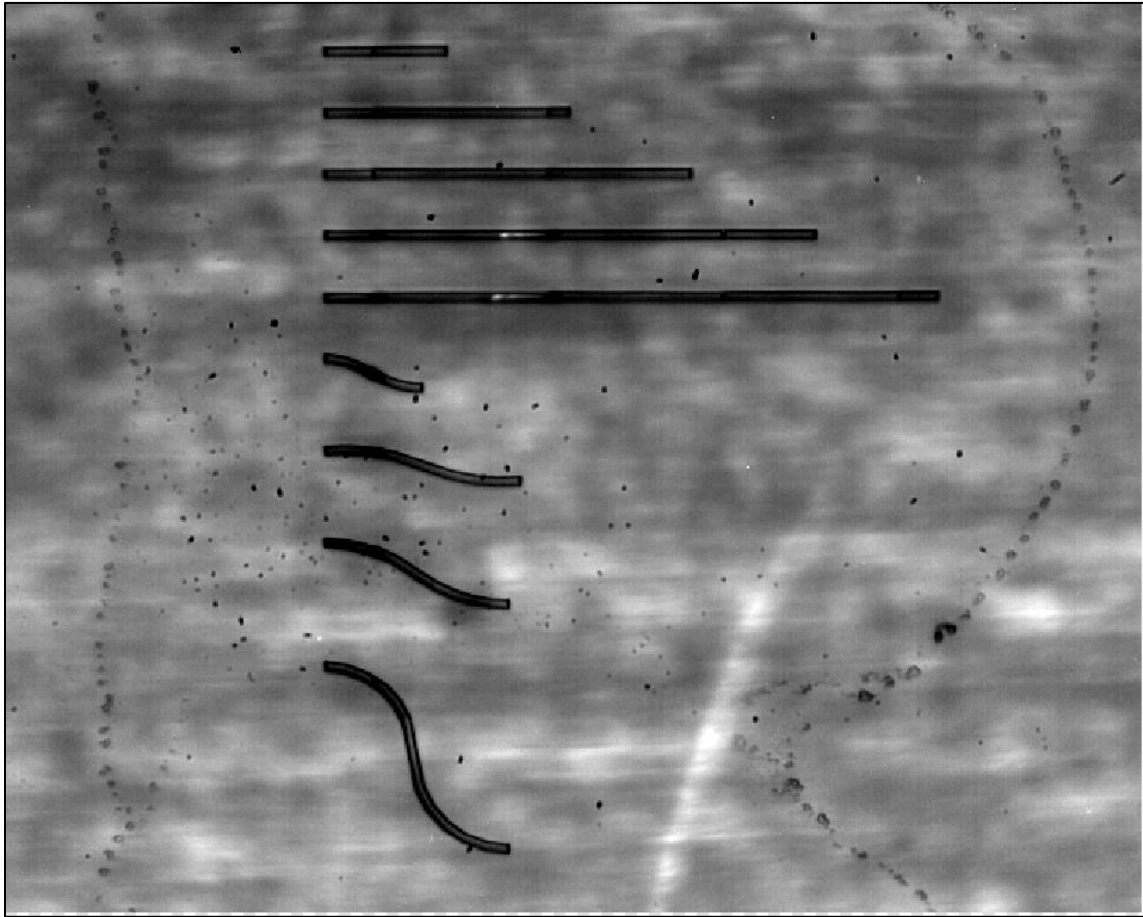
Print 3

Taken on April 05th 2022

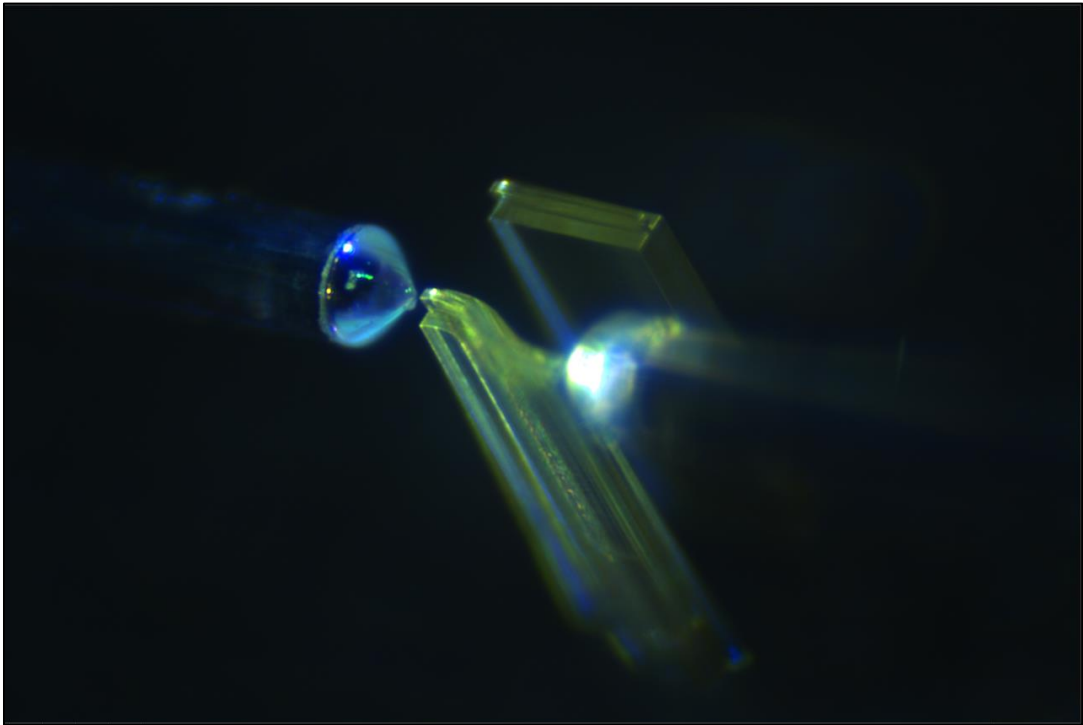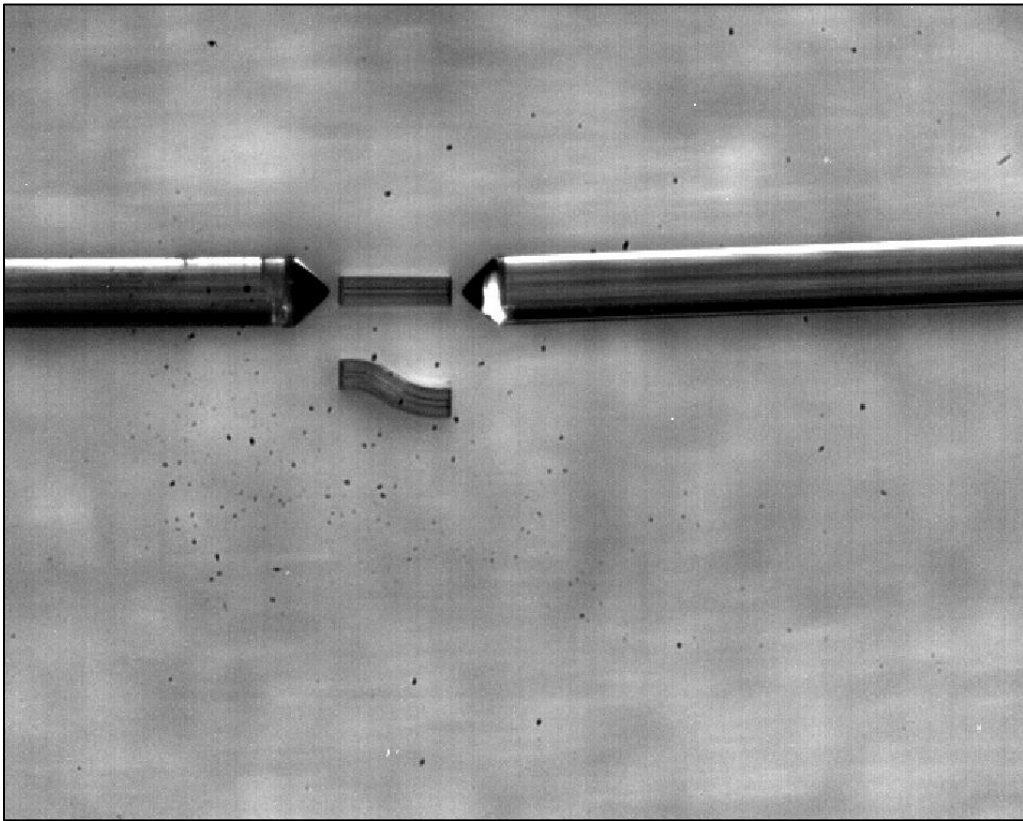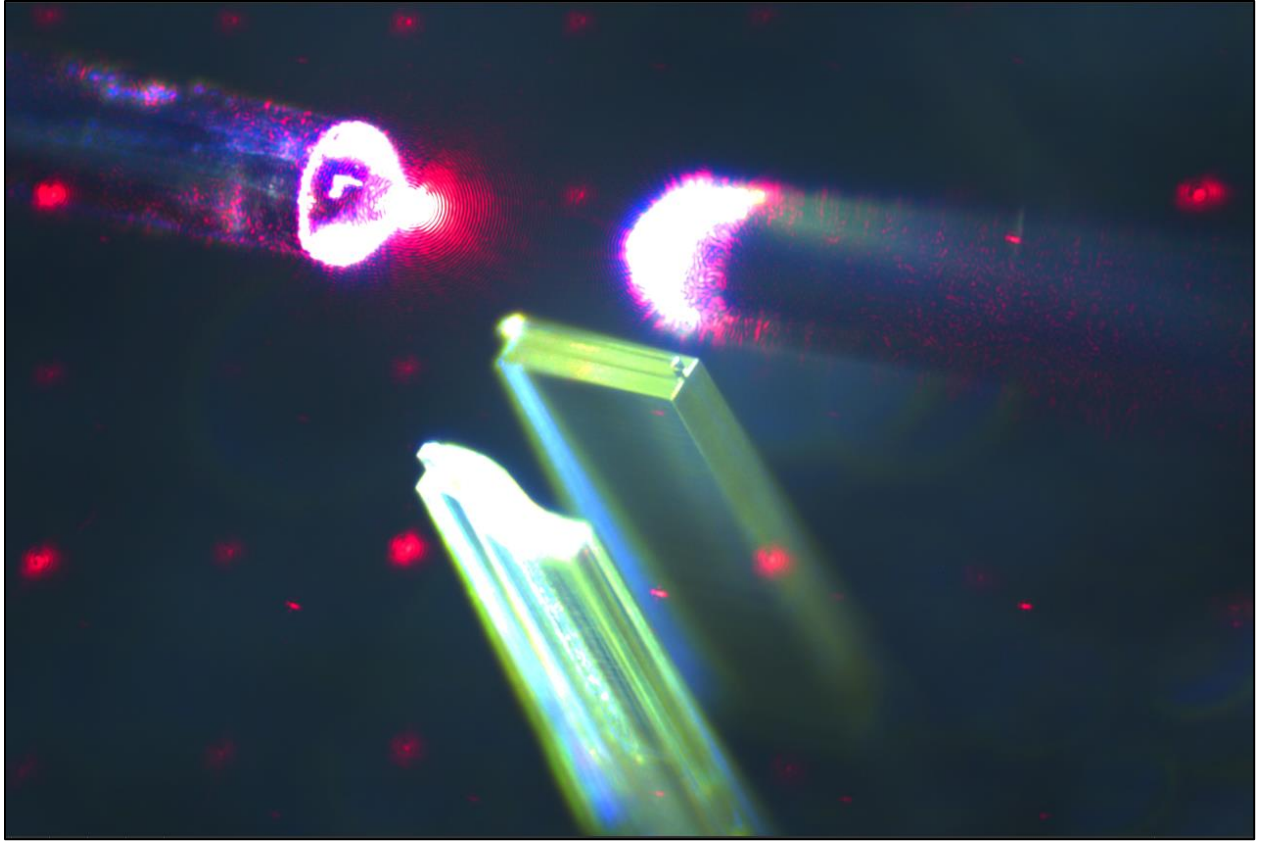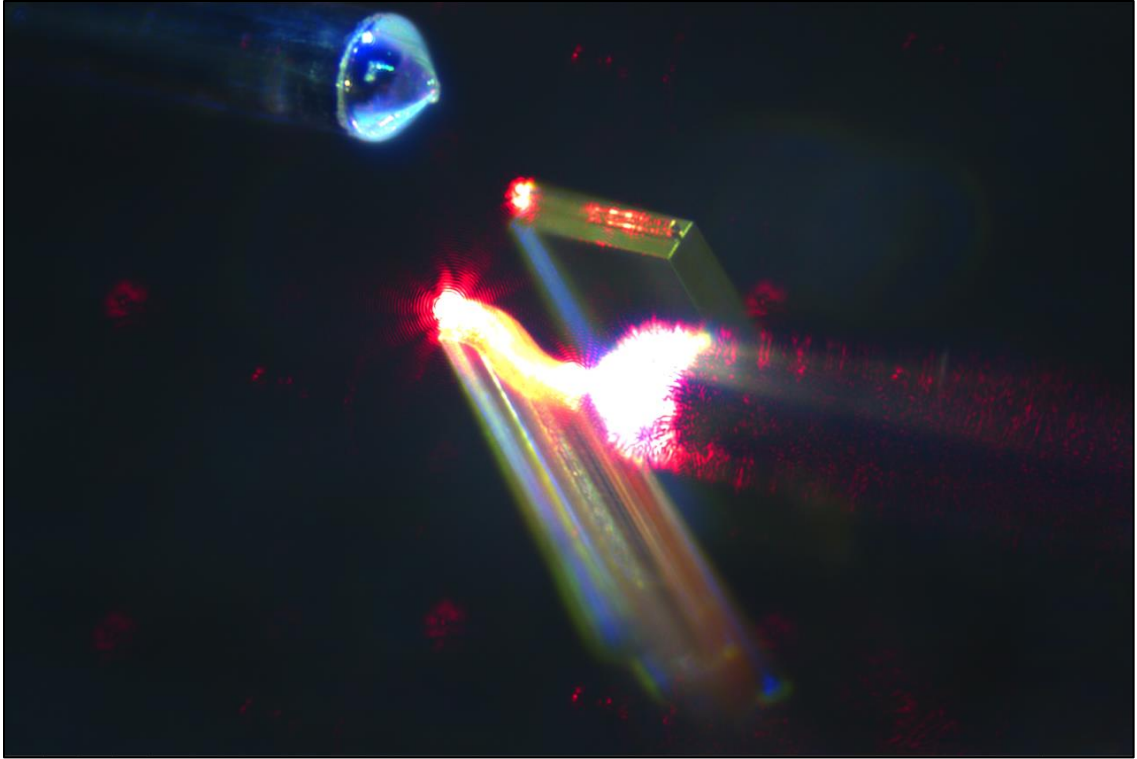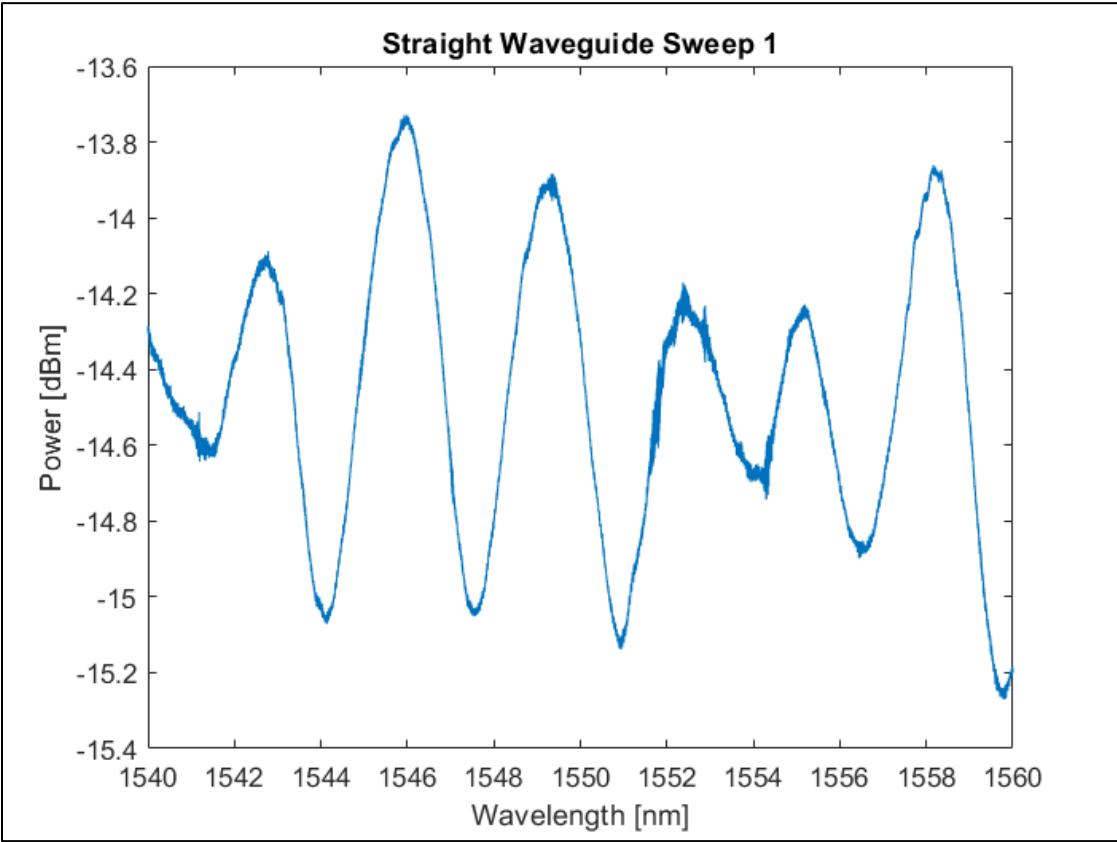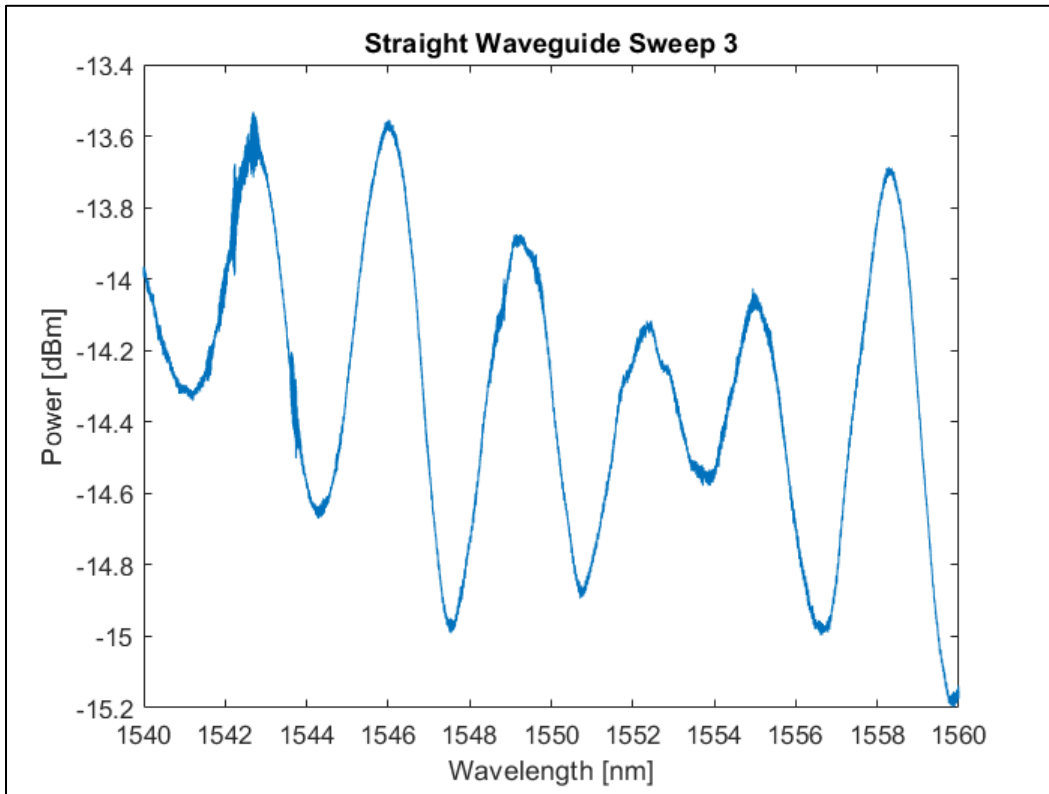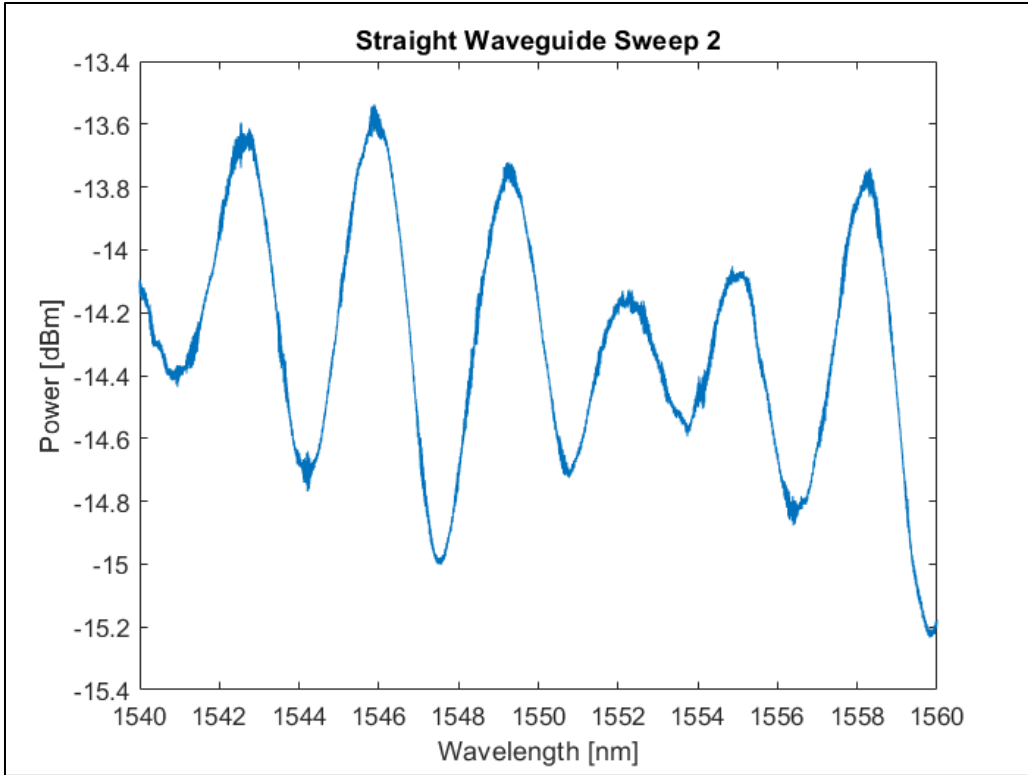Taken on April 05th 2022
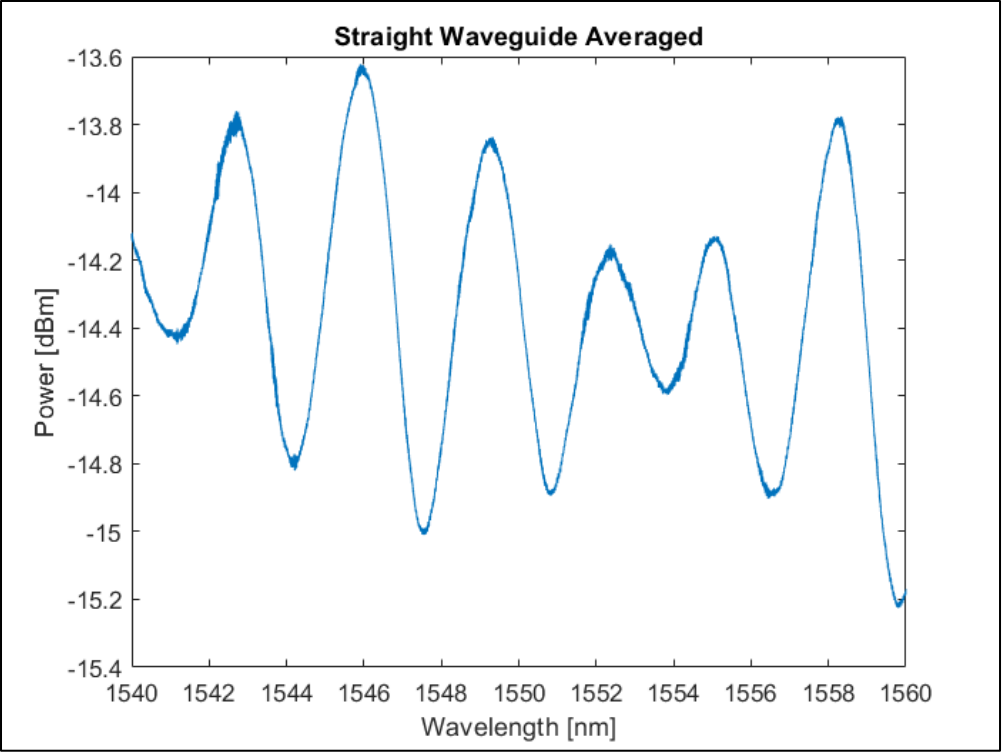
Taken on April 6th 2022

Appendix D: Data Graphs from Testing

Data was taken on April 06, 2022

Straight Waveguide

Waveguide Sweeps

Straight Waveguide Sweep 2

Straight Waveguide Sweep 3

Air Coupling Sweeps

S Bend Waveguide

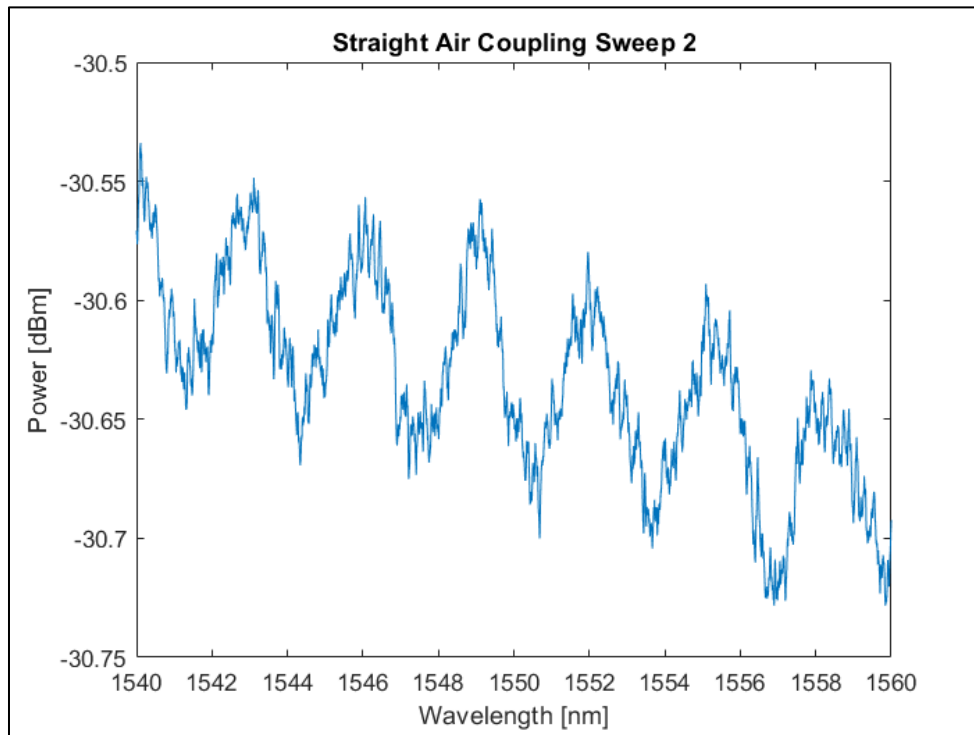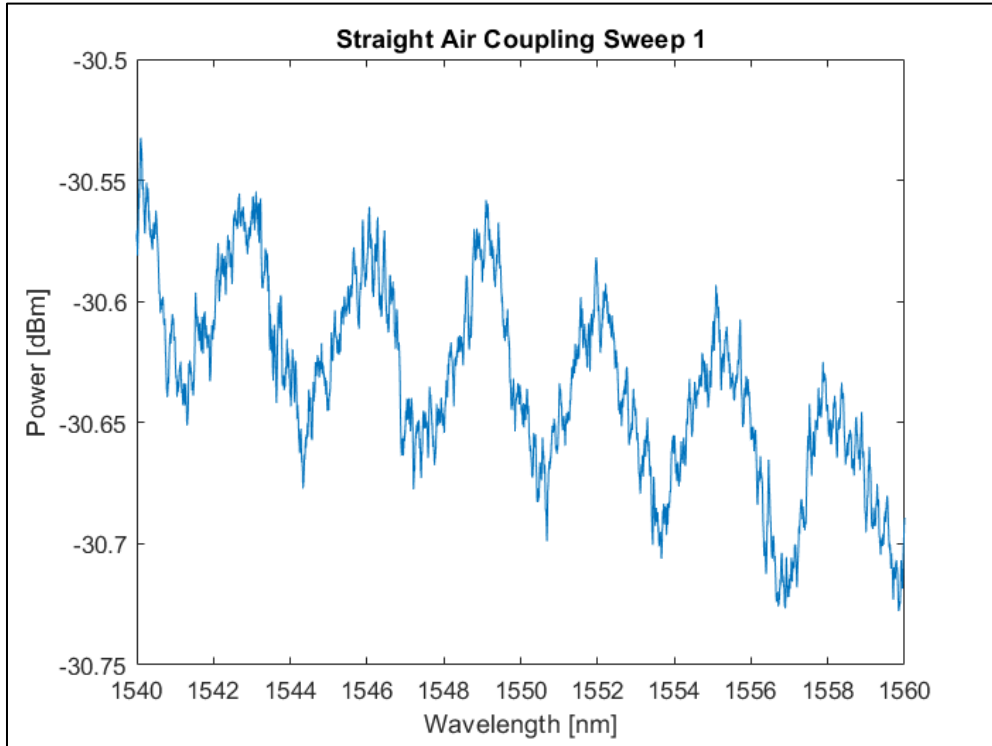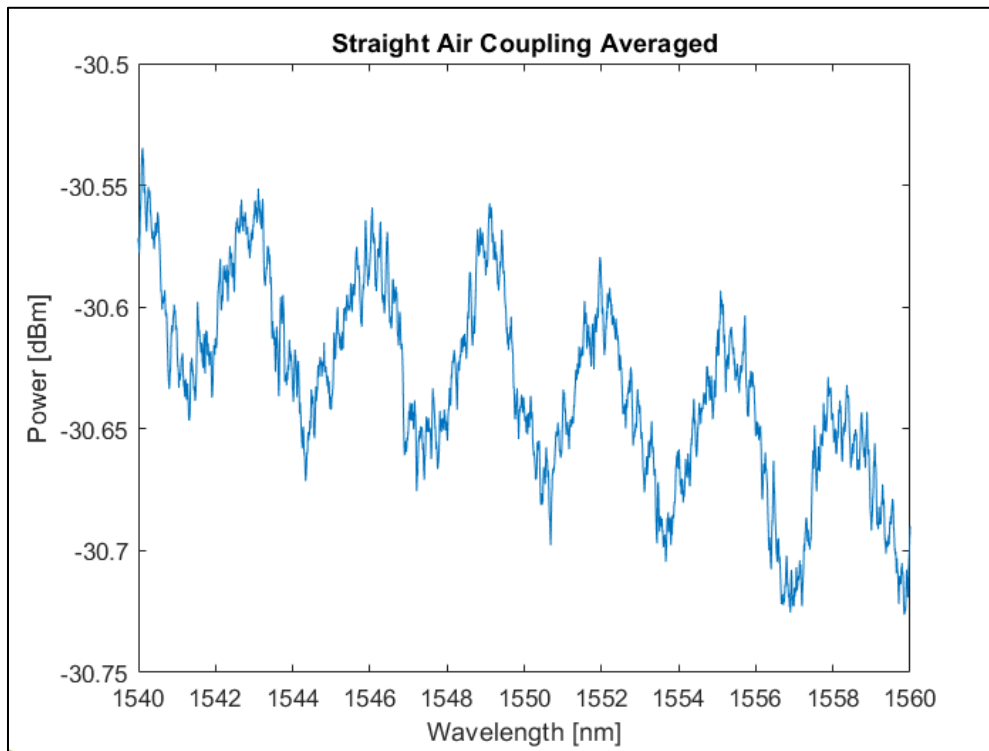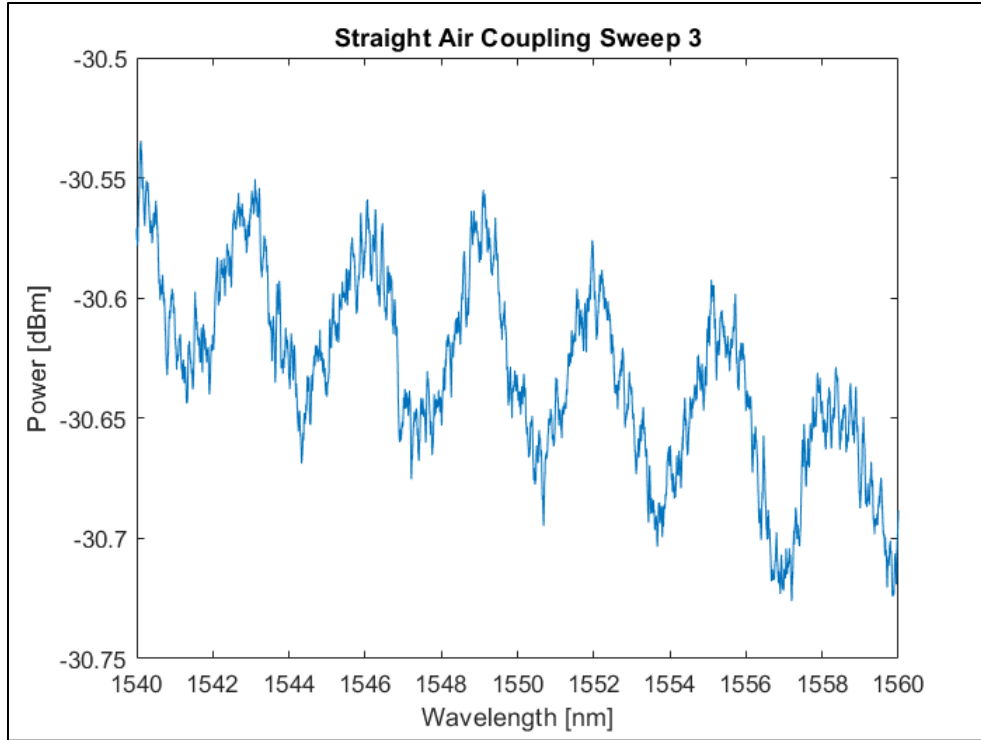Waveguide Sweeps

Air Coupling Sweeps

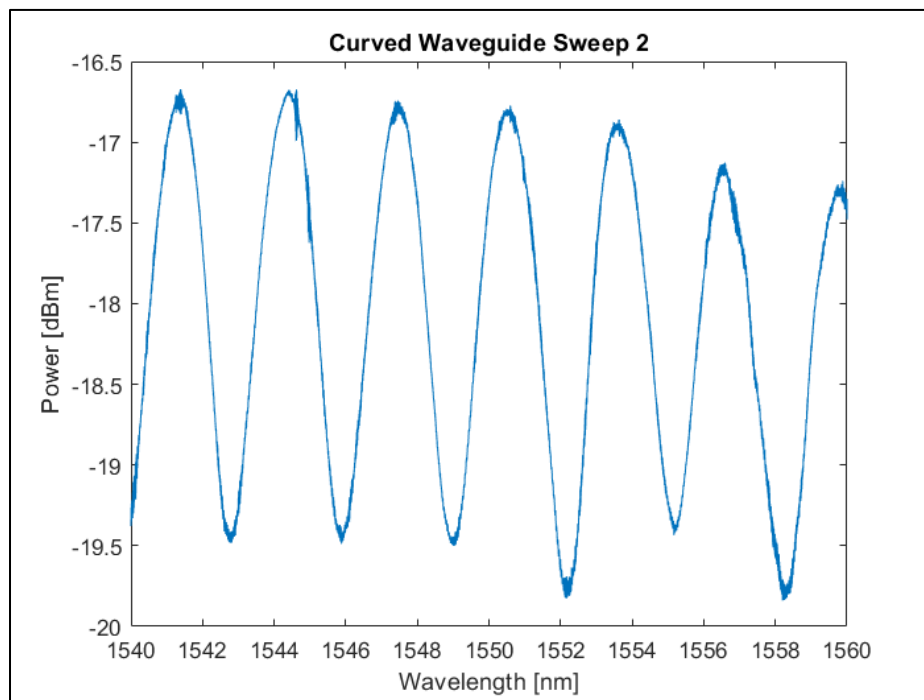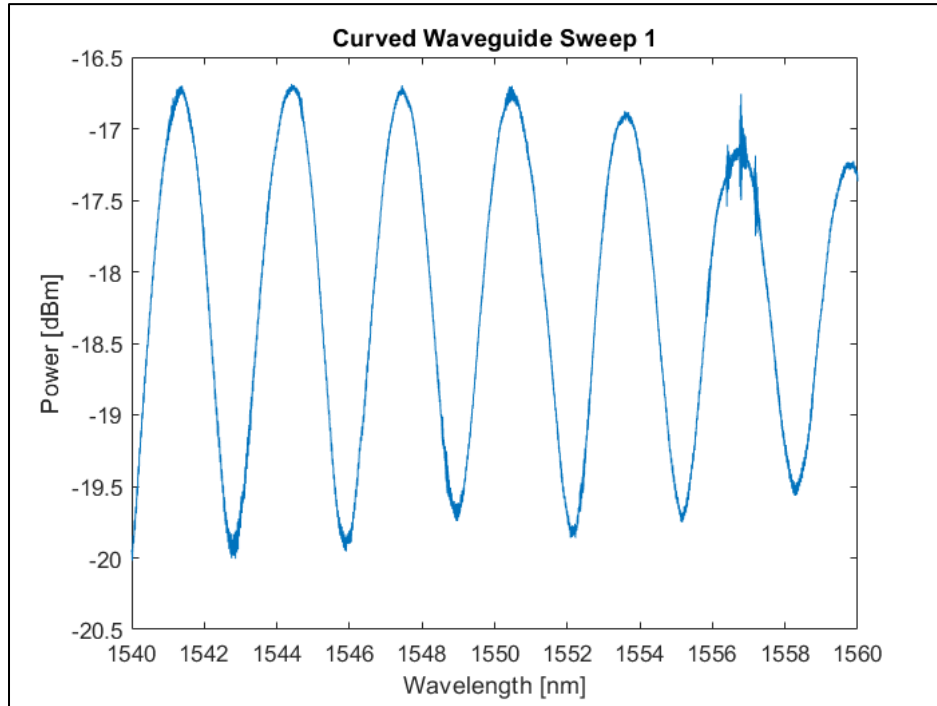Curved Air Coupling Sweep 3

Curved Air Coupling Averaged
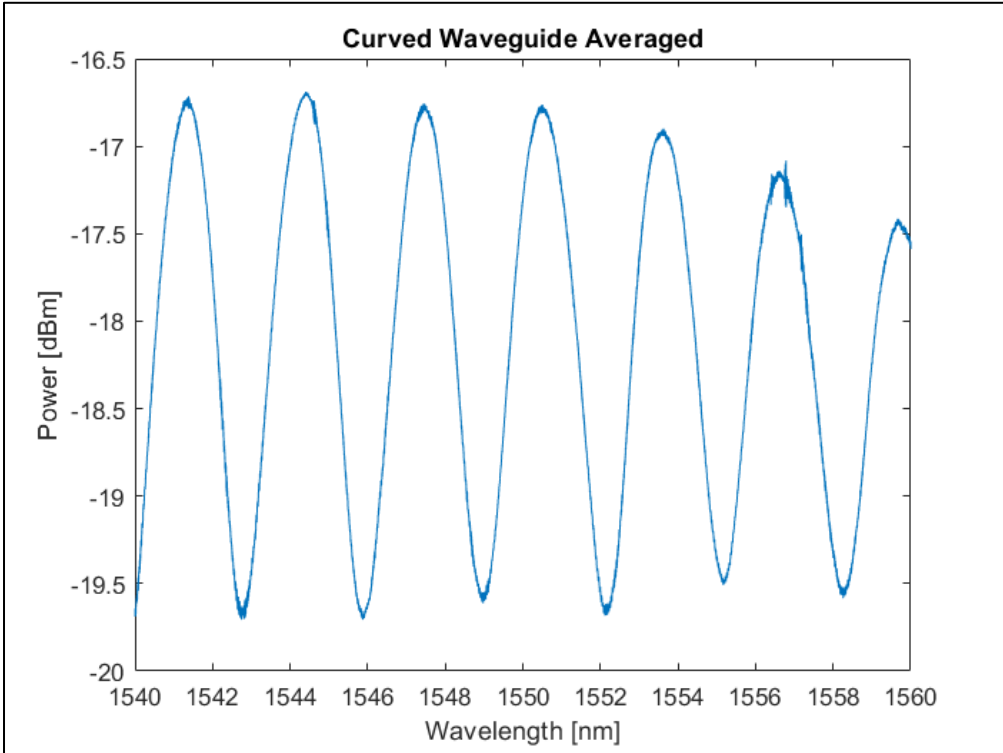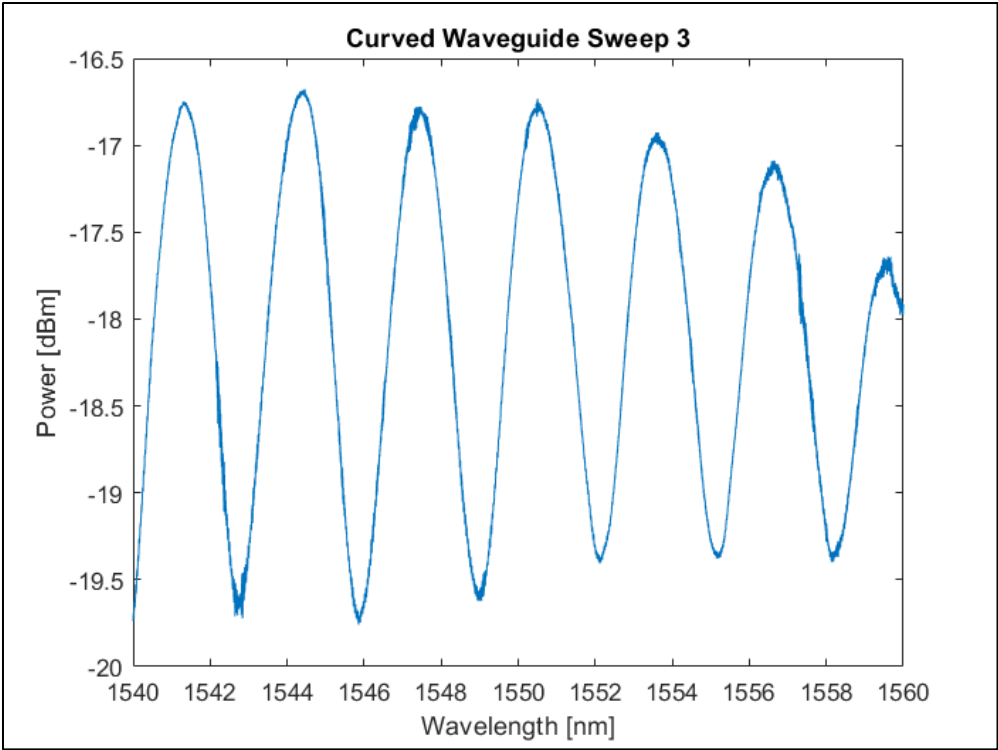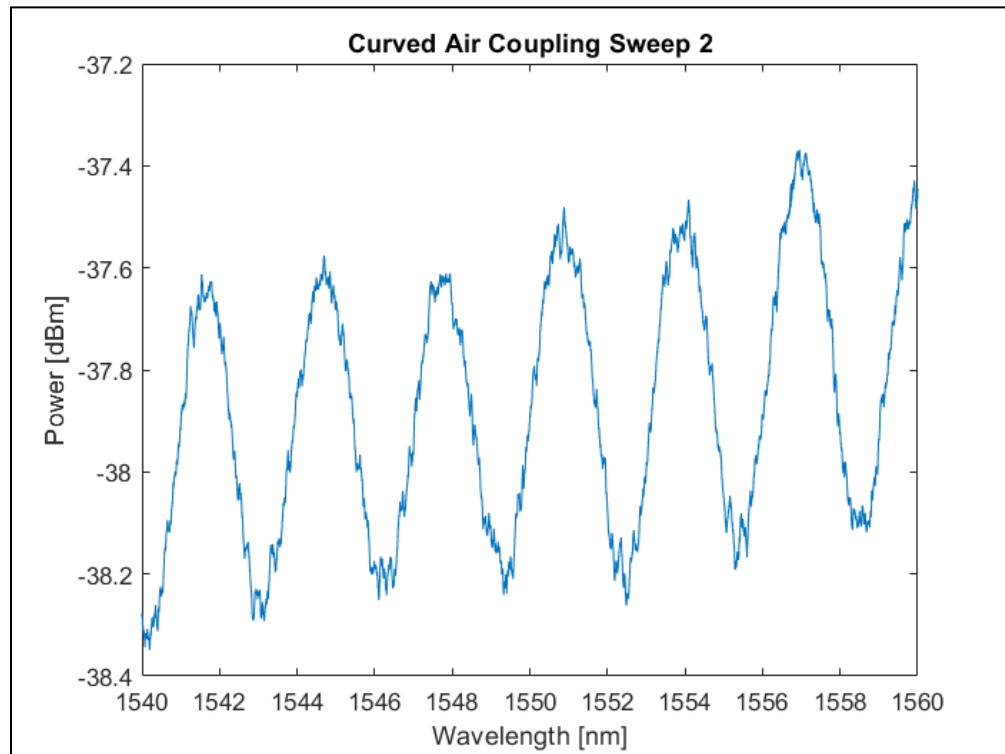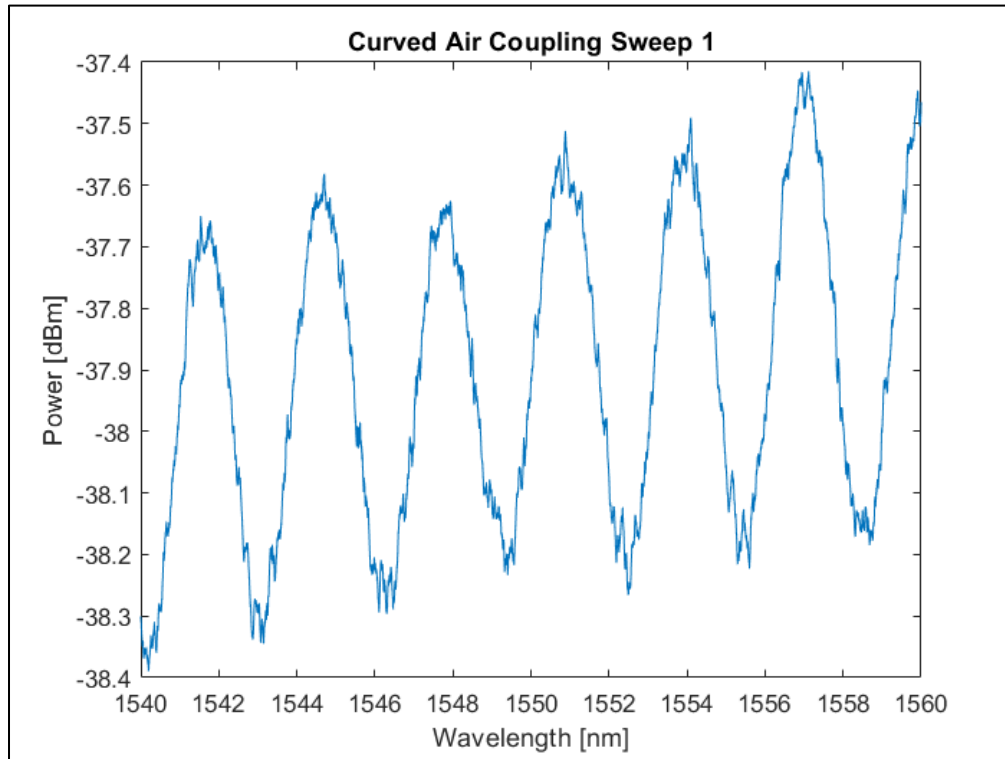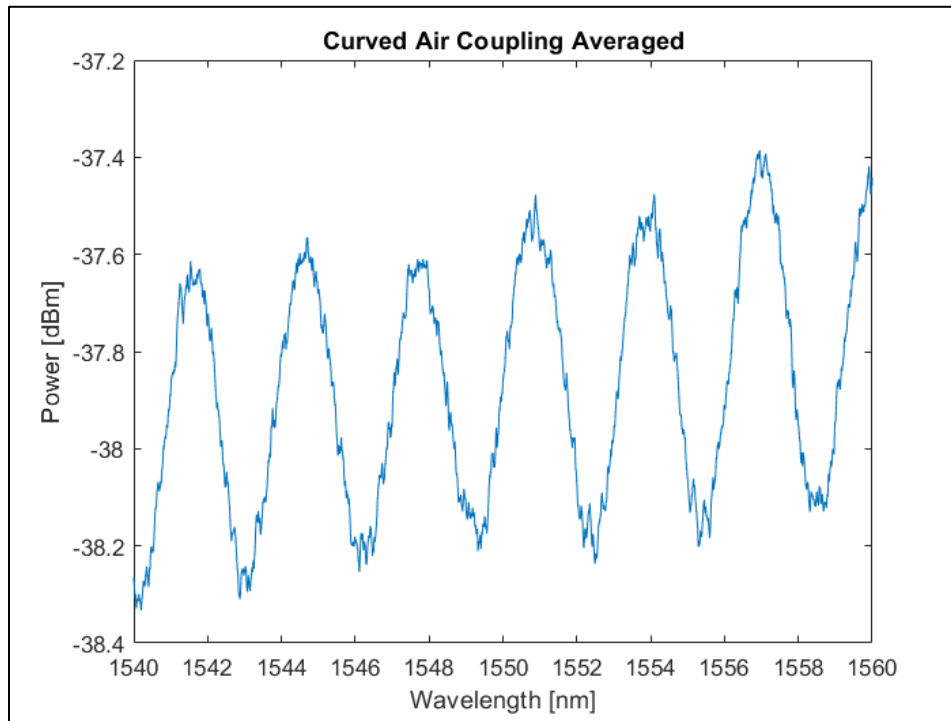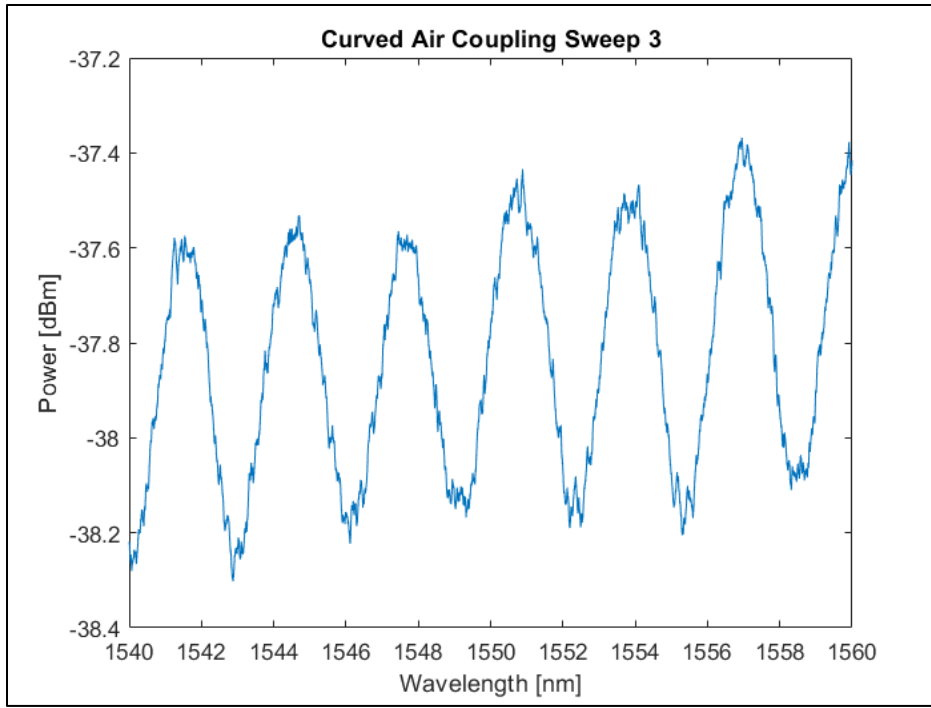
References

[1]   J. Bardeen and W. H. Brattain, "The Transistor, A Semi-Conductor Triode," *Physical Review,* vol. 74, no. 2, pp. 230-231, 07/15/ 1948, doi: 10.1103/PhysRev.74.230.

[2]   J. S. Kilby, "Miniaturized Electronic Circuits," United States Patent 3138743, June 23, 1964, 1964.

[3]   R. N. Noyce, "Semiconductor Device-and-Lead Structure," United States Patent 2,981,877, 1961.

[4]   F. Kish *et al.*, "System-On-Chip Photonic Integrated Circuits," *IEEE Journal of Selected Topics in Quantum Electronics,* vol. PP, pp. 1-1, 06/22 2017, doi: 10.1109/JSTQE.2017.2717863.

[5]   R. N. Hall, G. E. Fenner, J. D. Kingsley, T. J. Soltys, and R. O. Carlson, "Coherent Light Emission From GaAs Junctions," *Physical Review Letters,* vol. 9, no. 9, pp. 366-368, 11/01/ 1962, doi: 10.1103/PhysRevLett.9.366.

[6]   N. H. Jr. and S. F. Bevacqua, "COHERENT (VISIBLE) LIGHT EMISSION FROM Ga(As1−xPx) JUNCTIONS," *Applied Physics Letters,* vol. 1, no. 4, pp. 82-83, 1962, doi: 10.1063/1.1753706.

[7]   S. E. Miller, "Integrated optics: An introduction," *The Bell System Technical Journal,* vol. 48, pp. 2059-2069, 1969.

[8]   G. Batra, R. Fletcher, K. Kasymaliev, A. Mahindroo, and N. Santhanam, "The next wave of innovation in photonics," *Advanced Electronics Insights*, June 28, 2021.

[9]   *Global Photonics Market - Forecasts from 2020 to 2025*. Research and Markets, 2020.

[10]   K. Amsalu and S. Palani, "A review on photonics and its applications," *Materials Today: Proceedings,* vol. 33, pp. 3372-3377, 2020/01/01/ 2020, doi: https://doi.org/10.1016/j.matpr.2020.05.184.

[11]   A. Einstein, "Zur Quantentheorie der Strahlung," *Physikalische Zeitschrift,* vol. 18, 1917.

[12]   R. Ladenburg, "Untersuchungen über die anomale Dispersion angeregter Gase," *Zeitschrift für Physik,* vol. 48, no. 1, pp. 15-25, 1928/01/01 1928, doi: 10.1007/BF01351571.

[13]   J. Hecht, "Short history of laser development," *Optical Engineering,* vol. 49, no. 9, p. 091002, 2010. [Online]. Available: https://doi.org/10.1117/1.3483597.

[14]   W. E. Lamb and R. C. Retherford, "Fine Structure of the Hydrogen Atom. Part I," *Physical Review,* vol. 79, no. 4, pp. 549-572, 08/15/ 1950, doi: 10.1103/PhysRev.79.549.

[15]   M. Bertolotti, *Masers and lasers: an historical approach*. Crc Press, 2015.

[16]   J. P. Gordon, H. J. Zeiger, and C. H. Townes, "Molecular Microwave Oscillator and New Hyperfine Structure in the Microwave Spectrum of NH3," *Physical Review,* vol. 95, no. 1, pp. 282-284, 07/01/ 1954, doi: 10.1103/PhysRev.95.282.

[17]   J.-I. Nishizawa, "Extension of frequencies from maser to laser," *Proceedings of the Japan Academy, Series B,* vol. 85, p. 454, January 01, 2009 2009, doi: 10.2183/pjab.85.454.

[18]   A. L. Schawlow and C. H. Townes, "Infrared and Optical Masers," *Physical Review,* vol. 112, no. 6, pp. 1940-1949, 12/15/ 1958, doi: 10.1103/PhysRev.112.1940.

[19]   A. Javan, "Possibility of Production of Negative Temperature in Gas Discharges," *Physical Review Letters,* vol. 3, no. 2, pp. 87-89, 07/15/ 1959, doi: 10.1103/PhysRevLett.3.87.

[20]   T. H. Maiman, "Optical and Microwave-Optical Experiments in Ruby," *Physical Review Letters,* vol. 4, no. 11, pp. 564-566, 06/01/ 1960, doi: 10.1103/PhysRevLett.4.564.

[21]   T. H. Maiman, "Stimulated Optical Radiation in Ruby," *Nature,* vol. 187, no. 4736, pp. 493-494, 1960/08/01 1960, doi: 10.1038/187493a0.
[22]   T. H. Maiman, "Stimulated Optical Emission in Fluorescent Solids. I. Theoretical Considerations," *Physical Review,* vol. 123, no. 4, pp. 1145-1150, 08/15/ 1961, doi: 10.1103/PhysRev.123.1145.
[23]   U. o. M. F. P. A. S. R. H. Ann Arbor Conference on Optical Pumping, "The Ann Arbor conference on optical pumping : the University of Michigan, June 15 through June 18, 1959," Ann Arbor, 1959: [publisher not identified].
[24]   K. C. Kao and G. A. Hockham, "Dielectric-fibre surface waveguides for optical frequencies," *Proceedings of the Institution of Electrical Engineers*, vol. 113, no. 7*,* pp. 1151-1158. [Online]. Available: https://digital-library.theiet.org/content/journals/10.1049/piee.1966.0189
[25]   N. Zlatanov, *Introduction to Fiber Optics Theory*. 2017.
[26]   J. Crisp and B. Elliott, *Introduction to Fiber Optics (Third Edition)*. Oxford: Newnes, 2005.
[27]   M. Azadeh, *Fiber Optics Engineering*. Springer US, 2009.
[28]   C.-L. Chen, *Foundations for guided-wave optics*. 2006.
[29]   S. K. Selvaraja and P. Sethi, "Review on Optical Waveguides," 2018.
[30]   C. Jain *et al.*, "Hollow Core Light Cage: Trapping Light Behind Bars," *ACS Photonics,* vol. 6, no. 3, pp. 649-658, 2019/03/20 2019, doi: 10.1021/acsphotonics.8b01428.
[31]   B. Jang, J. Gargiulo, R. F. Ando, A. Lauri, S. A. Maier, and M. A. Schmidt, "Light guidance in photonic band gap guiding dual-ring light cages implemented by direct laser writing," *Opt. Lett.,* vol. 44, no. 16, pp. 4016-4019, 2019/08/15 2019, doi: 10.1364/OL.44.004016.
[32]   J. Kim *et al.*, "The Optofluidic Light Cage – On-Chip Integrated Spectroscopy Using an Antiresonance Hollow Core Waveguide," *Analytical Chemistry,* vol. 93, no. 2, pp. 752-760, 2021/01/19 2021, doi: 10.1021/acs.analchem.0c02857.
[33]   D. O. Carvalho, L. R. P. Kassab, V. D. Del Cacho, D. M. da Silva, and M. I. Alayo, "A review on pedestal waveguides for low loss optical guiding, optical amplifiers and nonlinear optics applications," *Journal of Luminescence,* vol. 203, pp. 135-144, 2018/11/01/ 2018, doi: https://doi.org/10.1016/j.jlumin.2018.06.037.
[34]   R. Halir *et al.*, "Waveguide sub-wavelength structures: a review of principles and applications," *Laser & Photonics Reviews,* vol. 9, no. 1, pp. 25-49, 2015, doi: https://doi.org/10.1002/lpor.201400083.
[35]   L. Sun, Y. Zhang, Y. He, H. Wang, and Y. Su, "Subwavelength structured silicon waveguides and photonic devices," *Nanophotonics,* vol. 9, no. 6, pp. 1321-1340, 2020, doi: doi:10.1515/nanoph-2020-0070.
[36]   M. Smit, K. Williams, and J. v. d. Tol, "Past, present, and future of InP-based photonic integration," *APL Photonics,* vol. 4, no. 5, p. 050901, 2019, doi: 10.1063/1.5087862.
[37]   M. Smit *et al.*, "An introduction to InP-based generic integration technology," *Semiconductor Science and Technology,* vol. 29, no. 8, p. 083001, 2014/06/01 2014, doi: 10.1088/0268-1242/29/8/083001.
[38]   K. Williams, "InP Integrated Photonics: State of the Art and Future Directions," in *Optical Fiber Communication Conference*, Los Angeles, California, 2017/03/19 2017: Optical Society of America, in OSA Technical Digest (online), p. M3B.5, doi:

10.1364/OFC.2017.M3B.5. [Online]. Available: http://www.osapublishing.org/abstract.cfm?URI=OFC-2017-M3B.5

[39]   Y. Jiao *et al.*, "InP membrane integrated photonics research," *Semiconductor Science and Technology,* vol. 36, no. 1, p. 013001, 2020/01/01 2020, doi: 10.1088/1361-6641/abcadd.

[40]   S. Y. Siew *et al.*, "Review of Silicon Photonics Technology and Platform Development," *Journal of Lightwave Technology,* vol. 39, no. 13, pp. 4374-4389, 2021, doi: 10.1109/JLT.2021.3066203.

[41]   S. Meister *et al.*, "Photonic Integrated Circuits for Optical Communication," *Optik & Photonik,* vol. 7, no. 2, pp. 59-62, 2012, doi: https://doi.org/10.1002/opph.201290052.

[42]   F. A. Kish, "The past, present, and future of photonic integrated circuits in optical communications," presented at the 73rd Annual Device Research Conference (DRC), Columbus, OH, USA, 2015.

[43]   I. P. Kaminow, "Optical Integrated Circuits: A Personal Perspective," *Journal of Lightwave Technology,* vol. 26, no. 9, pp. 994-1004, 2008, doi: 10.1109/JLT.2008.922149.

[44]   H. Sasaki, "Development of Silicon Photonics Integrated Circuits for Next Generation Optical Access Networks," in *2019 2nd International Symposium on Devices, Circuits and Systems (ISDCS)*, 6-8 March 2019 2019, pp. 1-4, doi: 10.1109/ISDCS.2019.8719259.

[45]   E. A. Rank *et al.*, "Toward optical coherence tomography on a chip: in vivo three-dimensional human retinal imaging using photonic integrated circuit-based arrayed waveguide gratings," *Light: Science & Applications,* vol. 10, no. 1, p. 6, 2021/01/05 2021, doi: 10.1038/s41377-020-00450-0.

[46]   R. Chandrasekar, Z. Lapin, A. Nichols, R. Braun, and A. Fountain, "Photonic integrated circuits for Department of Defense-relevant chemical and biological sensing applications: state-of-the-art and future outlooks," *Optical Engineering,* vol. 58, no. 2, p. 020901, 2019. [Online]. Available: https://doi.org/10.1117/1.OE.58.2.020901.

[47]   N. Anscombe, "Direct laser writing," *Nature Photonics,* vol. 4, no. 1, pp. 22-23, 2010/01/01 2010, doi: 10.1038/nphoton.2009.250.

[48]   Z.-L. Wu *et al.*, "Polymer-Based Device Fabrication and Applications Using Direct Laser Writing Technology," *Polymers,* vol. 11, no. 3, p. 553, 2019. [Online]. Available: https://www.mdpi.com/2073-4360/11/3/553.

[49]   A.-I. Bunea, N. del Castillo Iniesta, A. Droumpali, A. E. Wetzel, E. Engay, and R. Taboryski, "Micro 3D Printing by Two-Photon Polymerization: Configurations and Parameters for the Nanoscribe System," *Micro,* vol. 1, no. 2, pp. 164-180, 2021. [Online]. Available: https://www.mdpi.com/2673-8023/1/2/13.

[50]   C. R. Ocier *et al.*, "Direct laser writing of volumetric gradient index lenses and waveguides," *Light: Science & Applications,* vol. 9, no. 1, p. 196, 2020/12/03 2020, doi: 10.1038/s41377-020-00431-3.

[51]   T. Baghdasaryan, K. Vanmol, H. Thienpont, F. Berghmans, T. Geernaert, and J. Van Erps, "Design and two-photon direct laser writing of low-loss waveguides, tapers and S-bends," *Journal of Physics: Photonics,* vol. 3, 08/06 2021, doi: 10.1088/2515-7647/ac1b7d.

[52]   P. K. Gill and D. M. Marom, "Single Mode, Air-Cladded Optical Waveguides Supported by a Nano-Fin Fabricated with Direct Laser Writing," *Applied Sciences,* vol. 11, no. 14, p. 6327, 2021. [Online]. Available: https://www.mdpi.com/2076-3417/11/14/6327.

[53]   "On-chip 3D printing of hollow-core photonic waveguides," ed. Nanoscribe, 2020.

[54]   "Introduction to COMSOL Multiphysics," 5.6 ed: COMSOL, 2020.
[55]   "Introuction To Wave Optics Module," 5.6 ed: COMSOL, 2020.
[56]   "Wave Optics Module Users Guide," 5.6 ed: COMSOL, 2020.
[57]   "Simulating Optical Waveguides with COMSOL Multiphysics." COMSOL.
        https://www.comsol.com/video/waveguide-simulation-with-the-beam-envelope-method
        (accessed February 6, 2022).
[58]   "Photonic Professional GT2: World's highest resolution 3D printer." Nanoscribe.
        https://www.nanoscribe.com/en/products/photonic-professional-gt2 (accessed March 29,
        2022).
[59]   H. Wei and S. Krishnaswamy, "Polymer micro-ring resonator integrated with a fiber ring
        laser for ultrasound detection," *Opt. Lett.,* vol. 42, no. 13, pp. 2655-2658, 2017/07/01
        2017, doi: 10.1364/OL.42.002655.
[60]   *Photonic Professional GT2*, Nanoscribe.
[61]   "MD-100 Optical Probe Station Specification Sheet," Maple Leaf Photonics.
[62]   "Multi-Die Probe Station," ed. Maple Leaf Photonics.
[63]   *8164B Lightwave Measurement System Data Sheet*, Keysight Technologies.
[64]   "8164B Lightwave Measurement System." Keysight.
        https://www.keysight.com/us/en/product/8164B/lightwave-measurement-system.html
        (accessed April 4, 2022).
[65]   *N7744A 4-Channel Optical Multiport Power Meter Data Sheet*, Keysight Technologies.
[66]   "N7744A Optical Multiport Power Meter." Keysight.
        https://www.keysight.com/us/en/product/N7744A/optical-multiport-power-meter-4-
        sensor-ports.html (accessed April 4, 2022).
[67]   "PM100D - Compact Power and Energy Meter Console, Digital 4" LCD " ThorLabs.
        (accessed April 7, 2022).
[68]   "Digital Microscope - VHX-7000 Series." Keyence.
        https://www.keyence.com/products/microscope/digital-microscope/vhx-7000/ (accessed
        April 4, 2022).
[69]   "Digital Microscope VHX-7000 Series."
[70]   H. Golub *et al.* (2000) Delivering Value to Customers. *McKinsey Quarterly*.
[71]   WPI. "About LEAP." Worcester Polytechnic Institute.
        https://www.wpi.edu/research/core-research-facilities/leap/about (accessed October 17,
        2021).
[72]   WPI. "Major Qualifying Project." https://www.wpi.edu/academics/undergraduate/major-
        qualifying-project (accessed October 26, 2021).
[73]   "The WPI Plan." Worcester Polytechnic Institute. https://www.wpi.edu/project-based-
        learning/wpi-plan (accessed October 26, 2021).
[74]   M. Goraus, D. Pudis, P. Urbancova, I. Martincek, and P. Gaso, "Surface-relief Bragg
        grating waveguides based on IP-Dip polymer for photonic applications," *Applied Surface
        Science,* vol. 461, pp. 113-116, 2018/12/15/ 2018, doi:
        https://doi.org/10.1016/j.apsusc.2018.05.185.
[75]   H. Gao, G. F. R. Chen, P. Xing, J. W. Choi, H. Y. Low, and D. T. H. Tan, "High-
        Resolution 3D Printed Photonic Waveguide Devices," *Advanced Optical Materials,* vol.
        8, no. 18, p. 2000613, 2020, doi: https://doi.org/10.1002/adom.202000613.
[76]   *Nanoscribe Printing Materials*, Nanoscribe.

[77] "NanoGuide." Nanoscribe. https://support.nanoscribe.com/hc/en-gb (accessed April 3, 2022).

[78] S. Dottermusch, D. Busko, M. Langenhorst, U. W. Paetzold, and B. S. Richards, "Exposure-dependent refractive index of Nanoscribe IP-Dip photoresist layers," *Opt. Lett.,* vol. 44, no. 1, pp. 29-32, 2019/01/01 2019, doi: 10.1364/OL.44.000029.

[79] T. Gissibl, S. Wagner, J. Sykora, M. Schmid, and H. Giessen, "Refractive index measurements of photo-resists for three-dimensional direct laser writing," *Opt. Mater. Express,* vol. 7, no. 7, pp. 2293-2298, 2017/07/01 2017, doi: 10.1364/OME.7.002293.

[80] *TSMJ_TMMJ_TPMJ-Tapered-Lensed-Fibers-OZ-Optics-Datasheet*, AMS Technologies.

[81] X. C. Tong, *Advanced Materials for Integrated Optical Waveguides*. Springer, 2014.

[82] X. Zhu *et al.*, "Single-transverse-mode output from a fiber laser based on multimode interference," *Opt. Lett.,* vol. 33, no. 9, pp. 908-910, 2008/05/01 2008, doi: 10.1364/OL.33.000908.

[83] Q. Wu, Y. Semenova, P. Wang, and G. Farrell, "High sensitivity SMS fiber structure based refractometer – analysis and experiment," *Opt. Express,* vol. 19, no. 9, pp. 7937-7944, 2011/04/25 2011, doi: 10.1364/OE.19.007937.

[84] P. Karioja and D. Howe, "Diode-laser-to-waveguide butt coupling," *Appl. Opt.,* vol. 35, no. 3, pp. 404-416, 1996/01/20 1996, doi: 10.1364/AO.35.000404.

[85] C. Xiong *et al.*, "Optical Fiber Integrated Functional Micro-/Nanostructure Induced by Two-Photon Polymerization," (in English), *Frontiers in Materials,* Review vol. 7, 2020-October-28 2020, doi: 10.3389/fmats.2020.586496.

[86] "Ansys Lumerical Photonics Simulation & Design Software." Ansys. https://www.ansys.com/products/photonics (accessed April 12, 2022).

[87] "Product Overview." Ansys Lumerical. https://www.lumerical.com/products/#system (accessed April 12, 2022).

[88] H. Wang, "Measurement of optical waveguide scattering loss: an improved method by the use of a Coblentz mirror," *Appl. Opt.,* vol. 33, no. 9, pp. 1707-1714, 1994/03/20 1994, doi: 10.1364/AO.33.001707.